

ALMA MATER STUDIORUM - UNIVERSITÀ DI BOLOGNA

---

DOTTORATO DI RICERCA IN INGEGNERIA CIVILE,  
CHIMICA, AMBIENTALE E DEI MATERIALI  
Ciclo XXXII

08/A1 - Idraulica, Idrologia, Costruzioni Idrauliche e Marittime  
ICAR/02 - Costruzioni Idrauliche e Marittime e Idrologia

**DEVELOPMENT AND TESTING OF  
NUMERICAL HYDRODYNAMIC TOOLS FOR  
LARGE-SCALE FLOOD HAZARD AND RISK  
ASSESSMENT**

Presentata da:  
**Iuliia Shustikova**

Supervisore:  
**Prof. Attilio Castellarin**

Co-supervisore:  
**Dr. Alessio Domeneghetti**

Coordinatore del Dottorato:  
**Prof. Luca Vittuari**

---

Esame Finale - Anno 2020

*In memory of my mother and father*

# Abstract

Hydrodynamic modelling of inundation events is associated with a large array of uncertainties. This aspect is especially evident in the models run for geographically large areas. Recent studies suggest using fully two-dimensional (2D) models with high resolution in order to avoid uncertainties and limitations coming from the incorrect interpretation of flood dynamics and unrealistic reproductions of the terrain topography. The increasing availability of high-resolution topographic data and the ever growing computational potential of workstations enable us to simulate inundation events with a high level of hazard parameters details (i.e. water depth, inundation extent, flow velocity, etc.). The EU Floods Directive requires the Member States to update their flood hazard and risk maps every six years, and this requires high resolution simulations over large areas for successful flood management solutions. Additionally, low-frequency high-magnitude events bring additional challenges as conventional structural flood protection systems (e.g. levees), which are omnipresent in floodplain landscapes, might collapse due to hydraulic conditions such as high water loads, durations and velocities, or geotechnical factors that weaken structures (e.g. burrowing animal activities). Therefore, it is important to jointly consider the distribution of the inundated zones, potential levee breaching and holistic river-system behaviour when assessing flood hazard. In order to address the abovementioned challenges the present research focuses on the high-resolution flood simulations performed on geographically large areas using 2D inundation models with particular focus on complex topography (e.g. main and minor levees, embankments, small canals, etc.). Moreover, this Thesis aims at developing and testing a new tool, which allows for an efficient levee breach modelling and river dynamic tracking in fully 2D mode.

First, our study evaluates and compares numerical models of different complexity by testing them on a floodplain inundation event that occurred in the basin of the Secchia River, Northern Italy, on 19th January, 2014. The event was characterized by a levee breach

and consequent flooding of over 75 km<sup>2</sup> of the plain behind the levee within 48 hours causing population displacement, one death and economic losses in excess of 400 million Euro. We test the well-established HEC-RAS 2D, and LISFLOOD-FP codes implemented using different grid size (25, 50, 100 m) based on 1 m digital elevation model resolution. The two models are based on different governing equations and mesh representation. Our study quantitatively compares modelling strategies highlighting differences in terms of the ease of implementation, accuracy of representation of hydraulic processes within floodplains and computational efficiency. Additionally, we look into the different grid resolutions in terms of the results accuracy and computation time. This study is a preliminary assessment that focuses on smaller areas in order to identify potential modelling schemes that would be efficient for simulating flooding scenarios for large floodplains.

Then, we simulate the flood which occurred in October, 2000 on the mid-lower portion of the Po River (c.a. 350 km long reach), Northern Italy and produced significant damages in the area, particularly in the upper portion of the river. Due to its peculiar flood protection system, which consists of a complex network of minor and main embankments, flood management in this region is a great challenge. In order to represent the complexity of the floodplain we simulate the event along the study reach using a LISFLOOD-FP model in fully 2D mode. The model is run based on high-resolution digital elevation data (from 30 m to 100 m) in order to reproduce the inundation patterns of the event. The main objective of this task is to investigate how high resolution data together with the 2D hydraulic model may contribute to the large-scale hazard assessment. We test different terrain configurations, which account for protection measures (i.e. embankments) differently and derive an optimal solution in terms of the resolution and computation costs. Importantly, the current work advances previous studies performed for the flood simulations on the Po River which employed one-dimensional (1D) and quasi-2D schemes that have significant limitations (e.g. quasi-2D schemes lack the representation of spatial distribution of flood depth and flow velocity).

Finally, to reproduce the river system behaviour as a response to the levee breach we simulate flooding events using the LISFLOOD-FP 2D with its new levee-breaching extension developed within this PhD project. This accurate yet computationally efficient tool allows for levee breaching simulations run on large-scale with minimum setup effort. In order to investigate the performance of the extension we test it against the identical setup of the full-momentum 2D solver HEC-RAS 2D on a synthetic case study. Moreover, we evaluate the performance of the new extension on two historical events in terms of inundation extent: a small-scale Secchia River flood (January 2014) and large-scale catastrophic Polesine flood (November 1951), both occurred in the Northern Italy and resulted in vast damages and life losses. Numerical stability, as well as computation costs were assessed accounting for the accuracy of the results and sensitivity of the model

parameters. Our levee-breaching extension will allow breach simulations to be undertaken over geographically larger areas in order to capture the inundation patterns and changes in flow hydrographs downstream from the breach. Moreover, the designed tool is expected to be applied in near-real time and emergency flood risk management solutions.



# Contents

<b>ABSTRACT .....</b>	<b>1</b>
<b>INTRODUCTION.....</b>	<b>1</b>
Structure and contributions of the Thesis .....	6
<b>CHAPTER 1. FLOOD HAZARD MAPPING METHODS .....</b>	<b>9</b>
1.1. Introduction .....	9
1.2. Empirical methods: application, limitations and advantages .....	10
1.3. DEM-based methods: application, limitations and advantages .....	13
1.4. Numerical hydrodynamic models: application, limitations and advantages .....	14
1.4.1. 1D schematization .....	16
1.4.2. 2D schematization .....	18
1.5. Flood modelling: recent advances and further steps.....	23
1.6. Research questions addressed in this Dissertation .....	25
<b>CHAPTER 2. COMPARING 2D CAPABILITIES OF HEC-RAS AND LISFLOOD-FP ON COMPLEX TOPOGRAPHY .....</b>	<b>27</b>
2.1. Introduction .....	27
2.2. Tools and study scope.....	29
2.2.1. HEC-RAS (5.0.3) .....	29
2.2.2. LISFLOOD-FP .....	31
2.2.3. Objective of the study .....	31

<b>2.3. Study event and data used, models setup and calibration .....</b>	<b>32</b>
2.3.1. Study event and data .....	32
2.3.2. Models configuration and setup .....	36
2.3.3. Models calibration.....	37
<b>2.4. Results .....</b>	<b>38</b>
<b>2.5. Discussion.....</b>	<b>43</b>
2.5.1. Performance comparison .....	43
2.5.2. Limitations .....	46
<b>2.6. Conclusions.....</b>	<b>48</b>

### **CHAPTER 3. LARGE-SCALE HIGH-RESOLUTION SIMULATIONS USING 2D RASTER-BASED MODEL. THE PO RIVER CASE STUDY .....**

<b>3.1. Introduction .....</b>	<b>51</b>
3.1.1. Study area.....	52
3.1.2. Flood modelling on the mid-lower portion of the Po River. Review of existing research.....	57
3.1.3. Research objectives.....	61
<b>3.2. Methods and data.....</b>	<b>62</b>
3.2.1. Study event and data .....	62
3.2.2. Model set up and calibration .....	65
<b>3.3. Results and discussion .....</b>	<b>66</b>
<b>3.4. Conclusion .....</b>	<b>71</b>

### **CHAPTER 4. LEVEE BREACHING: A NEW EXTENSION TO THE LISFLOOD-FP MODEL.....**

<b>4.1. Introduction .....</b>	<b>73</b>
<b>4.2. Methods.....</b>	<b>76</b>
4.2.1. Levee breach module.....	76
4.2.2. Synthetic test description .....	78
4.2.3. Secchia inundation .....	79
4.2.4. November 1951 Polesine catastrophic flood of the Po River.....	82
<b>4.3. Results .....</b>	<b>84</b>
4.3.1. Synthetic tests .....	84
4.3.2. Secchia inundation .....	85
4.3.3. November 1951 Polesine catastrophic flood, Po River.....	87

<b>4.4. Discussion</b> .....	<b>88</b>
4.4.1. Synthetic cases .....	88
4.4.2. Historic events simulations.....	89
4.4.3. Assumption and limitation of the levee failure extension.....	90
<b>4.5. Conclusion</b> .....	<b>91</b>
<b>SYNTHESIS</b> .....	<b>93</b>
<b>LIST OF FIGURES</b> .....	<b>101</b>
<b>LIST OF TABLES</b> .....	<b>105</b>
<b>BIBLIOGRAPHY</b> .....	<b>107</b>
<b>ACKNOWLEDGEMENTS</b> .....	<b>125</b>



# Introduction

Floods are a greatly impactful natural disaster, which over the years have taken millions of human lives and caused tremendous socio-economic damages around the globe (Alfieri et al. 2017). Floods may have a different origin, and may thus be classified accordingly: coastal, riverine, flash floods and ice-jam floods. Compared to other natural hazards such as droughts, earthquakes, extreme temperatures, landslides, mass movements, storms, volcanic activity and wildfire, floods are the most frequently occurring disasters throughout 2008-2017 globally (CRED 2019b). In 2018 floods affected more people than all other natural hazards combined (Figure 1).

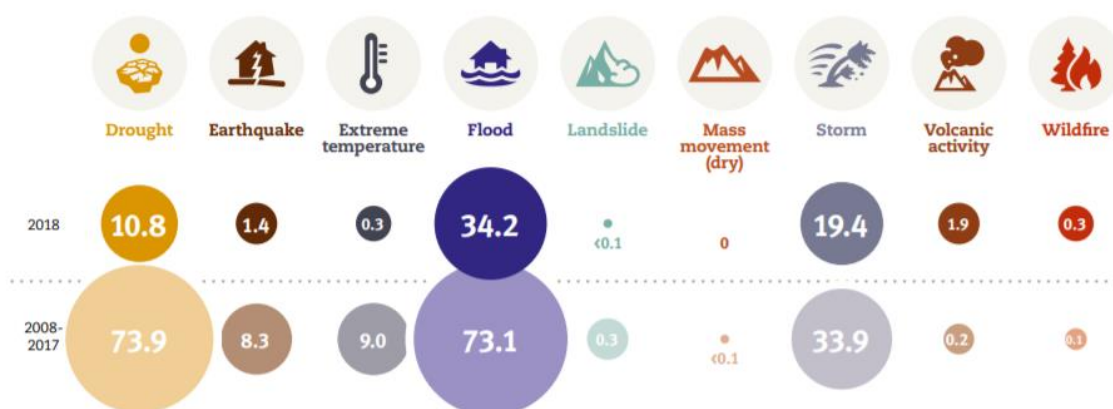


Figure 1. Number of affected people (million) by disaster type: 2018 compared to 2008-2017 annual average. Taken from (CRED 2019b)

Spatially (Figure 2), most affected regions are Asia and Africa, from which in Pakistan, Vietnam, India and Bangladesh floods occur several times a year and tremendously impact local communities. In 2018 some African countries such as Somalia and Nigeria suffered severe floods, having direct and indirect impacts on almost 5 million inhabitants (CRED 2019a). Developing countries with high-level flood protection system and efficient flood management solutions also suffer from the increasing water levels.

## Introduction

Extreme rainfalls in Japan generated catastrophic floods, resulting in 230 deaths (CRED 2019a). In terms of monetary losses, according to CRED (2019b) in 2018 floods contributed to third largest share of monetary losses (about \$19.7 billion) after storms and wildfire.

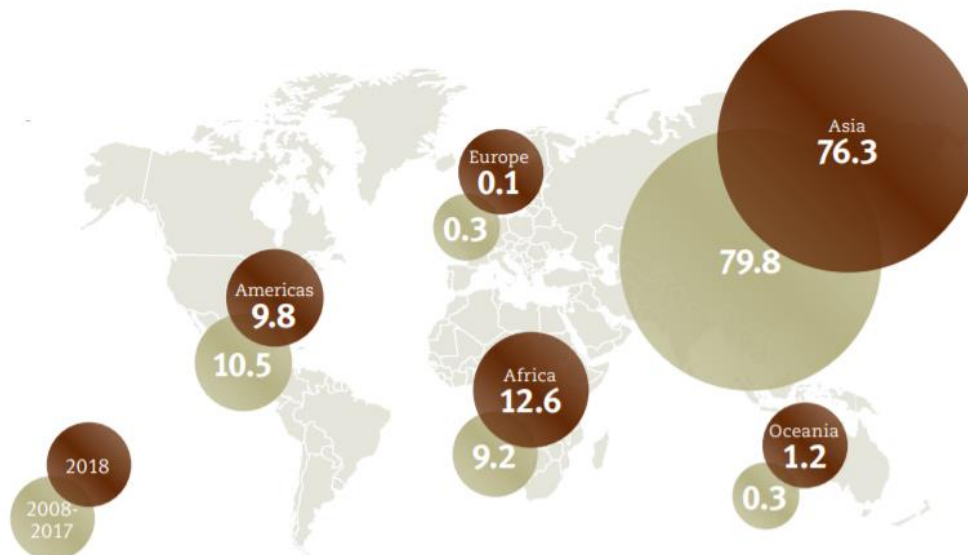


Figure 2. Share of affected people (%) by continent (million). Taken from (CRED 2019b)

In human record, one of the deadliest floods occurred on the Yellow River (China) in 1931. According to various sources, the death toll reached between 1 and 4 million people, which is difficult to accurately estimate because of the spatial extent and the accessibility of the data back in 1931. 25 million people were displaced, the territory as large as 70,000 square miles was flooded and overall damages reached \$2,000,000,000 (National Flood Relief Commission 1933).

There have been a series of large-scale floods in recent decades also on the European continent. An event, which was recorded as one of the most damaging in terms of monetary losses is the November 1994 flood in Italy, which devastated some areas of Piedmont, Lombardy, Liguria, Aosta Valley and Emilia-Romagna, with \$9.3 billion overall and \$65 million insured losses. According to Munich RE (2016) the event of August 2002 across central Europe, which mainly affected Germany, Austria, Czech Republic, Switzerland and Slovakia, are among the 10 costliest floods worldwide in the period between 1980-2015. These events resulted in 39 deaths and \$16.5 billion of overall losses, from which \$3.4 billion were insured losses. Following this event, a catastrophic flood impacted Austria, Czech Republic, Germany, Hungary, Poland and Switzerland in 2013. Insured losses were of the same magnitude as in 2002, but overall losses were somewhat lower (\$12.5 billion) and the event caused 25 fatalities. Extensive research has shown that, despite the fact that the 2013 event was more severe in hydrologic terms, it was possible to reduce the overall economic losses compared to the 2002 event. This effect is attributed to increased preparedness and

higher level of adaptation in some regions after the 2002 event (Kienzler et al. 2015; Kreibich et al. 2011).

Numerous studies (Alfieri et al. 2017; Bubeck et al. 2019; Hallegatte et al. 2013; Winsemius et al. 2016; IPCC 2014) conclude that flood risks will only increase in future decades due to economic development, urban migration of population and global climatic changes. Alfieri et al. (2018) highlighted that flood risk is likely to increase in Central and Western Europe. Dottori et al. (2018) explored the impact of different levels of climate warming and socio-economic scenarios, and found that socio-economic dynamics will be the crucial element in changes in riverine flood risk in the 21<sup>st</sup> century. Under different mitigation targets, including those set in Paris agreement (United Nations 2015), the flood risks are subject to change. In their research on impact of different levels of climate warming they investigated three thresholds: 1.5°C, 2°C and 3°C (of global temperature warming) and summarised that in all areas globally, the flood damages related to agriculture, residential and capital will upsurge with temperature increase (Dottori et al. 2018). Regarding future risks on railway network in Europe, the damages related to railway tracks disruption is likely to increase by 310% (under the 3°C of global warming scenario) (Bubeck et al. 2019).

Despite obvious direct consequences, such as deaths, direct damages to buildings and infrastructure, agricultural losses, floods may have a vast array of indirect impacts. Some of them are infrastructure disruption and related economic losses, spread of infections, famine, household displacement, long-term environmental impacts, etc. Koks et al. (2019) suggests that financial damages associated with indirect impacts on macroeconomic level in Europe will increase in the light of increasing occurrence of extreme flood events. Indirect losses is a subject to 65% increase compared to direct, as due to the severity of the natural hazards it will be more challenging to supply products from alternative sources (Koks et al. 2019).

In order to address increasing flood risk issues the European Commission developed the European Floods Directive 2007/60/EC, which is aimed to *“establish a framework for the assessment and management of flood risks, aiming at the reduction of the adverse consequences for human health, the environment, cultural heritage and economic activity associated with floods in the Community”* (Article 1, European Commission 2007). The implementation of the Floods Directive is supposed to be in cooperation with the Water Frame Directive (2000/60/EC), meaning that flood risk management and river basin management should be performed in close collaboration and agreement. The Floods Directive defines a flood as *“temporary covering by water of land not normally covered by water. This shall include floods from rivers, mountain torrents, Mediterranean ephemeral water courses, and floods from the sea in coastal areas, and may exclude floods from sewerage systems”*. While, flood risk is defined as *“combination of the probability of a flood event and of the potential adverse consequences for human health, the environment, cultural heritage and economic activity associated with a flood event”* (Article 1, European Commission 2007). Hereafter, we will refer to the definitions stated in

the Floods Directive. The EU countries (also Member States) should assess flood risks related to coastal and river floods and develop strategies taking into account long term developments (climate change) and be addressed through sustainable land-use solutions. Member states are obliged to provide flood hazard (magnitude and probability of the flood, (Moel et al. 2009a)) and flood risk maps, which would display potential negative effects of various flooding scenarios using “best available technologies” (European Commission 2007). The outcomes such as maps, plans, other supplementary materials are supposed to be accessible to public (European Commission). The flood scenarios produced by responsible authorities should cover:

- Extreme flood events
- Floods with medium probability (likely return period  $\geq 100$  years)
- High probability floods

Based on the Floods Directive requirement, the flood hazard maps should include flood extent, water levels and flow velocity or water flow (where appropriate) (European Commission 2007). Flood hazard maps illustrate a spatial distribution of several flooding parameters and their combination, such as water depth, flow velocities, duration of flood and in some cases time of arrival of the flood at a certain location. Flood hazard maps are the basis for calculating associated risks, therefore flood mapping is an essential step in reducing flood risks. Flood risk maps visualise an aggregated information on the risk zones, which are usually described as e.g. low, medium and high.

With the changing physical environment, and scientific methods and tools, existing methods and maps get outdated after certain period of time. For this reason, the Floods Directive establishes that every six years the hazard and risk maps need to be revised and updated (European Commission 2007). Moreover, it is stated in the document that management plans should be developed for each river basin or sub-basin. These plans should satisfy the condition that they do not increase flood risks (in countries) upstream or downstream of any given river. In order to achieve such goals, flood risk assessments and mapping should be undertaken considering the catchment response to any given flood scenario (see above). Vorogushyn et al. (2018) question the assumption that Member States utilise state-of-art scientific methodologies and approaches in flood risk mapping. Incomplete/fragmented spatial coverage used in the undertaking of flood risk management and mapping may lead to inefficient adaptation strategies, where complex river system effects are poorly addressed or not considered entirely (Vorogushyn et al. 2018). This, in turn violates the solidarity principles outlined in the Floods Directive, which means some changes are required to overcome current challenges in implementation of the EU Floods Directive.

Large-scale flood risk assessment, which spatially covers the whole river system rather than a single reach, is an essential concept in the development of effective flood management strategies. The evolution of the physical environment over time, as well as

climate change, needs to be considered, especially in light of substantial economic investments, e.g. installing flood protection infrastructure (levees, embankments, retention basins, etc.) (Vorogushyn et al. 2018).

As a crucial part of the large-scale flood mapping it is important to consider a complex interaction between floodplains and flood protection measures and related risks in cases of their failures. Flood protection measures such as levees and embankments, may fail due to a series of various internal or external factors. A levee failure may bring catastrophic consequences to the communities and assets located behind levees. Sudden lowering of embankment crests in densely populated areas leads to human losses and a vast array of direct and indirect socio-economic and environmental impacts. Therefore, it is of great importance to consider remaining (residual) risks and plan the adaptation and mitigation measures appropriately. Therefore, it is a common phenomenon when the communities in the protected floodplains are not aware of the possible risks in case the levee is breached, so the consequences become catastrophic when failures occur (Ludy and Kondolf 2012). In Greater New Orleans this effect was seen after the passage of Hurricane Katrina in 2005, which caused over 1100 deaths and claimed to be the costliest hurricane on human record (Andersen 2007). The protecting levee breached in several locations inundating the majority of New Orleans and affecting the community for many years ahead. Another example is Polesine flood that occurred on the Po River in 1951, when the levee breached in 3 locations on the left embankment, letting an enormous amount of water penetrate the floodplain. The floodwaters reached the Adriatic coast and spread for an area of 1000km<sup>2</sup>, killing 114 people and leaving about 180,000 people homeless (Viero et al. 2019). The recovery after such devastating events may last decades and in some cases, certain parts of the flooded communities may never be able to recover to the pre-event state. Thus, it is highly important to investigate and assess residual risks and inform the communities about possible remaining risks.

Despite negative impacts outlined above, retention of flood waters in off-line floodplains may have overall positive effects, by reducing the peak water flow and water levels downstream from the breach (Sanders et al. 2006; van Mierlo et al. 2007). This can be undertaken by controlled levee failure, when a portion of the levee is removed in a pre-defined location under the supervision of responsible local authorities. Controlled flooding is considered an important element for flood management strategies and practiced globally, e.g. Italy, The Netherlands, Vietnam, Germany, Belgium, Bangladesh, The USA etc. (van Staveren et al. 2017). In such case, a floodplain upstream the river reach gets inundated taking certain volume of floodwater and reducing risks of possible levee failures downstream. This is of specific importance in places where residual risks are high behind the levees. A complex interaction between channel flow and floodplains is also known as river system behaviour (van Mierlo et al. 2007). In order to address associated effects and their consequences we need to produce accurate flood risk maps.

In view of the above, flood hazard mapping across geographically large areas, considering possible levee breaches, can provide policy makers with valuable input for the development of correct and holistic flood management strategies. This aspect is highly important and our work is focused on further deepening understanding in this topic.

In order to meet requirements of the EU Floods Directive and develop effective flood risk management plans, the European Member States established responsible bodies (European Commission 2007). These bodies carry out a large scope of activities associated with the implementation of the Floods Directive, i.e. production of the flood hazard maps. As mentioned above, flood hazard mapping is a preliminary and compelling step in developing flood risk maps and mitigation strategies. There are two main approaches for the development of flood hazard maps, named probabilistic and deterministic flood modelling (Apel et al. 2006). The general algorithm of probabilistic flood mapping usually consists of hydrological simulation, flood frequency analysis and eventually hydraulic modelling (Alfieri et al. 2015). Hydrological simulations are performed using hydrological models: mathematical models that simulate hydrological processes (snowmelt, surface runoff, infiltration, groundwater drainage, etc.) over an extended period of time. The outcome of such simulations is streamflow, which is then analysed using statistical models to derive extreme flow peaks (Alfieri et al. 2015). The peak flows are then used in the flood inundation model to generate flood maps for given probability levels, usually expressed in terms of return period e.g. 100-yr, 500-yr or 1000-yr floods. Some of the most spread inundation models are hydrodynamic models which represent different complexity and dimensionality (Di Baldassare et al. 2010). Using probabilistic models like this is one of the possible methods for flood hazard maps construction. Deterministic approach for floodplain mapping uses historical hydrographs and distributed rainfall and catchment models to produce hydrological input (synthetic design flood events, e.g. 1 in 50 year flood (Di Baldassare et al. 2010) to the inundation model, which then simulates a particular event or a set of events (Apel et al. 2006). As outlined earlier, flood hazard maps normally contain information on the flood extent, water depth and velocities, inundation time, etc. This information is combined to produce hazard maps, which are then used to calculate risks.

## Structure and contributions of the Thesis

The current Dissertation focuses on the latter element of flood hazard mapping, namely flood inundation modelling. In particular, we investigate the flow dynamics on geographically large areas by developing and applying state-of-art scientific methods and numerical algorithms to high-resolution datasets in order to better understand the potential of such tools to improve flood risk assessment and modelling and to reduce associated uncertainties. As mentioned earlier, we particularly aim to look at improved representation

of the flooding scenarios due to levee breaches on large scale. In order to address the issues stated above in most logical way, the Dissertation is structured as follows:

Chapter 1 presents an exhaustive literature review on main methods used in riverine flood modelling, including empirical methods, terrain-based approaches and hydrodynamic models. As the focus of the dissertation is centred on the latter method, the whole spectrum of available methods is described. There, the models of different dimensionality and complexity (one-dimensional - 1D, two-dimensional - 2D, combined 1D/2D) are presented, addressing most spread software packages and codes, their areas of application, related limitations and existing challenges. We highlight the differences of the schemes, grid representation and geometry used. In addition, it discusses potential application of certain methods or tools in large-scale studies.

Chapter 2 presents a thorough comparison of two fully 2D codes, which are tested on a Secchia River flood of 2014, when a levee breach caused vast inundation in Modena municipality. The chapter describes a performance of two well-known 2D models of different complexity. As the two codes operate with different mesh representation and governing equations used in flow calculation, we evaluate their effect on the results accuracy. We apply the two models on a complex terrain around two small towns located in the affected area. Moreover, we implement various grid size (25-100 m) based on 1 m Digital Elevation Model (DEM) resolution in order to evaluate the potential and limitations of the two models to be run on a large-scale study also considering their computational efficiency as one of the crucial elements.

In Chapter 3 we look into a larger scale study and importance of the DEM pre-processing in high-resolution fully 2D flood modelling. For this reason, we review existing research done on the study area (Po River, Italy) by using flood inundation models and we discuss remaining gaps which would potentially contribute to the Floods Directive implementation on the Po River. We apply a 2D model to simulate the flood, which happened in October 2000 and produced significant damages in the area. Specifically, we are dealing with the middle-lower stretch of the river, which is of particular interest for the responsible authorities. Due to its peculiar flood protection system, which consists of the complex network of main and minor embankments with different design return period, the flood management in this region is a great challenge (Castellarin et al. 2011a). In order to represent the complexity of the floodplain we simulate the event on the 350 km long river reach using a fully 2D model. The model is run using 30, 50 and 100 m raster resolution data resampled from 2 m resolution terrain data with and without addition of the actual embankment height. We describe how the deliberate inclusion of the embankments' height influences the accuracy of the model at each resolution and computational effort needed to run simulations on a large-scale study. We evaluate the benefits gained from large-scale 2D model by presenting water depth, local distribution of flow velocities and discharge along the reach.

Chapter 4 is dedicated to the description of a new levee-breaching extension (module) of a widely-known 2D model, namely LISFLOOD-FP. The extension was developed as a part of the PhD studies in cooperation with the research group of Bristol University. The new extension allows simulating levee breaches in one single simulation (which was previously unavailable). In order to evaluate the accuracy and efficiency of the new module we compare the outcomes with the identical simulations performed by full-momentum 2D solver. Furthermore, we test the updated model on a Secchia River flood of 2014, where we simulate the whole chain of the flooding process, including the water dynamics within the river channel, levee breaching link and consequent inundation of initially dry floodplain. To test the potential of the new extension to simulate levee-breaching scenarios on a large-scale study, we simulate a historic Polesine flood, which occurred in 1951 on the downstream portion of the Po River. We compare the outcomes obtained from the new feature with those available in reports and scientific literature. In order to identify applicability of the model on different scales, we assess the computation time in relation to the sizes of modelled domains. Finally, in Synthesis, we present the main outcomes of the performed work and possible implications of the obtained results.

# Chapter 1. Flood hazard mapping methods

## 1.1. Introduction

A crucial element in the flood risk assessment is efficient and accurate flood hazard mapping, which enhances the overall quality of risk analysis and allows the illustration of the flood. According to the Floods Directive 2007/60/EC, the hazard maps should consider extreme, medium (return period of about 100 years) and more frequent events providing the insight about the flood extent, water depth or water levels and flow velocity, where appropriate (European Commission 2007). Implementation of the Floods Directive 2007/60/EC triggered the development of manifold methods and techniques to assess and represent spatial distribution of river floods. The hazard assessment methods vary not only between countries, but also between different parts and institutions within one country (Nones 2017).

A considerable number of studies showed an extensive use of the one- and two-dimensional (1D and 2D) numerical models to delineate floodplains (Bates and Roo 2000; Aronica et al. 2002; Horritt and Bates 2002; Penning-Rowsell et al. 2005; Büchele et al. 2006; Moel et al. 2009b; Di Baldassare et al. 2009b; Di Baldassare et al. 2010; Alfieri et al. 2014; Neal et al. 2012b; Falter et al. 2013), which enable the users to produce an accurate representation of river hydraulics and floodplain inundation dynamics. Some models, however apply different principles in calculating inundated areas, those would be approaches that mainly rely on Digital Elevation Model (DEM) analysis (Manfreda et al. 2014). Alongside numerical models, other methods occupy a rather large niche in flood modelling. Among those are empirical methods, which include various on-ground measurements and historic data collection, as well as remotely sensed images processing (Teng et al. 2017). Remote sensing gives an opportunity to capture flood extent of the occurred disaster and assists hydrodynamic models by providing input data and observation for calibration and validation.

It has been recognised that the correct method selection increases the overall efficiency and accuracy of hazard assessment, which in turn attributes to the risk analysis. There has been a wide array of mapping options suggested by numerous research groups and institutions (Teng et al. 2017; Néelz S. and Pender G. 2013). The selection of the approaches to delineate floodplains usually depends on numerous factors such as the data availability, computational and time capacity, scale, output requirements, etc. This chapter reviews well-known methods and tools together with auxiliary schemes to capture river flood inundation extent and related hazard characteristics such as water depth and flow velocity. Moreover, the research provides a comprehensive insight on their differences in terms of the background principles, complexity and designed application. In order to outline most widely spread flood hazard mapping methods, they are grouped as following: empirical methods with remote sensing techniques, DEM-based methods and numerical hydrodynamic models. Below we demonstrate the application of such methods and their main limitations based on extensive literature review.

### **1.2. Empirical methods: application, limitations and advantages**

One of the most basic methods to delineate flood-prone areas is the retrospective information collection and mapping. Surveys, ground measurements, sediments sequencing, dendrochronology, eye-witness interviews, remotely sensed images play a great role in this process ( Zhang et al. 2018; Kakar et al. 2014; Zielonka et al. 2008). Data collection allows for reconstruction based on numerous data inputs from various sources. Historic floods leave traces in the environment; there has been a series of studies performed in order to identify geochemical proxies that are reflected in the floodplain and deltaic sediments (Zhang et al. 2018; Zhao et al. 2017). Such proxies help to investigate the climatic and anthropogenic interplay in the river basins on high-resolution dated hundreds years back (Zhang et al. 2018). These methods are a very approximate representation of reality and are subject to uncertainties. The results of such methods are also used as a supplement to other modelling methods (DEM- based or hydraulic numerical models) as a reference for calibration and validation. For instance, remote sensing is a fast evolving approach for flood forecasting and monitoring (Teng et al. 2017). In order to support flood modelling, remote sensing offers significant inputs. Remote sensing data can be used either for empirical mapping (observed or historical event used for mapping), for constructing hydrodynamic modelling (1D and 2D), or for applying simplified DEM-based methods.

Flood mapping can now be supported by satellite observations (Schumann et al. 2009; Li et al. 2016). From one side, such data can be an auxiliary tool for hydraulic modelling in terms of data derivation (DEM, morphological properties of channels) and

model calibration/validation (Schumann et al. 2009; Li et al. 2016; Horritt and Bates 2002). From the other side, remote sensing is a (semi-) independent instrument which helps flood monitoring, capturing the inundation extent and depth levels during and after a flood event (Townsend and Walsh 1998; Brivio et al. 2010; Patel and Srivastava 2013; Hoque et al. 2011). Furthermore, we would like to focus on the remote sensing methods of inundation maps derivation.

There are different types of data acquisition techniques: optical sensors, passive microwave instruments and synthetic aperture radars (SAR). They vary by the way the images are obtained, their resolution and cost. For instance, optical sensors allow acquiring images with very high spatial resolution, visible and invisible spectrum range compositions, where the inundation extent is obtained by digitizing the contours of water-surface boundary (Schumann et al. 2009). This approach has gained a very high spread around the world and is used by numerous research groups, governmental and commercial institutions due to its straightforward nature. An advantage is that such images may be provided free of charge (Landsat 5, 7, 8; MODIS aqua and terra, SPOT, COANE, etc.), however in case of a specific mission, they may be expensive. Despite broad successful application (Marcus and Fonstad 2008; Townsend and Walsh 1998; Sanyal and Lu 2004; Joyce et al. 2009; Ward et al. 2014; Khan et al. 2011; Villaret et al. 2013; Proud et al. 2011), optical imagery has a serious limitation: it is unable to capture the terrain in case of dense cloud cover over the catchment and vegetation presence (Hoque et al. 2011; Schumann et al. 2009; Ward et al. 2014; Wilson et al. 2007).

Unlike optical sensors, microwaves are capable of passing through the clouds. Passive microwaves enable data acquisition day-and-night regardless weather conditions, since radiometers capture thermal emissions (Rees 2001). As emissivity of land and water surfaces are different, it is possible to detect inundated areas. Despite this capability, due to the large angular beams, the resulting resolution of such images is rather coarse, therefore it is applicable for very large river catchments only (approx.  $10^3$  km<sup>2</sup>) (Smith 1997; Schumann et al. 2013; Schumann et al. 2009; Li et al. 2016). Among the passive sensors there are SSM/I, SSMIS, SMMR, MIMR, TRMM-TMI, AMSR-E, etc. They are extensively used for the flood monitoring and forecasting (Bindlish et al. 2009; Temimi et al. 2005; Temimi et al. 2011; Singh et al. 2013; Lacava et al. 2015), in fact Groeve (2010) points out on the potential of using passive imagery in the global and national flood monitoring because of its high temporal resolution. Yet, the flood mapping and modelling requires higher spatial resolution than the one offered by passive microwave imagery (Schumann et al. 2009). Some studies, however, are dedicated to overcoming this limitation by e.g. downscaling the images and involving social media geotagged posts into the flood extent estimations (Sun et al. 2015).

A suitable tool to capture the terrain during the flood is the synthetic aperture radar (SAR) (Horritt et al. 2010b; Hess et al. 1995; Brivio et al. 2010; Joyce et al. 2009; Smith 1997;

Townsend and Walsh 1998; Sanyal and Lu 2004; Matgen et al. 2007; Dewan et al. 2007; Ward et al. 2014), which is able to penetrate the clouds, creating “cloud-free” images of high resolution. This feature is of great importance, as normally during a flood event the sky is overcast; more notably, SAR operates in the night time, which allows efficient hazard monitoring (Smith 1997). Active microwave imagery is obtained by the backscattered microwave pulses from the surface to the antenna; once the higher spatial resolution is needed, the beam “footprint” has to be reduced. Depending on the surface roughness, shape and dielectric properties the amount of backscattered pulse varies (Grimaldi et al. 2016); thus, the water surfaces cleared off vegetation are precisely defined in the imageries (Smith 1997). One of the examples of the flood extent capture using SAR images can be seen in Figure 3. Different colour lines are a part of the post-processing done by Schumann and Moller (2015) to delineate the flooded areas. Most of the measurements are free of charge or rather less expensive and provided by space agencies (Grimaldi et al. 2016).

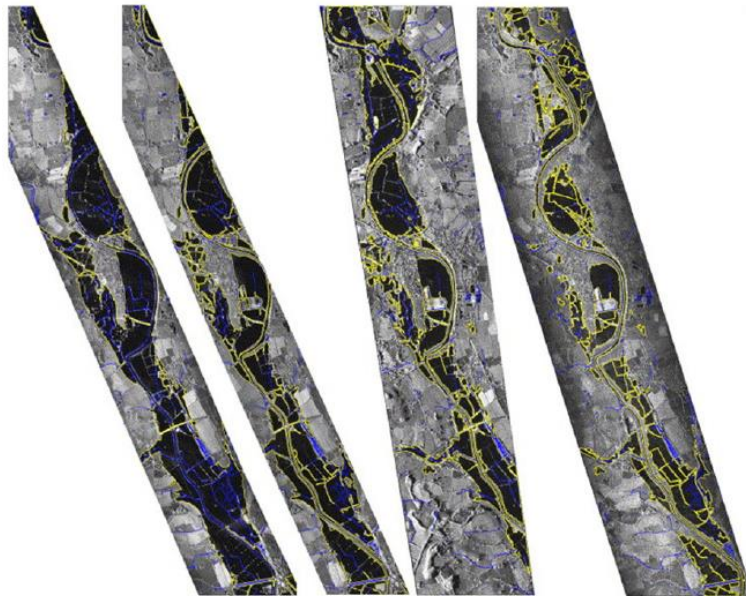


Figure 3. Flood extent delineation on airborne SAR images at four different dates during one event. Taken from (Schumann and Moller 2015)

Different algorithms exist to process the satellite images in order to delineate floods; among them are: basic visual interpretation, multitemporal change detection (Calabresi 1996; Dellepiane and Angiati 2012), automated processing (Hess et al. 1995; Matgen et al. 2011; Twele et al. 2016; Oberstadler et al. 1997), supervised classification (Roo et al. 1999), fuzzy logic (Pulvirenti et al. 2011), image histogram thresholding (Brivio et al. 2010), etc.

### 1.3. DEM-based methods: application, limitations and advantages

This group of methods uses terrain elevation data as a basic component of delineating flood-prone areas on different scales. Such delineation is normally performed using various methods to calculate the possible spread of the “inundated” areas, such as impact zonation or geomorphic characteristics of given terrain (Manfreda et al. 2014). One of the main advantages of DEM-based methods, is that they are highly efficient in terms of computation time and can be used on very large areas (national or continental scales). However, they all have a significant limitation: such methods do not capture flow dynamics and some of them are unable to report water elevations. The most spread tools and approaches are presented next.

Height Above Nearest Drainage (HAND) method is a low-complexity DEM-based approach, which has been used in numerous studies for large-scale domains (Nobre et al. 2016; McGrath et al. 2018; Johnson et al. 2019; Jafarzadegan and Merwade 2017). The basic principle is that it first processes DEM in a way that the flow pathway is defined from the local drain direction grid in 8 directions. Then the DEM is rebuilt to remove incoherent areas (those which are not hydrologically connected with the stream network). The drainage is delineated by identifying a threshold value (Nobre et al. 2016). Based on that, the drainage network is normalised and can be used for outlining flood inundation extent. This method is applied on large-scale areas (over 1000 km<sup>2</sup>), as well as probabilistic flood modelling due to its computational efficiency and data requirements (Teng et al. 2017). Nevertheless, such a method does not include the momentum transfer and velocity fields, moreover, it is known to overestimate flood-prone areas (Nobre et al. 2016).

Some other methods can be based on different assumptions and approaches, among them are: modified Topmodel index approach, linear binary classifier and inundation hydro-geomorphic characterization algorithm, etc. (see e.g., Manfreda et al. 2014 and references therein). All of them rely on different aspects related to geomorphic features that can be derived from the DEM datasets. For instance, modified Topmodel index approach takes the topographic index, which is a function of the local upslope contributing area and the local slope (Manfreda et al. 2014). The linear binary classifier is based on five features which are calculated from a given DEM to delineate flood-prone areas: distance from a DEM cell to the nearest stream, difference of elevation between a given cell and closest stream, surface curvature, contributing area and local slope (Jafarzadegan and Merwade 2017). The hydro-geomorphic method outlines the flood-prone areas in regard to the river basin properties. It considers a set of natural physical processes, which take part in the formation of the river networks and specifies the interconnections between the width of the possible flooded area and contributing area (Nardi et al. 2006). Similar to HAND approach,

all these methods are limited in their application for a preliminary identification of flood-prone areas due to the absence of hydrodynamics in the delineation of floodplains. DEM-based approaches are not able to take into account hydraulic structures and flow velocities. Therefore, in order to comply with the Floods Directive 2007/60/EC requirements in flood hazard map production, such methods should be applied along with hydrodynamic models.

Another method to delineate the flood is Rapid Flood Spreading Methodology (RFSM) developed at HR Wallingford (Gouldby et al. 2008). It was built in order to perform large-scale simulations for the regional flood risk assessments in relatively short time comparing to hydraulic models. Its main input is generated from (multiple) breached or overtopped defences and discharge into the floodplain (Lhomme et al. 2009). The automatic approach is based on two steps, first step includes a DEM pre-processing, which results in the model mesh calculation (irregular cells shape) and impact zones delineation. This is done by analysing the floodplain gradient in 8-directional expansion from the low-elevated DEM points using a search algorithm, and the consequent definition of the storage cells (Gouldby et al. 2008). Second step is the distribution of the certain water volume over the storage cells by simple flux-approximations and stage-volume functions (Falter et al. 2013). Such method is a rapid and efficient flood mapping tool (Gouldby et al. 2008), however it is linked to certain limitations such as neglecting the flow dynamics, terrain obstacles and the sensitivity of the model to the time steps observed by Falter et al. (2013). Nevertheless, RFSM performed considerably well in comparison with fully 2D codes in terms of flood depth and extent representation, and, importantly, computational efficiency. Overall, the approach has a great potential for time-saving large-scale risk mapping (Pender and Liu 2012; Falter et al. 2013; Lhomme et al. 2009; Krupka et al. 2007; Pender and Liu 2012; Liu Y. 2010).

### **1.4. Numerical hydrodynamic models: application, limitations and advantages**

Recent studies have shown a large interest to and exploitation of numerical modelling schemes of different complexity to simulate hydraulic processes (Néelz S. and Pender G. 2013). Such tools are widely applied by engineers and researchers around the globe; numerous studies proved the applicability of hydraulic models (Bates and Roo 2000; Horritt and Bates 2002; Néelz S. and Pender G. 2013; Hunter et al. 2008; Neal et al. 2012a; Teng et al. 2017; Di Baldassare et al. 2010). Unlike DEM-based mapping methods, hazard characteristics are derived from the numeric computations of physical equations. In this

sub-chapter we would like to present hydraulic models and their main application areas, as well as discuss their differences and advantages.

Any model requires a certain amount of pre-processing and setup. Depending on the model complexity and dimensionality, the data collection and pre-processing may require much longer time than the software setup itself (Sosa et al. 2019). Flood hazard mapping consists of steps described in Figure 4.

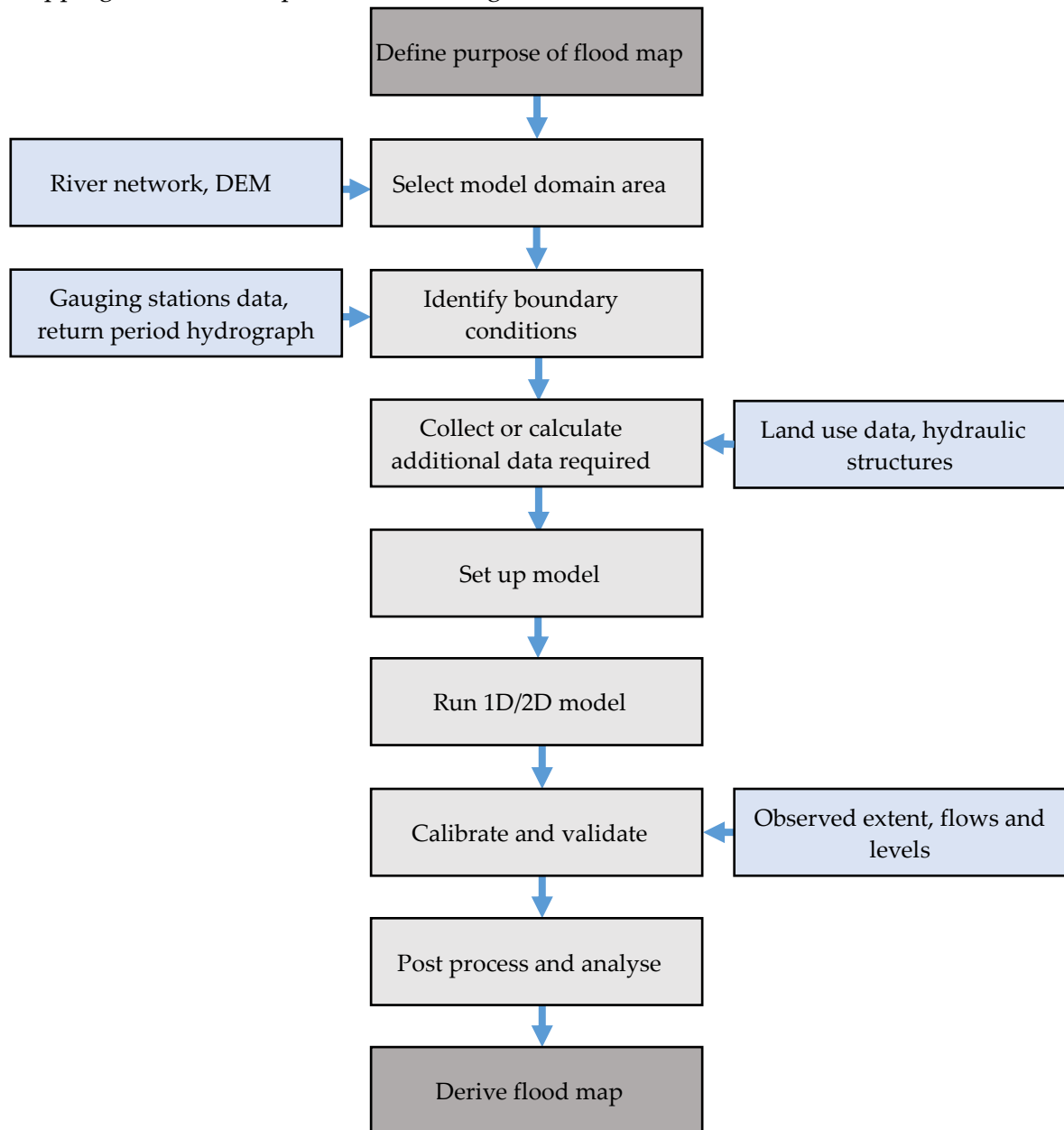


Figure 4. Schematics of the steps commonly used in flood mapping when hydraulic models are applied. Based on Hoch and Trigg (2019) and Caribbean handbook of Risk Information Management .

As illustrated in Figure 4, the domain must be carefully outlined first, to consider all possible flow directions and be large enough to account for correct representation of boundary conditions. Depending on the purpose of the flood modelling, a modeller may apply deterministic or probabilistic approach. If the hydrograph represents an estimated or historic extreme event, flow hydrograph data can be used as the upstream boundary condition to route the flow. Alternatively, it can be a series of flow hydrographs derived using statistical models, which represent a particular given exceedance probability.

The models can be grouped following the criteria of their dimensionality as 1D, 2D and 3D (see for the further details below). Regardless modelling scheme, the model needs to be calibrated using certain parameters and then validated if possible. These stages are crucial in producing most accurate flood maps, however the accuracy is also a subject of the selected method used. Below we discuss 1D and 2D modelling schemes which are employed in hydraulic models. 3D models are not discussed below, as they are used to study vertically stratified fluid properties: temperature, salinity, velocity, sediment transport or ecological studies (Popescu et al. 2015; van Ballegooyen et al. 2004; Lee et al. 2014). For instance, dam break dynamics or tsunami simulations require the application of 3D codes. Due to the aspects mentioned above 3D models are not applied for regional or large-scale floodplain inundation modelling.

### 1.4.1. 1D schematization

General principle of one-dimensional models lies in the evaluation of the water volume flowing through the channel cross-sections. Different models may operate with steady or unsteady and primarily uni-directional, homogeneous flows. Most models solve full 1D Saint Venant equation, represented by continuity or mass conservation equation and momentum conservation equation (Néelz and Pender 2009):

Conservation of mass:

$$\frac{\partial Q}{\partial x} + \frac{\partial A}{\partial t} = 0 \quad (1)$$

Conservation of momentum:

$$\frac{1}{A} \frac{\partial Q}{\partial t} + \frac{1}{A} \frac{\partial (\frac{Q^2}{A})}{\partial x} + g \frac{\partial h}{\partial x} - g(S_0 - S_f) = 0 \quad (2)$$

Where,  $Q$  is discharge,  $t$  is for time,  $h$  is the water depth,  $g$  is the gravitational acceleration,  $S_f$  is the friction slope and  $S_0$  is the channel bed slope,  $A$  is the flow cross-section area and  $x$  is the distance between cross-sections.

This solution assumes that the flow is parallel to the centreline of the channel and varies slowly in the cross-sections. The geometry of the model is represented as cross-sections, which describe the riverbed morphology (river bed, banks and adjacent relevant areas) (Figure 5). Figure 5 represents main elements of the 1D models simulation. Flow boundary condition is a hydrological input to the model, which reflects the volume of water coming into the model and is normally represented as discharge hydrograph, water levels or water stage. The modelling scheme is routing the flow within the channel and flow parameters are calculated at each cross-section. When the water levels in the cross-section exceed river banks, it spills to the adjacent indicated terrain.

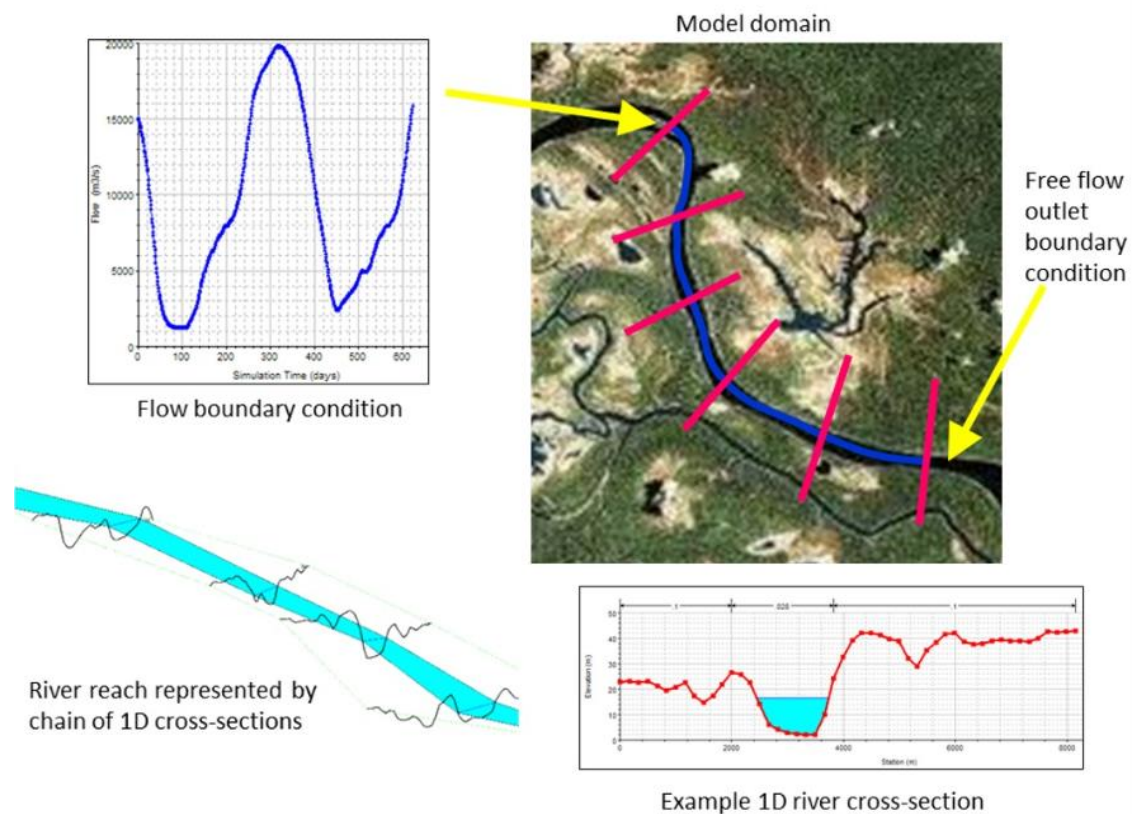


Figure 5. Example of 1D geometry and boundary conditions. Upper right panel is a top view on the channel and cross-sections, where yellow arrows point on the upstream and downstream boundary conditions, which in this case are represented as the relevant cross-section, located on the edges of the domain. The lower images graphically show the geometry of the cross-sections and associated water levels. Taken from (Caribbean handbook of Risk Information Management).

The numerical modelling scheme depends on discretization of the initial equation and in the majority of 1D codes it is finite-difference method (Néelz and Pender 2009). Some of the models that use finite-difference method are: HEC-RAS 1D (U.S. Army Corps of Engineers), SOBEK 1D Flow (Deltares), ISIS 1D (now Flood Modeller Pro), MIKE 11 (Danish Hydraulic Institute), InfoWorks RS 1D (MWH Soft/Innovyze). These are only the most popular packages, which differ by their interface features, availability (some of those, e.g. HEC-RAS, are non-commercial), etc. Overall, the numerical scheme of 1D models makes

the computation time faster compared to 2D. However, the depth mapping and evaluation of the flood extent is not always straight forward, it may require the use of interpolation methods (such as Inverse Distance Weighting) and supplementary Geographical Information System (GIS) tools (Werner 2004). In some cases, the floodplain may be represented as a part of a cross-section, it is then possible to capture the inundation extent. Therefore, 1D packages may be used to simulate inundation extent (with data post-processing), water depth, flow velocity (averaged per cross-section) and hydraulic structures: bridges, weirs, pumps, gates, etc. (Néelz and Pender 2009). One of the most crucial parts is the accurate representation of the cross-sections topography, which, in most cases, can be achieved solely by the detailed ground survey. This, and considerable amount of other input parameters may produce more room for errors. One of the most limiting factors is that 1D configuration requires the modeller to evaluate the river behaviour and dynamics, reproducing the main connections of the river with lateral floodplains or other minor reaches by means of hydraulic connections (e.g., weirs, culvert, gates and so on). This introduces subjectivity and the model performance may vary from one application to another. These models do not reproduce the real two-dimensional behaviour that characterizes some conditions but rather provide average hydraulic variables, not appropriate for real hazard representation, especially in large floodplain, where 2D dynamics are relevant (Teng et al. 2017). Due to very high computation efficiency, 1D models are commonly used for flood modelling on different scales, including large-scale studies with the limitations mentioned above (Horritt and Bates 2002; Castellarin et al. 2009).

### 1.4.2. 2D schematization

The availability of the high-resolution Light Detection and Ranging (LiDAR) DEMs (2 m and finer) prompted the application of more complex solutions for flood hazard mapping (Hawker et al. 2019). The fundamental difference between 1D and 2D models lies, firstly, in the representation of topography. In 2D models there is a complete 2-dimensional coverage of the terrain (Figure 6). The river dynamics are driven by the topography and do not depend on the river schematization provided by the modeller. Most of 2D models' solvers are based on the depth-averaging Navier-Stokes equations, which are implemented as two-dimensional shallow-water equations, which preserve mass and momentum conservation.

Conservation of mass:

$$\frac{\partial h}{\partial t} + \frac{\partial(hu)}{\partial x} + \frac{\partial(hv)}{\partial y} = 0 \quad (3)$$

Conservation of momentum:

$$\frac{\partial(hu)}{\partial t} + \frac{\partial}{\partial x} \left( hu^2 + \frac{1}{2} gh^2 \right) + \frac{\partial(huv)}{\partial y} = 0 \quad (4)$$

$$\frac{\partial(hv)}{\partial t} + \frac{\partial(huv)}{\partial x} + \frac{\partial}{\partial y} \left( hv^2 + \frac{1}{2} gh^2 \right) = 0 \quad (5)$$

where  $x$  and  $y$  are spatial dimensions, estimates of  $u$ ,  $v$ , and  $h$  over space and time (Teng et al. 2017). Due to the fact that 1D and 2D formulations do not have analytical solution for the vast majority of real world applications, different numerical schemes are implemented in order to compute the approximated flows (finite-element, finite-volume, finite-difference). Regarding spatial representation, the computational grids may have different shapes (i.e. triangular, square, rectangular, etc.) and be structured or unstructured (Figure 6).

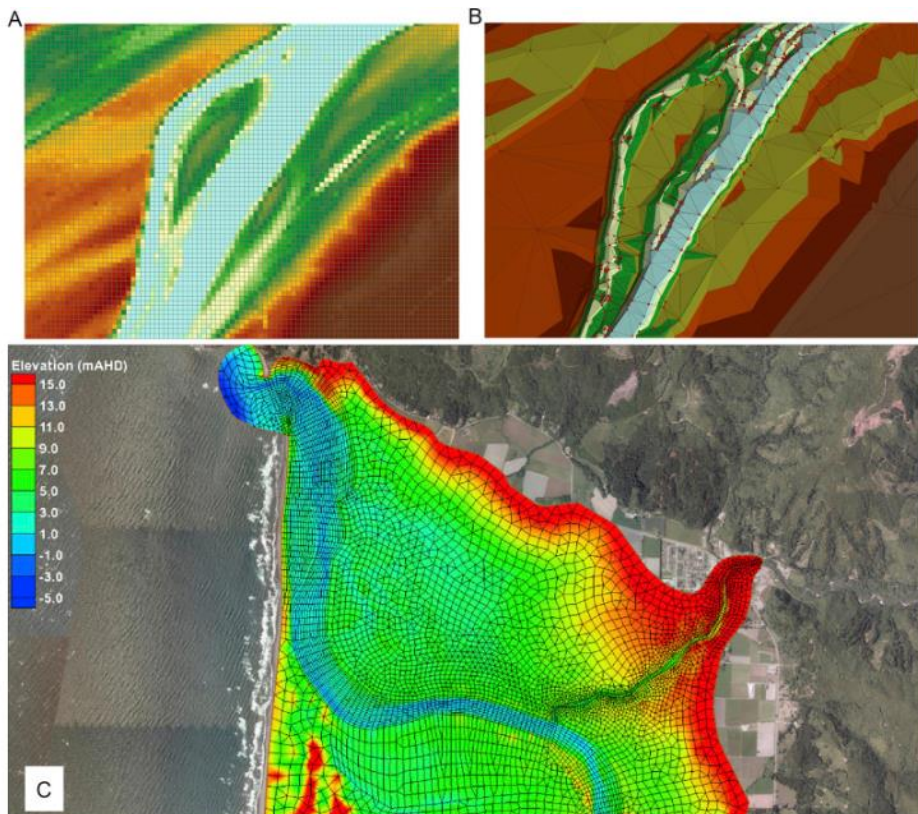


Figure 6. Different meshes used in 2D modelling: a) structured mesh; b) unstructured mesh; c) flexible mesh. Taken from (Teng et al. 2017)

Grid geometry plays an important role in the model accuracy: the more topographical details are captured in mesh building, the more detailed/accurate the results are. Unstructured and flexible meshes, which are able to contain fine topographic features such as embankments, canals, levees, etc. would greatly benefit the flood dynamic over complex topography (Shustikova et al. 2019). Meanwhile structured grid might be less efficient in this case.

2D models are able to compute the inundation extent over complex topography as well as in urban areas, and provide water depth and depth-averaged velocities, yet they are less sensitive to smaller hydraulic structures (Néelz and Pender 2009).

### *Combined 1D/2D models*

It must be noted that certain software packages allow combining 1D and 2D models (See Table 1). Normally it is represented as a link between 1D river flow model and 2D floodplain grid (Figure 7). Such method is used when the channel representation requires the terrain model with a significantly higher resolution, which sometimes is impossible/inefficient to use. 1D/2D combining is widely spread (see Table 1) as it gives an opportunity to considerably reduce the computation time compared to fully 2D models and keep the representation of the two-directional flow over the floodplain (Brunner 2016).

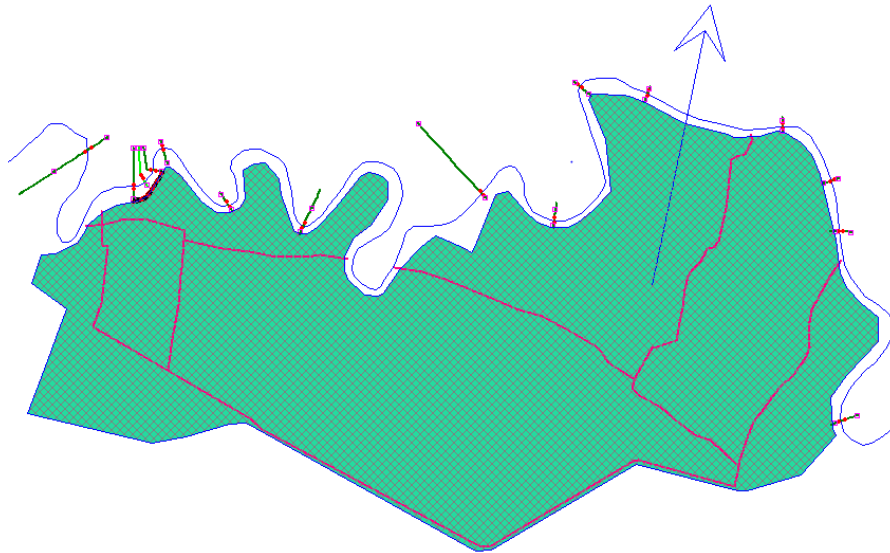


Figure 7. Schematic representation of 1D (cross-sections, green lines) and 2D (floodplain, green polygon with mesh) areas and lateral link between them (black line at left top corner in the image).

Below are presented some of the most used 2D packages (Néelz and Pender 2009).

## Chapter 1. Flood hazard mapping methods

Table 1. Some of most common 2D software used for river flood modelling.

Name	Developer	Numerical scheme	Mesh	1D coupling	License
<b>TELEMAC 2D</b>	EDF	finite-element	structured/ unstructured, triangular	+	free
<b>MIKE 21</b>	DHI	finite-difference	structured/ unstructured, triangular or quadrilateral	+	proprietary
<b>ANUGA</b>	Australian National University and Geoscience Australia	finite-volume	triangular	-	free
<b>InfoWorks RS</b>	MWH Soft/Innovyze	finite-volume	structured/ unstructured, triangular	+	proprietary
<b>FESWMS-2DH</b>	Federal Highway Administration	finite-element	triangular or quadrilateral	+	free
<b>FLO-2D</b>	FLO-2D Software, INC	finite-difference	raster-based	+	proprietary
<b>HEC-RAS 2D mode</b>	US Army Corps of Engineers	finite-volume	structured/ unstructured, up to 8 sides	+	free
<b>ISIS 2D (Flood Modeller Pro)</b>	Flood Modeller	finite-difference	structured/ unstructured, triangular or quadrilateral	+	proprietary
<b>SOBEK 2D</b>	Deltares	finite-difference	staggered grid	+	proprietary
<b>TUFLOW</b>	BMT-WBM	finite-difference	square	+	proprietary
<b>Delft3D (FLOW module)</b>	Deltares	finite-difference	structured/ unstructured (flexible mesh)	+(couples with another model)	free

Due to the differences that can be observed in Table 1, the results obtained from modelling also differ. A benchmark study performed by the UK Environment Agency on 2D hydraulic modelling packages revealed that 2D models based on shallow-water

equations deliver better results in terms of flood water velocity, than the ones which use simplified equations (Néelz and Pender 2009). Nevertheless, for the representation of the flood extent all 2D packages perform comparably. Then, predictably, it is suggested that possibility to link 2D model with 1D channel model gives a wide array of options that are provided by both codes, however the type of 1D/2D linkage is an essential threshold for the river-floodplain water volume exchange (Néelz and Pender 2009). Moreover, the numerical scheme used in software influences the ability to represent the levee breaches, and those which are able to capture shocks (mostly finite-volume schemes perform better in such conditions (Néelz and Pender 2009)). Therefore, finite-volume schemes are more popular (Teng et al. 2017). Combined 1D/2D models are widely used in large-scale flood mapping, as they allow to cover vast areas with lower computation costs compared to fully 2D schemes (Di Baldassare et al. 2010; Castellarin et al. 2011a).

### *Raster-based hydrodynamic models*

A distinction of raster-based hydrodynamic models, hereafter referred to also as raster-based models, is that they operate with regular rectangular mesh (e.g. LISFLOOD-FP, JFLOW, PRIMo, PARFLOOD) (Neal et al. 2012a; Vacondio et al. 2014; Sanders and Schubert 2019; Bradbrook 2006). The flow in raster-based models moves in  $x$  and  $y$  directions (Figure 8). Raster-based models can pose a limitation, due to the fact that some critical topographical features might be not captured in such mesh, which would result in errors in flow parameters. These errors can be avoided by applying smaller mesh size (or higher terrain data resolution). Specific characteristics related to the mesh building vary from one model to another. Below we describe several examples of how such models function.

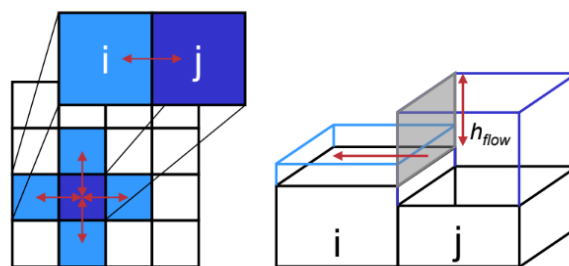


Figure 8. Schematics of the raster-based model representation. Taken from (Bates 2009-2019)

Numerous studies utilise 2D LISFLOOD-FP model, developed by the University of Bristol and freely accessible for the research purposes (Bates et al. 2010; Di Baldassare et al. 2010; Neal et al. 2012a). The 2D flow is solved based on inertial formulation of shallow-water equation coupled in  $x$  and  $y$  directions (Bates et al 2010). The above mentioned simplification allows for the substantial reduction of the computational time (Alfieri et al.

2014; Néelz and Pender 2009). LISFLOOD-FP operates with square grid of same resolution as the input raster, however, it may represent channel thanks to its subgrid capabilities (Neal et al. 2012a). This model is proven to be efficient specifically for large-scale hazard modelling. This feature has been tested by various research groups, among them are the studies conducted on regional (Horritt and Bates 2002; Schumann et al. 2013; Fewtrell et al. 2011; Bates and Roo 2000; Maugeri 2012), basin (Savage et al. 2016; Dimitriadis et al. 2016; Amarnath et al. 2015; Schumann et al. 2013) and continental/global (Alfieri et al. 2014; Schumann et al. 2016; Sampson et al. 2015) scales.

A similar approach is used in JFLOW (JBA consulting), a commercial software developed for the engineering and consultancy purposes (Bradbrook 2006). It was tested and showed an excellent performance in terms of computational efficiency working with high resolution DEMs (Lamb et al. 2009). It utilizes full-momentum shallow water equation on regular grid, utilising graphical processing units (GPU) capabilities, which makes the computation fast (Néelz and Pender 2009). In addition, this tool is supplied by a built-in GIS interface for convenient mapping.

Unlike LISFLOOD-FP and JFLOW, The Parallel Raster Inundation Model (PRIMo) model solves full-momentum shallow water equation on upscaled grid, which can be of different size than the input raster dataset. Meaning, e.g. the topographic data can be of 5 m resolution, while the mesh cell size can be any larger (>5 m). This can drastically decrease the computation time, while preserving high accuracy. Moreover, PRIMo allows for subcritical, supercritical and transitional flows because of the approximate Riemann solver used to estimate fluxes (Sanders and Schubert, 2019).

There are, however, some significant weaknesses of all 2D models: most importantly, they require much longer computational time comparing to 1D and combined 1D/2D models. This difference would depend on the number of cells within the domain and water volume. At the same time some simplified models (i.e. LISFLOOD-FP) are faster than conventional 2D codes, as they are based on inertial formulation of the shallow water equation and have been tested on large and continental scales (see above). Yet, the factor of computational capacity and data availability may pose the main source of the limitations for the users.

### **1.5. Flood modelling: recent advances and further steps**

Future climatic changes and shifts in flood risk towards the increase in frequency and severity of the events triggers the community to develop, test and implement updated modelling methods in order to reduce damages. Among the fastest developing empirical

methods for flood modelling is remote sensing (Schumann et al. 2009). The overall quality of the images (SAR) and improved timing of the acquisition plays a great role in flood forecasting and monitoring. The integration of remote sensing into flood forecasting have gained a large attention in recent years, however it requires a further improvement for streamflow predictions (Li et al. 2016). Satellite data is processed using significantly faster computation capacity via cloud computing (Morsy et al. 2018). In order to reduce the limitations related to hydrological data quality acquired from satellite images, a new generation Surface Water Ocean Topography (SWOT) mission is expected to be launched in 2020 (Biancamaria et al. 2016). Moreover, machine learning and deep learning are now extensively used for the remote sensing image processing and classification, which allows for more efficient and accurate flood mapping (Lamovec et al. 2013; Schnebele and Cervone 2013; Lim and Lee 2018). There is a clear trend in increasing use of remote sensing in not only flood modelling but also providing necessary data such as Shuttle Topography Radar Mission (SRTM) and Light Detection and Ranging (LiDAR) DEM. (Teng et al. 2017).

Regarding hydrodynamic models, recent advances in computational resources and availability of high-resolution (30 m or higher) large-scale datasets (Yamazaki et al. 2017) drive the tendency on development and application of state-of-art hydrodynamic numerical models. Each new model or its updated version has target applications. Simple 1D codes have been applied to calculate the discharge through cross-sections and are still widely applied on specific case studies. The overview above showed, that nowadays, most commonly used methods to map floods are combined 1D/2D or fully 2D codes of different complexity. The model choice is commonly justified by data availability, computation capacity and access to specific modelling software. Numerous studies in recent years utilise fully 2D codes, which provide a better overlook on flow parameters (water depth, flow velocities, inundation extent) and their spatial distribution (Shustikova et al. 2019). Moreover, 2D codes allow for river system dynamic tracking, which is largely unavailable in combined 1D/2D models, due to architecture of one-directional links between channel and floodplain. While 2D codes are able to capture flow and backwater effects between channel and floodplains.

Each modelling approach discussed above has their own uncertainties associated with input data or modelling techniques. Identifying and quantifying uncertainties is a fundamental component of flood hazard modelling. Further studies should focus on the reduction of uncertainties and finding best solutions.

Regarding computation efficiency, as shown above, low-dimensional models require much less time for simulations, whereas the most time-consuming are full-momentum models. This, and data availability play a great role in the models application on large scale. In the meantime, it has been proved that cloud computing and GPU-parallelisation significantly increase the use of 2D codes not only for local studies but for very large areas (catchment and continental scales). The integration of one method into

another may be greatly beneficial in flood modelling, for instance applying updated techniques in terrain data acquisition (LiDAR) would provide much improved input into hydrodynamic and DEM-based models. Therefore, we may expect even greater use of 2D schemes in large-scale flood modelling.

Building spatially complete and accurate flood maps is a crucial component in flood risk management and compliance with national and international laws and regulations. To sum up, all mentioned models have their application suitability, the codes have their strength and weaknesses. The approach selection is a matter of each specific case and requirements skills of the modeller and should be considered with great care. The subsequent chapters will provide a closer look into the testing and analysing the performance of different modelling techniques (software), which have a potential to be applied on large-scale studies.

### **1.6. Research questions addressed in this Dissertation**

The research questions addressed in the Dissertation are:

1. How do two-dimensional hydrodynamic models with different complexity contribute to flood hazard mapping with a specific focus on areas with complex topography? What is their potential relative to large-scale studies?

We focus on the testing of two models, namely the 2D full-momentum HEC-RAS and raster-based LISFLOOD-FP, we apply them for modelling the inundation event which occurred on the Secchia River (Italy) in January 2014. During the event, the morphologic complexity of the terrain had a pivotal impact on the inundation dynamics, therefore we tested the fully-2D schematization of both models, which differ in their governing equations and mesh representation, to see how these elements influence the accuracy of the outcomes as well as the computational efficiency (i.e. runtime).

2. What is the potential of raster-based 2D models for simulating inundations across large geographical areas characterized by heavily anthropogenically modified terrain? What is the impact of terrain pre-processing and resolution under such circumstances?

Here we look into application of fully-2D LISFLOOD-FP to the Po River flooding event that occurred in October 2000. A complex network of main and minor embankments that protect floodplains along 350 km river reach pose a great challenge for modellers, therefore we apply various techniques in DEM pre-processing and consider different horizontal resolutions (i.e. 30, 50, 100 m). This helps to identify the configuration that would be able to correctly depict water extent, local flow velocities and water surface elevations, and at the same time it would be computationally efficient.

3. Concerning a new levee breaching extension for LISFLOOD-FP model, what are its main advantages and potential?

We develop and test an additional extension to LISFLOOD-FP model, which allows for levee breaching in one or multiple locations, pre-defined by the user. We analyse the performance of the tool on a synthetic case study, as well as for two historic inundation events of different magnitude, that occurred in Italy in 1951 and 2014. We then discuss the potential of the new extension for the application across different scales and geographical regions.

# Chapter 2. Comparing 2D capabilities of HEC-RAS and LISFLOOD-FP on complex topography

## 2.1. Introduction

Recent studies suggest using fully 2D models with high level of details in order to avoid uncertainties and limitations coming from the incorrect interpretation of flood dynamics and unrealistic reproductions of the terrain topography (Morsy et al. 2018). Some studies, point out that for the large-scale studies, coarser resolution (i.e. 50 m) is an optimum between the accuracy and computational expenses for 2D simulations (Savage et al. 2016). Using fully 2D codes can, however, be difficult, as most areas are not covered by the high-resolution terrain datasets (LiDAR surveys) that such modelling requires. In addition, another evident constraint of using fully 2D codes lies in their higher computational burden relative to simplified combined 1D/2D codes (Apel et al. 2009; Falter et al. 2013; Dimitriadis et al. 2016). Yet, the tendency to run high-resolution global and regional flood scenarios is increasing (Falter et al. 2013; Sampson et al. 2015; Savage et al. 2016; Schumann et al. 2016, 2016). Furthermore, with increasing computational capacity, parallelization techniques and affordable access to cloud computing services, the utilisation of 2D codes in combination with high-resolution DEMs becomes more and more viable for hydraulic engineers and researchers (Morsy et al. 2018). Moreover, the 20x and 100x speed-ups gained by executing codes on graphical processing units (GPU) hardware comparing

to central processing unit (CPU) clusters show the potential in applying high-resolution flood models over large areas (Vacondio et al. 2014; Morsy et al. 2018).

Building on the existing literature, our study aims at further deepening our knowledge and understanding of the potential and capabilities of different types of 2D inundation models in the context of flood hazard assessment and mapping. In particular, our study compares two models, the well-known LISFLOOD-FP (Horritt and Bates 2002) and the recently launched 2D version (release 5.0.3) of Hydrologic Engineering Center-River Analysis System (HEC-RAS) model. As mentioned above, LISFLOOD-FP is a raster-based 2D model based on inertial formulation of the shallow-water equations, while HEC-RAS is a widespread modelling tool for hydraulic engineers that can be used for a large spectrum of applications and deploy different schematization complexities, and, in more recent releases, solves the full-momentum 2D equations.

A previous study performed by Horritt and Bates (2002) looked into differences in terms of flood extent for a 2D diffusion-wave LISFLOOD-FP model, a 1D HEC-RAS model and a 2D finite-element TELEMAC 2D model. They identified that HEC-RAS and TELEMAC 2D are different from LISFLOOD-FP because of their different response to friction coefficients used in calibration (Horritt and Bates 2002). It is important to point out, that the study of (Horritt and Bates 2002) is based on the older version of the models. For instance, HEC-RAS has been improved and is now used not only for 1D but also for fully 2D simulations with additional advantages of implying fully momentum shallow water equation on high resolution DEMs with unstructured grid. LISFLOOD-FP has also been updated from a diffusion wave to inertial formulation of the shallow water equation and now uses an adaptive time step, which ensures numerical stability of the code.

LISFLOOD-FP and HEC-RAS codes are governed not only by different schemes, but mesh representations, capabilities and input data requirements, and hence a thorough comparison is needed to better understand their advantages and limitations relative to topographical complexity, inundation dynamics and data availability of the codes updated versions. Regional and continental applications of LISFLOOD-FP are already a reality (Alfieri et al. 2014; Schumann et al. 2016; Sampson et al. 2015), while such applications can be envisaged in the near future for fully 2D HEC-RAS due to the rapid expansion of computational means and strategies cited above. For instance, a recent study by Liu et al. (2019) compared the 1D and 2D modules of HEC-RAS and LISFLOOD-FP where the channel flow is linked to the floodplain by lateral structures using a uniform grid resolution of 30 m. They concluded that the 2D models showed slightly better results than 1D. It is crucial to remember, that small and big changes made to the codes together with emerging accuracy of LiDAR data may drastically affect models' performance and results. Therefore, in this study we focus on the newest versions of the codes and investigate the advantages and disadvantages and their correlation with the DEM resolution for floodplain modelling.

This study aims at quantitatively highlighting differences and similarities in terms of accuracy of representation of inundation processes within heterogeneous floodplains and computational efficiency between the models with regard to different grid and terrain resolutions. We focused our study on such aspects as the capabilities and accuracy of 2D models of different complexity to capture flood extent and water depth in areas with complex topography. Additionally, we discuss model limitations in the context of future large-scale applications of detailed fully 2D models.

## 2.2. Tools and study scope

### 2.2.1. HEC-RAS (5.0.3)

HEC-RAS (5.0.3) was developed to perform fully 2D computations, and solves both the 2D Saint Venant equations and the 2D Diffusion Wave equations through an implicit finite volume scheme. The selection of the equation depends on the study case (dam breach, wave propagation analysis, existence of multiple hydraulic structures within the area) (Brunner 2016). Previous studies done on benchmarking of the codes with different physical complexity showed that, in cases where subcritical flow is unlikely (gradually varied flow), simpler codes perform comparably well in terms of water depth and velocity (Neal et al. 2012b; Almeida and Bates 2013). In order to utilise more stable numerical solutions and reduce the computation time for the current case, we selected the 2D Diffusion Wave solver. It identifies the barotropic and bottom friction terms as prevailing.

$$\frac{n^2|V|V}{(R(H))^{4/3}} = -\nabla H \quad (6)$$

The above equation can be further rearranged by dividing both sides by the square root of their norm,

$$V = \frac{-(R(H))^{2/3}}{n} \frac{\nabla H}{|\nabla H|^{1/2}} \quad (7)$$

Where  $V$  is the velocity vector,  $R$  is the hydraulic radius and  $-\nabla H$  is the surface elevation gradient,  $n$  is Manning's  $n$ .

The differential form of the Diffusion Wave Approximation of the Shallow Water equation can be obtained by combining the diffusion wave equation in the mass conservation equation,

$$\frac{\partial H}{\partial t} - \nabla \cdot \beta \nabla H + q = 0 \quad (8)$$

Where,

$$\beta = \frac{(R(H))^{5/3}}{n|\nabla H|^{1/2}} \quad (9)$$

(Brunner 2016).

Mesh computation is done automatically within the 2D flow areas and meshes can be structured (i.e. regular connectivity) or unstructured (irregular connectivity). The selection of the grid type (structured/unstructured) depends on the terrain topography and data availability, enabling the user to adopt reduced mesh resolution in more homogenous areas and a highly detailed description along critical terrain features such as embankments or levees. Additionally, the model gives an opportunity to reduce the computation time by implementing a coarser grid on fine topographic details through a so-called subgrid bathymetry approach (Figure 9) (Brunner 2016).

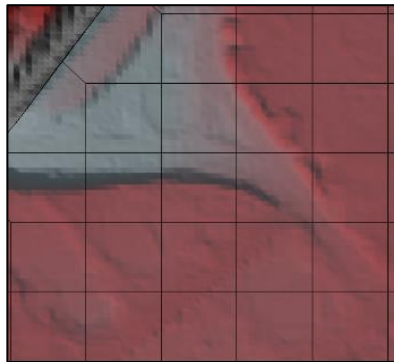


Figure 9. RasMapper representation of 2 m subgrid DEM and 25 m mesh cell size of HEC-RAS 2D (adapted from Brunner (2016)).

For instance, the DEM resolution might be 2 meters, while the mesh cell size is 25 m (see Figure 9). During a pre-processing step, hydraulic radius, volume and cross-sectional data are collected for each mesh cell using the finer resolution data and stored in property tables (a function for cell face area ( $A$ ) and water surface elevation ( $H$ ); see Figure 10). The subgrid approach allows the computation of more detailed property tables for larger mesh cell sizes.

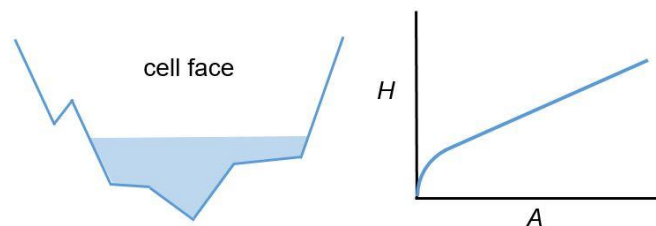


Figure 10. Cell face terrain data (left) and schematic representation of  $A$  (area) –  $H$  (elevation) relationship reproduced with the Property Table (right) (adapted from Brunner (2016)).

### 2.2.2. LISFLOOD-FP

The raster-based LISFLOOD-FP model used here is employed in 2D mode and solves an inertial formulation of the shallow-water equations in explicit form through a finite difference scheme (Bates et al. 2010; Savage et al. 2016). The model further simplifies the computation by decoupling flows in the  $x$  and  $y$  directions and treating the 2D problem as a series of 1D calculations through the cell face boundaries. Therefore, the water flow through each cell face is calculated as:

$$q_{t+\Delta t} = \frac{q_t - gh_t \Delta t \frac{\Delta(h_t+z)}{\Delta x}}{(1+gh_t \Delta t n^2 q_t/h_t^{10/3})} \quad (10)$$

Where,  $q_{t+\Delta t}$  is a unit flow at the next time step  $t$ ,  $g$  is gravitational acceleration,  $h$  is depth,  $n$  is a Manning's roughness coefficient,  $\Delta$  is the cell resolution,  $z$  is cell elevation,  $h_t$  is the difference between highest bed elevation and highest water surface elevation between two cells (Savage et al. 2016; Bates et al. 2010).

The discharge through the four faces of each cell is then used to update the water depth in each cell at each time step:

$$\frac{\Delta h^{i,j}}{\Delta t} = \frac{Q_x^{i-1,j} - Q_x^{i,j} + Q_y^{i,j-1} - Q_y^{i,j}}{\Delta x^2} \quad (11)$$

Where,  $i$  and  $j$  are the coordinates of a cell (Coulthard et al. 2013).

In order to secure the model stability we used an adaptive time step based on the Courant-Friedrichs-Lewy (CFL) condition which is estimated as (Bates et al. 2010):

$$\Delta t_{max} = \alpha \frac{\Delta x}{\sqrt{gh_t}} \quad (12)$$

Where  $\alpha$  is a coefficient ranging from 0.3 to 0.7, which ensures the numerical stability (Coulthard et al. 2013).

Despite the governing equations used to compute the flow between cells, another important distinction between the two models is the way in which the codes treat topographic data. Differently from HEC-RAS, mesh size in LISFLOOD-FP is forced by the resolution of the input DEM data and cannot be further manipulated. There is not an option to include subgrid (see details above) terrain in the 2D computations with larger mesh sizes, meaning the mesh face cross-section profile has a rectangular shape.

### 2.2.3. Objective of the study

This study tests and compares the models on an inundation event that occurred on the 19<sup>th</sup> January, 2014 in the dike-protected floodplain of the Secchia River (a right bank tributary of the Po River), Northern Italy. We compare HEC-RAS with LISFLOOD-FP using

various grid sizes 25, 50 and 100 m generated from a LiDAR DEM of 1 m resolution. Moreover, along with the resampled DEMs we use the subgrid capabilities of HEC-RAS by applying subgrid terrain of 1 m resolution within the 25, 50 and 100 m sized meshes.

We explicitly focus on the fully 2D formulations for both models addressing the representation of the floodplain wave dynamics, i.e. no 1D component is included in the simulations (no channel flow simulated). This is done in order to see the difference in the codes' ability to simulate inundation propagating over complex topography and an initially dry floodplain.

## 2.3. Study event and data used, models setup and calibration

### 2.3.1. Study event and data

The event was characterized by a levee breach and consequent flooding of over 50 km<sup>2</sup> of the plain behind the dike within 48 hours causing significant population displacement, one death and economic losses in excess of 400 million Euro (D'Alpaos et al. 2014; Carisi et al. 2018). It occurred around 6:00 am on January 19 when a part of the levee in the right bank of Secchia River collapsed (see Figure 11). Although the water levels in the river did not exceed the designed embankment crest height, right after the breach the crest lowered by about 1 m compared to the water elevation in the Secchia River. The conclusion driven from the post-event analysis is that the reason for the levee collapse was the activity of burrowing animals in the area (Vacondio et al. 2016; Orlandini et al. 2015).

Over the event the breach width reached nearly 80 m (Figure 12) and the inflow water volume that penetrated the floodplain reaching the municipalities of Modena, Bastiglia and Bomporto was estimated in 38.7·10<sup>6</sup> m<sup>3</sup> (Figure 13). Previous studies showed that linear terrain irregularities strongly affected the flooding dynamics (Castellarin et al. 2014; Hailemariam et al. 2014; Carisi et al. 2018; Domeneghetti et al. 2015; Domeneghetti 2014). The water flowed northward for nearly 16 km, where it started accumulating due to the presence of an embankment (see Strada di Cavezzo in Figure 11).

Figure 11 illustrates the study area outline, which is identified by the embankments from east and west and the roads and Strada di Cavezzo from the north. As can be seen from the figure, once the inundation reached Bastiglia, it turned in a south-westerly direction and further reached the municipality of Bomporto from the south-west; Bomporto was completely flooded at about 11:00 AM on January 20th. Figure 12 shows the place of the breach and inundated areas in Bomporto and Bastiglia.

## Chapter 2. Comparing 2D capabilities of HEC-RAS and LISFLOOD-FP on complex topography

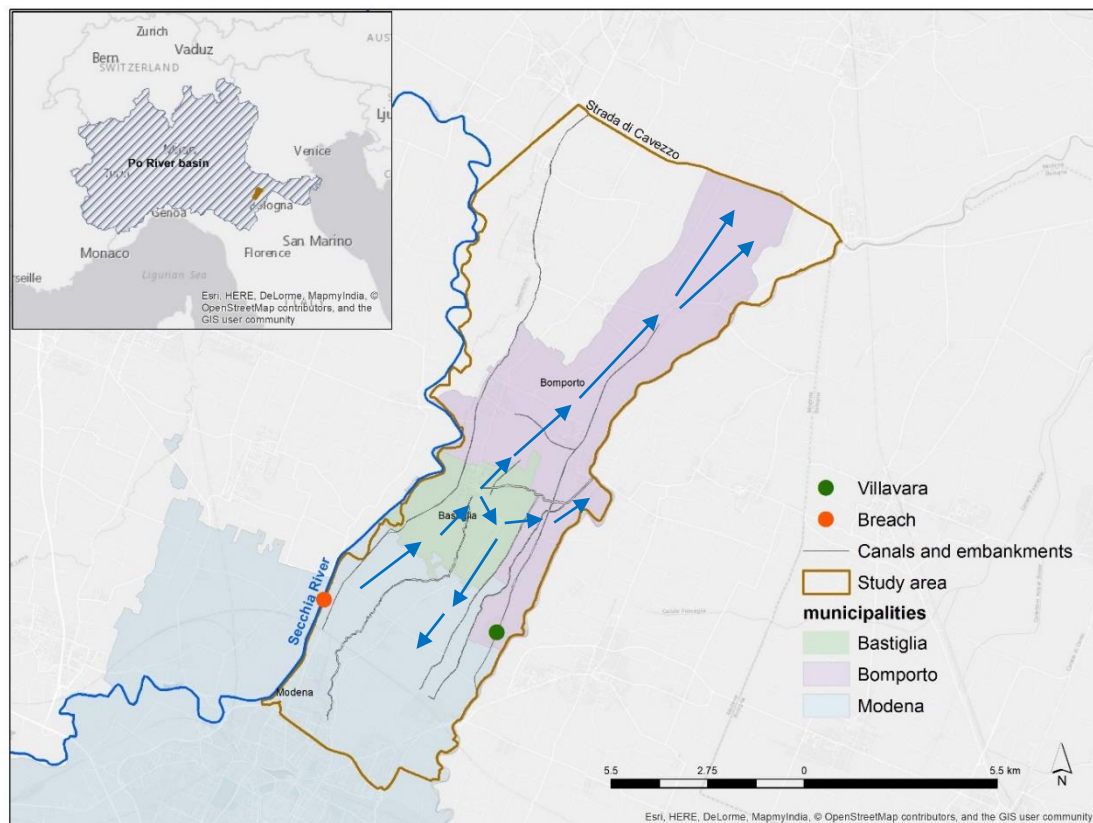


Figure 11. Breach location and flow direction during the event.



Figure 12. Images of the January 2014 Secchia River flooding event. Upper left corner is the breach location. Upper right shows the inundated houses and fields in the affected area. Two lower images show the inundation in Bomporto. Taken from (Raggini 2016).

Due to the system of linear terrain features such as embankments and channels (see Figure 11), the inundation dynamics followed depressions in the relief. After overtopping the embankment near Villavara eastwards, the water moved to the north, direction Bomporto. At the same time, a channel, which divides the study area in half (the line following from Bastiglia southern direction to Modena), filled up with water and contributed to the inundation of Bomporto from the west (see Figure 11). Post event field surveys made by the local authorities together with other publicly available data (photographs, videos and Google Earth images) provided us with the water marks (maximum water depths) at certain points. The study of Horritt et al. (2010a) shows that the post-event collection and evaluation of the water marks and wreck marks is not always matches the actual maximum values. Field measurement methods and their interpretation done by surveying groups, approximations of the elevation of water marks acquired from images may produce uncertainties. Horritt et al. (2010a) reports that accuracy range in such estimations is likely to be up to 0.5 m, which could be a potential source of errors. In order to check the liability of the observed water marks, we plotted them in relation to the 1 m LiDAR DEM in order to see if there are water surface elevation outliers (points in closer vicinity with the large difference in depth). We looked at their weighted average and observations difference and removed the outliers ( $>0.5$  m). As the result we further used 46 water mark points to validate the maximum simulated water depth. We, however, left the points in very close distance from each other ( $<50$  m) in order to look at the models' performance with different subgrid configurations.

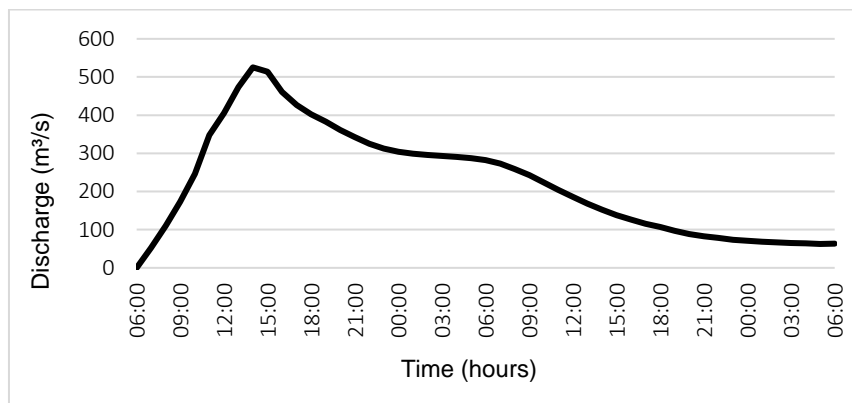


Figure 13. Outflowing discharge at the levee breach point over time (adopted from D'Alpaos et al. 2014).

Official reports recorded vast damage in the small town of Bomporto (Carisi et al. 2018). During the event the area within the embankment was completely flooded (Figure 14). We selected the area surrounding this particular town due to its complex and highly anthropogenically altered terrain (e.g. minor levees, embankments, irrigation and drainage channel networks, etc.) to test how the models were able to reproduce the propagation of inundated extent in such topography. The water marks are located within the populated

areas; therefore they are concentrated within the affected settlements of Bastiglia and Bomporto and the close vicinity around them. Fewtrell et al. (2008) in their study explicitly showed that the 2D models behaviour is strongly affected by the heterogeneity of the urban fabric and requires a very fine mesh to represent the building dimensions. Thus, we are particularly interested how the selected models will perform in built-up zones. We used these data to validate the models by comparing them to maximum water depths observed during the event (Carisi et al. 2018). The study by Carisi et al. (2018) reproduced the Secchia event simulating the inundation dynamic.

The simulations of Carisi et al. (2018) were based on the higher resolution 1 m LiDAR DEM with unstructured mesh, whose faces ranged in size from 1 to 200 m in more homogenous zones. The linear terrain irregularities were explicitly represented. The official reports done on the post-event field data collection and simulations made possible to reconstruct the flood extent as detailed as possible (D'Alpaos et al. 2014). The simulations showed a high correspondence with the maximum flood extent records (up to 0.9 in terms of CSI, Eq.13) (Carisi et al. 2018).

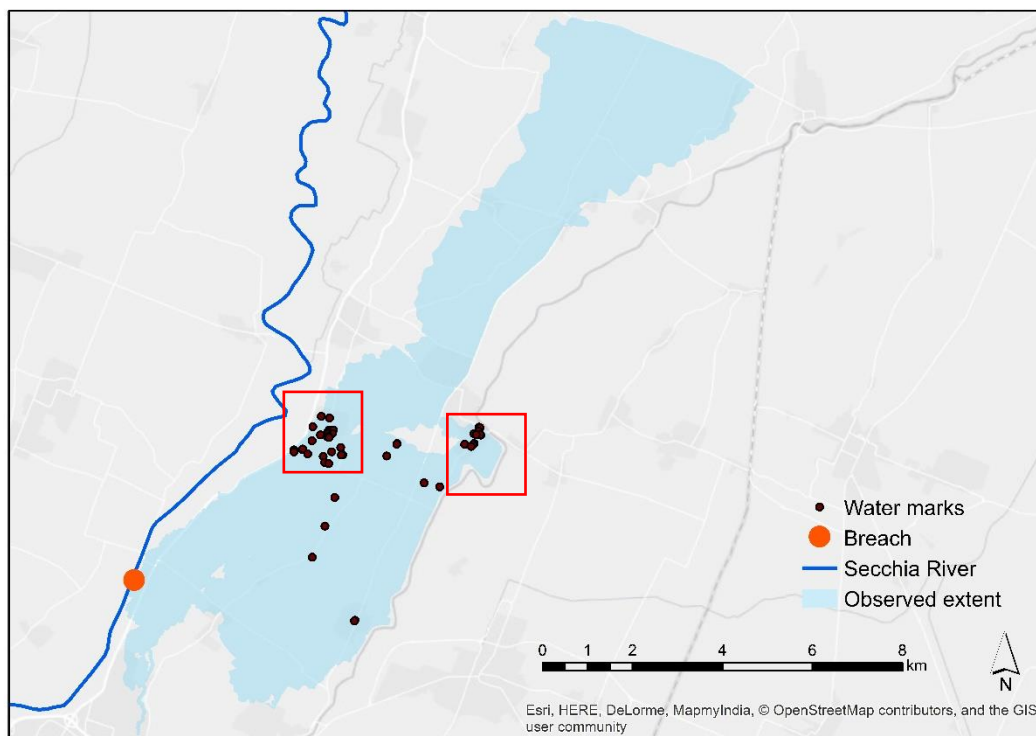


Figure 14. Observed flood extent, hotspot focus areas (red boxes) and water marks (control points). Left red box captures the inundation in Bastiglia; right red box shows the inundation extent in Bomporto.

### 2.3.2. Models configuration and setup

Previous modelling studies of the January 2014 inundation event showed that the topography of the area strongly controls the model performance (Vacondio et al. 2016; Carisi et al. 2018).

As our interest is to show how the models behave on large scales, we considered downscaling the 1 m LIDAR DEM to 25, 50 and 100 meters by taking the mean of the pixels' value. The vertical accuracy of the bare earth DEM is  $\pm 0.15$  m (Geoportale Nazionale 2017). The study of Savage et al. (2016) on regional flood modelling showed that resolution coarser than 100 m decreases the reliability of the model's outcomes, therefore, we avoided using lower resolutions. The same study showed that probabilistic flood mapping does not benefit much from resolution higher than 50 m. Nevertheless, as our study is specifically focused on heterogeneous topography, we intentionally included a 25 m DEM in order to have a more profound comparison of the two different models.

The flow leaving the breach was estimated based on the difference between observed discharge hydrographs 200 m upstream and 200 m downstream along the reach (see Figure 13) (Vacondio et al. 2016).

Both models were constructed adopting the same hydraulic loads. The upstream boundary condition was represented by the discharge flowing through the levee breach and it was fixed in each simulation as a point (a pixel) located at the failure location. The breach width was set in all simulations equal to 100 m, simultaneously involving 1, 2 and 4 pixels in the simulations using 100 m, 50 m and 25 m resolutions, in this order. The inflow hydrograph was represented by the values retrieved from the studies of Carisi et al. (2018), Vacondio et al. (2016) and Orlandini et al. (2015). In order to avoid possible errors coming from different widths of the upstream boundary (levee breach breadth), we insured that the water marks are located further downstream from the inflow location.

We referred to the CORINE Land Cover (European Environment Agency 2007) and OpenStreetMap (Contributors OSM 2012) data sets for classifying land use in the study area, which we represented in the models using spatially varying roughness coefficients. In particular, we adopted a subdivision of the study area into 2 main classes: built up (i.e. urban and industrial zones) and rural (i.e. all other land-use types mostly represented as agricultural fields) areas.

Fully 2D HEC-RAS was used and tested with and without its subgrid function capability with structured mesh cell sizes of 25x25, 50x50 and 100x100 m based on the 1 m LiDAR DEM. Structured mesh selection significantly decreases the model setup time and does not require additional data (i.e. linear infrastructure outlines) as is the case for configuration of an unstructured mesh. This is of a high importance for large-scale simulations, where such details might be unavailable or their implementation would require significant effort.

Table 2. Simulation configurations

Mesh Resolution	LISFLOOD	HEC RAS 1 m subgrid terrain resolution	HEC RAS 25/50/100 m subgrid terrain resolution
25	L25	HR25_1	HR25_25
50	L50	HR50_1	HR50_50
100	L100	HR100_1	HR100_100

The meshes were also used with the corresponding aggregated DEM (25x25 mesh with 25 m DEM resolution, 50x50 mesh with 50 m DEM resolution, 100x100 mesh with 100 m DEM resolution). Overall, we apply 9 mesh/terrain configurations as indicated in Table 2.

### 2.3.3. Models calibration

The models were calibrated using roughness coefficients for HEC-RAS and LISFLOOD-FP at 25 m resolution. We looked into previous research and post-event surveys done to describe and analyse this event. In particular, we considered the publication of Carisi et al. (2018) and the accurate reconstruction of the flood extent reported therein. We compared the maximum flood extent resulting from the models with the reference flood extent from Carisi et al. (2018) by means of a well-known Critical Success Index (CSI) method to compare binary maps (wet and dry areas) of the simulated and observed extents using a performance measure (Schumann et al. 2009):

$$CSI = \frac{A}{A+B+C} * 100 \quad (13)$$

Where  $A$  is the area correctly predicted as flooded (wet in both observed and simulated),  $B$  is the area overpredicting the extent (dry in observed but wet in simulated) and  $C$  is the underpredicted flood area (wet in observed but dry in simulated). CSI defined in (Eq. 13) varies between 0 and 100%, where 100% corresponds to a perfect match between the modelled extent and the reference inundation map (Horritt and Bates 2002).

Calibration consisted of varying the Manning's roughness coefficient,  $n$ , of rural areas from 0.03 to 0.2  $m^{-1/3}s$ , by 0.005  $m^{-1/3}s$  increments, while keeping  $n$  of urbanised zones constant (0.3  $m^{-1/3}s$ , (Syme 2008)) and referring to the land-use description resulting from CORINE Land Cover data (European Environment Agency 2007) and OpenStreetMap (2012). So, for each simulation we would use one roughness coefficient for rural and one for urban areas. LISFLOOD-FP resulted in the highest CSI value (81%) for a floodplain roughness coefficient  $n = 0.155 m^{-1/3}s$ ; with CSI varying between 73% for  $n = 0.030 m^{-1/3}s$  and 77% for  $n = 0.200 m^{-1/3}s$ . HEC-RAS showed similar performance, maximum value is equal to 78% at  $n = 0.195 m^{-1/3}s$ , however CSI values plateau at 78% for  $n$  values larger than

$0.185 \text{ m}^{-1/3}\text{s}$ . For the further analysis we selected the value of  $0.195 \text{ m}^{-1/3}$ . These values ( $0.195 \text{ m}^{-1/3}$  for rural and  $0.3 \text{ m}^{-1/3}$  for urban areas) do not reflect the actual vegetation/soil cover in the area, they are aimed at compensating for the possible errors coming from the overall flooding extent used to calibrate the model and possible limitations related to the inability of the terrain to capture the linear features, which played a crucial role in routing the flow. Also, we calibrated both models at 50 m and 100 m resolution, obtaining optimal values of the calibration parameters that differed from the optimal values at 25 m resolution by less than 1%. Therefore, we decided to use uniform optimal values for all resolutions.

Both models were validated against 46 water marks (see e.g. Figure 14) for which the maximum water depth (m) was surveyed in the event aftermath (water marks, post-event surveys, interviews and geolocating the marks using aerial and ground photographs). Dry simulated points were given zero value. Comparison was performed by means of Root Mean Square Error (RMSE). All simulations were performed on the 4 cores with the Intel Core i7 3.60 GHz CPU, 64 GB RAM.

## 2.4. Results

From Figure 15 we can see that the overall performance in terms of inundation extent (i.e. CSI values defined as in (13)) of LISFLOOD-FP is slightly better than HEC-RAS. The 25 m LISFLOOD-FP simulation (L25) was able to correctly simulate 81% of the flooding extent, while the 50 m LISFLOOD-FP simulation (L50) was as good as the HEC-RAS simulation with 1 m subgrid terrain (78%) (Table 3). All other configurations produced almost identical results, with a CSI value of  $\sim 77\%$ . However, the spatial pattern of the flooded areas differs for all configurations (Figure 15).

Together with the analysis of the overall inundation extent, the performance of each model was scrupulously assessed relative to specific areas in the towns of Bomporto and Bastiglia. Figure 14 illustrates the observed extent and the location of focus areas (red squares). From Figure 16 we can see that the LISFLOOD-FP model was able to correctly simulate the maximum flood extent in Bomporto for the fine resolution of 25 m, while with other LISFLOOD-FP resolutions the same results were not achieved. The red line in these maps demarcates the observed inundation extent, so we can see that the L25 configuration output is in good agreement with the observations (the flood propagated to the observed inundation boundary and covered all water marks).

The LISFLOOD-FP 50 m and 100 m simulations (L50 and L100) did not properly simulate the flood propagation in this area. The water marks display the accuracy of predicted water levels in relation to the observations. Figure 16 shows that the flood extent simulated by HEC-RAS for 25, 50 and 100 m mesh sizes with 1 m subgrid terrain was consistent with the observations, especially the larger meshes of 50 and 100 m.

Table 3. Critical Success Index (in %), inundation extent accuracy.

Mesh size[m]	LISFLOOD-FP	HEC-RAS 1 m subgrid	HEC-RAS 25/50/100 m subgrid
25	81	78	78
50	78	78	77
100	77	78	77

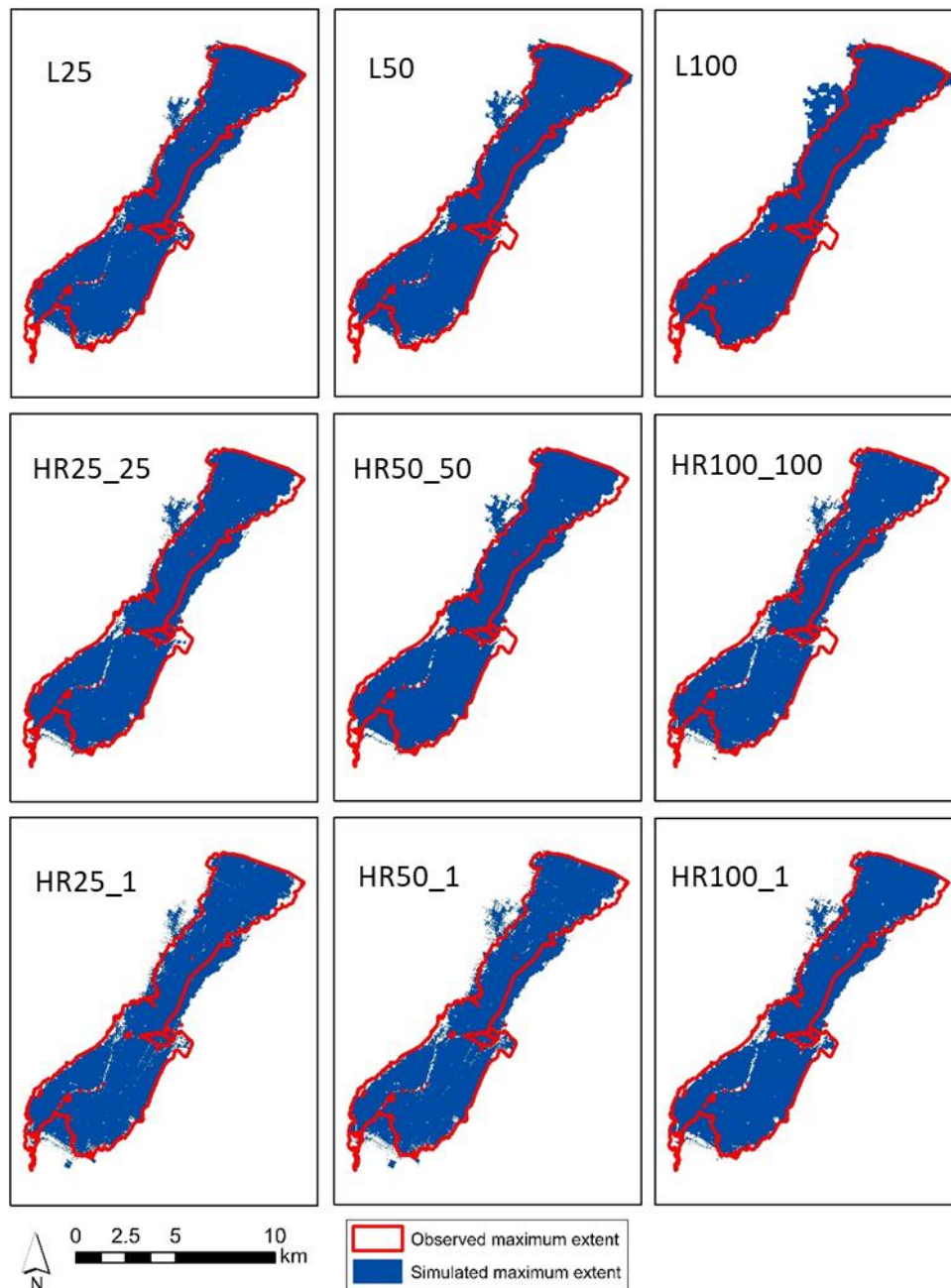


Figure 15. Overall simulated extent for all configurations (blue), compared to the observed extent (red outline)

The HEC-RAS models without subgrid terrain (HR25\_25, HR50\_50 and HR100\_100) were unable to simulate the flood wave propagation in the Bomporto focus area.

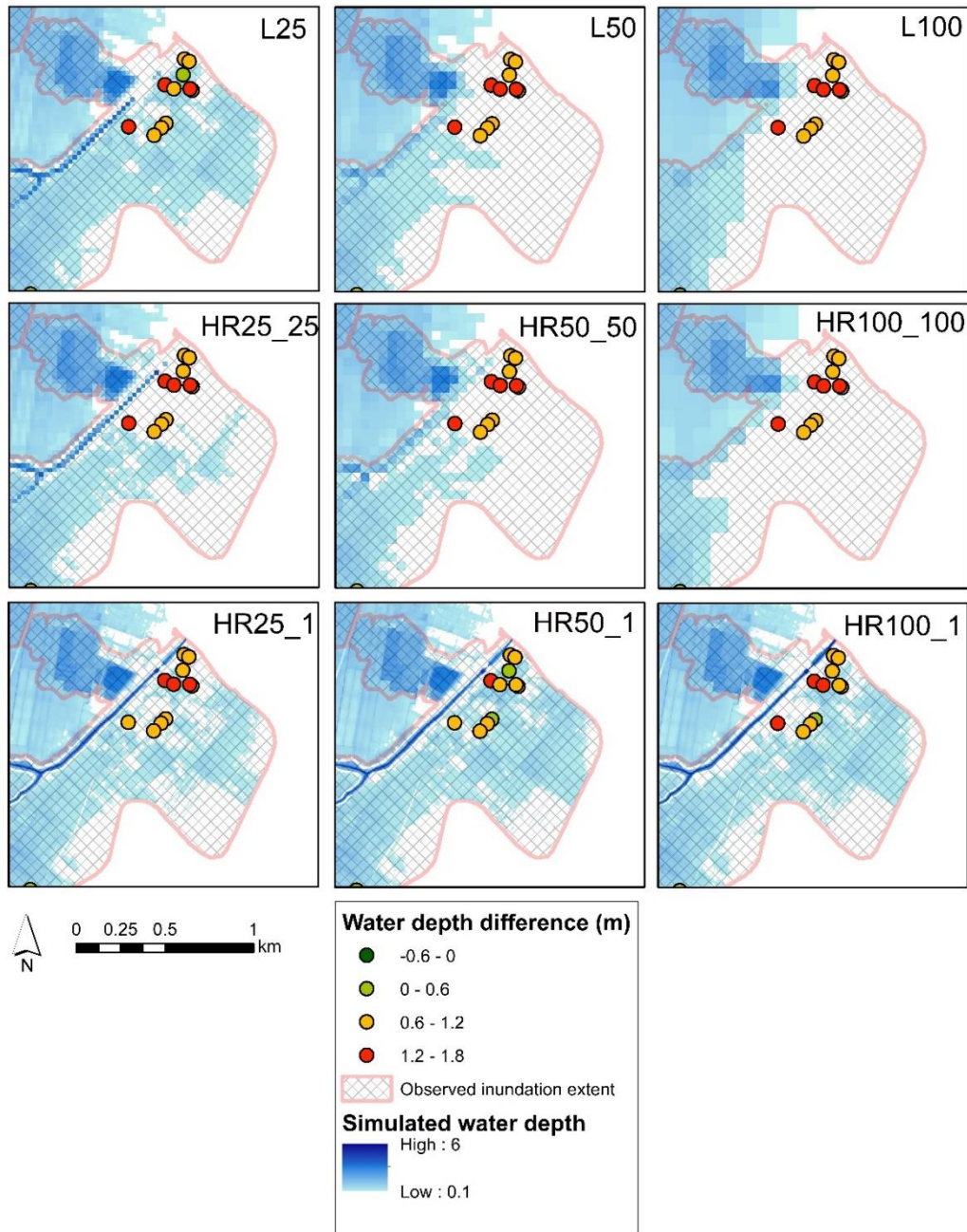


Figure 16. LISFLOOD-FP and HEC-RAS flood extent for different configurations at Bomporto (right red box in Figure 14). Water depth difference (m) between predicted and observed at water mark points.

As for the other focus area, from Figure 17 we can see that the flood extent in Bastiglia produced by all LISFLOOD-FP resolutions is in-line with the observed flood extent. The L25 configuration was more successful in reproducing the flood extent over the control areas, while the L50 and L100 models just slightly underestimate the flood

boundaries (see Figure 16 and Figure 17 ). HEC-RAS coarser grid simulations (25, 50 and 100 m subgrid), similar to LISFLOOD-FP (50 and 100 m), produce plausible results in terms of the inundation extent. The accuracy decreases with increasing mesh size. The HEC-RAS configurations using subgrid terrain of 1 m resolution struggle to produce a continuous inundation pattern, resulting in numerous dry islands.

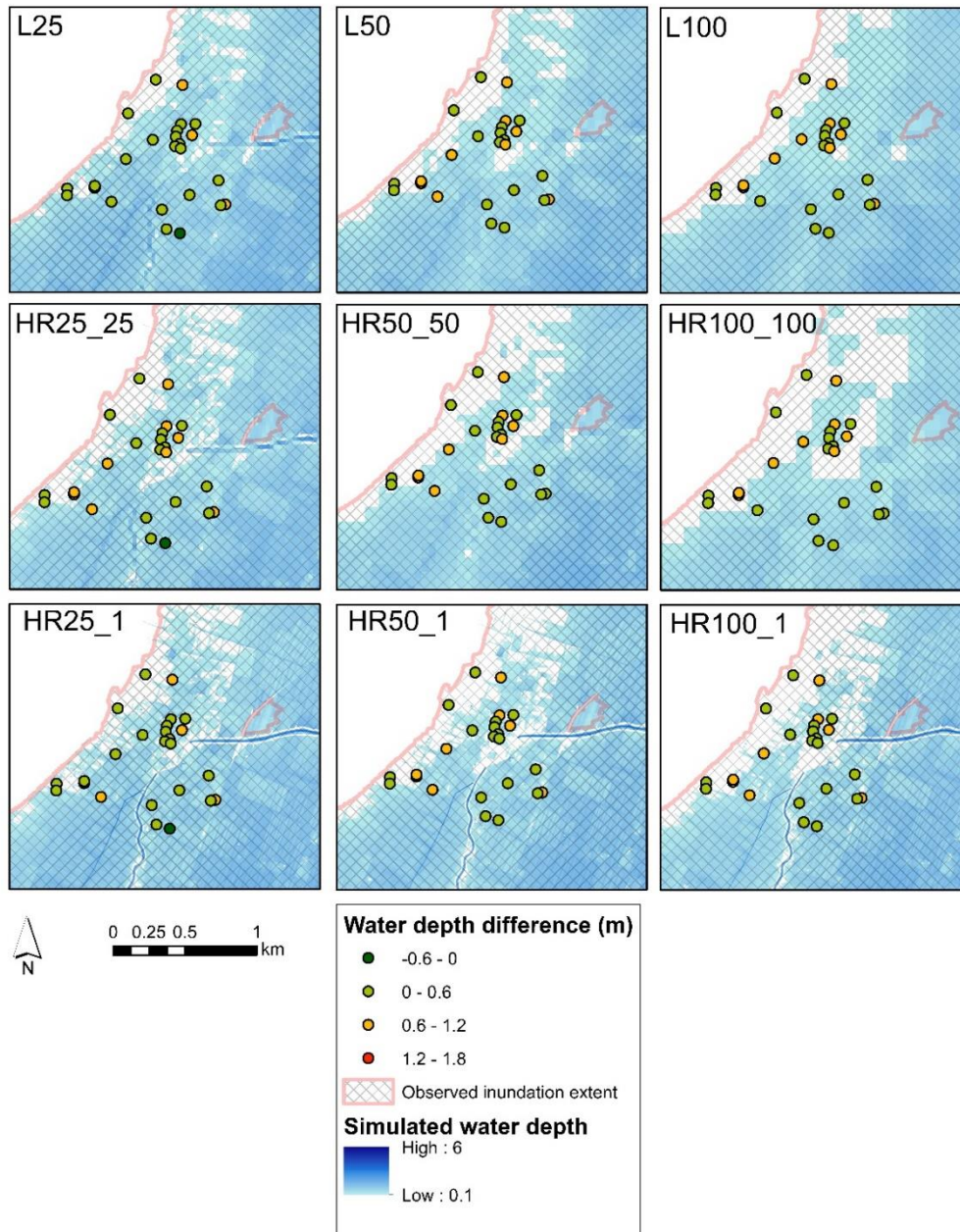


Figure 17. LISFLOOD-FP and HEC-RAS flood extent for different configurations at Bastiglia (left red box in Figure 14). Water depth difference (m) between predicted and observed at water marks.

Figures 16 and 17 display the water marks and the colour indicates on the level of absolute difference between simulated and surveyed maximum water levels through a red (underestimation) to dark green (overestimation) colour scale. The largest difference is

especially visible in Bomporto focus area (up to 1.8 meters), as most of the simulations did not succeed in inundating the town. While in Bastiglia such difference is less pronounced. There, the values vary between 0.1 m and 1.2 m. General tendency for all simulations is underestimation of the water depth values at water marks.

In addition, we compared observed and simulated maximum water levels using RMSE. Overall, the best results (see Table 4) are of L25 configuration (0.61m). Same performance was obtained from HEC50\_1 (0.62m). The results from L50 and L100 are similar to those gotten from HR25\_25, HR50\_50 and HR100\_100 (0.79-0.84m), while the other high-resolution subgrid terrain of HEC-RAS produced somewhat better outcomes 0.71m.

Table 4. RMSE [m] of the water depth at water marks

<b>Mesh size [m]</b>	<b>LISFLOOD-FP</b>	<b>HEC-RAS 1 m subgrid</b>	<b>HEC-RAS 25/50/100 m subgrid</b>
<b>25</b>	0.61	0.69	0.79
<b>50</b>	0.80	0.62	0.80
<b>100</b>	0.82	0.71	0.84

Another important factor to be considered in the mesh size and DEM resolution evaluation is the computation time. From Figure 18 we can see that in all simulations LISFLOOD-FP was significantly faster than HEC-RAS, no numerical instabilities reported. For instance, the 100 m resolution HEC-RAS simulation lasted about a minute, while the 25 m mesh size simulation with this model would take about 45 minutes (Figure 18).

LISFLOOD-FP was about 20 times faster than HEC-RAS for the same grids and time step (L50 was 1 min 20 sec computation time, HR50\_1 was 25 min computation time). HEC-RAS of 25 m resolution and 25 m subgrid terrain is faster than the same resolution with 25 m terrain, but this difference become less evident for large mesh. HEC-RAS of 100 m large mesh and 1 m subgrid resolution is 4 times slower than HR100\_100, it means that considering high performance (overall extent 78% accuracy and 0.71 m RMSE at water marks) HR100\_1 is the best choice in HEC-RAS simulations. When 1 m subgrid is implemented in HEC-RAS simulations, the model performs similarly in terms of flood extent (See Table 4), however the computation time can be drastically decreased by using large mesh (HR100\_1). L25 has shown best performance in terms of flood extent and water depth at selected control points, however it is 2 times slower than HR100\_1.

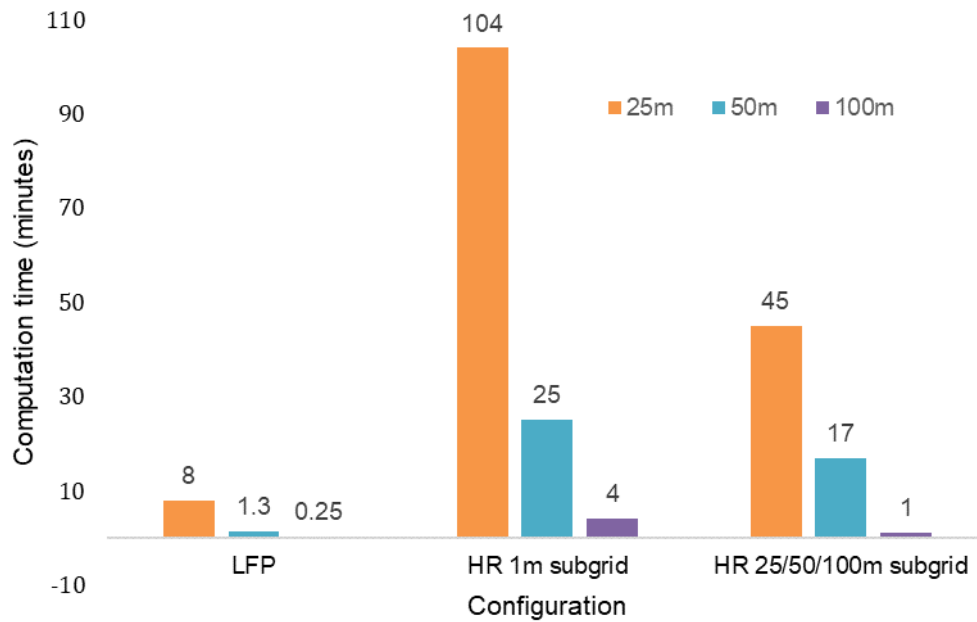


Figure 18. Approximate computation time of HEC-RAS and LISFLOOD-FP configurations.

## 2.5. Discussion

The two codes of different complexity and terrain resolution, used in this study, strongly affect the quality of the outputs. Diffusion wave model (HEC-RAS) and inertial formulation of the shallow water equation (LISFLOOD-FP) are distinct in different ways. The ability of HEC-RAS to include the subgrid bathymetry component makes it effective in terms of representation of topographic details by computing more informative property tables for each cell face. LISFLOOD in turn, operates with the rectangular mesh of the same resolution as the input terrain raster.

### 2.5.1. Performance comparison

As it was outlined in the Results section, the structured regular mesh of both models is able to reproduce the flooding event with sufficient correspondence with observations and capture the overall inundation extent and water depth marks at selected control points. The mesh size played a great role in the accuracy of the outputs of LISFLOOD-FP; the 25 m grid model performed somewhat better than coarser grids considering the inundation boundary. One of the main reasons for such performance is the ability of the finer resolution models to capture more terrain details and route the flow into the right direction considering depressions and the elevations of the relief. The flood extent of the 50 and 100 m models (L50 and L100, respectively) were virtually similar, differing by only 1% from each other in terms of the CSI. HEC-RAS, in turn had comparable results across the resolutions and subgrid terrain configurations considering flood extent in the whole study

area; nevertheless, compared to LISFLOOD-FP (L25), the CSI value is slightly less accurate. This is of specific importance for areas with complex topography. Overall extent differences between best performing L25 and the rest of configurations, however, are minimal. This can be explained by rather confined area, which is shaped by the embankments of the Secchia River from the west and another river from the east, moreover the northern boundary is also well-pronounced and acts as a barrier to the flood water preventing it propagating further north. Therefore, we suggest that the terrain configuration explains the similar performance of the models (77-78% accuracy, apart from L25 with 81% accuracy). This also confirms the previous findings that inundation extent over larger areas can be properly identified with the low-resolution datasets (in our case 50 or 100 m), with additional benefit of lower computational costs (Savage et al. 2016). Such findings can be relevant for areas with similar terrain configurations regardless geographical location. It is important to point out that CSI (spatially averaged performance measure) is not sensitive enough to inform about the resolution and local flow parameters, therefore it was necessary to additionally analyse the models' performance in selected spots in more details.

However, as predicted the behaviour of the models in the focus areas had diverse patterns. For instance, HR50\_1 and HR100\_1 were able to represent the inundation boundaries in Bomporto fairly well, unlike in Bastiglia (see Figure 16 and Figure 17). While LISFLOOD-FP was more accurate at high resolution of 25 m compared to 50 and 100 m. L25 performed strikingly better than HR25\_25 both overall and in the two focus areas (i.e. Bomporto and Bastiglia). We explicitly highlight such results, as L25 provided best outcomes in terms flood extent and water depth across all selected configurations (see Table 3 and Table 4). We suggest that this outcome of both models is strongly related to their ability to simulate floods in built-up areas with given resolution. It is known that the towns of Bomporto and Bastiglia are not only represented by urban fabric but also surrounded by a network of smaller channels and embankments, which in case of 2014 flood event played a crucial role in the inundation dynamics.

One of the similarities between both models is the performance of the 50 m and 100 m LISFLOOD-FP and HEC-RAS models when subgrid terrain resolutions are not considered for the latter code. For instance, by applying configurations L50 and HR50\_50 we attained rather comparable inundation patterns in Bastiglia (see Figure 17) and almost identical in Bomporto (see Figure 16).

The water mark errors evaluated in the current study show how models represented water depth spatially. A point that deserves attention is the vertical accuracy of the input and calibration data. As was discussed earlier, the vertical accuracy of the used LiDAR dataset ( $\pm 0.15$  m) and the observed data ( $\pm 0.5$  m), is a subject of uncertainties. Looking at the differences between observed and simulated water mark values, we may suggest that the RMSEs are within the input data error range. Despite eliminating the outliers, we cannot be 100% confident that the values perfectly match the reality. Therefore, here we treat the

results as a relative comparison between the two models rather than compare absolute observed and simulated values. In addition, the points also serve as an indicator to evaluate the simulations, where the water marks did not get inundated. Overall, in terms of RMSE HEC-RAS with 1 m subgrid terrain for all resolutions was better compared to coarser terrains (approx. 0.13 m difference in terms of RMSE between HEC-RAS 1 m subgrid and coarse subgrids, including LISFLOOD-FP simulations). The only exception is LISFLOOD-FP of 25 m resolution, which was comparable to high-detailed subgrid of HEC-RAS (RMSE error equal to 0.61 and 0.62 m correspondingly). We suggest that such performance can be reasoned by the fact that most of the points are located within rather short distance (up to 200 m) on heterogeneous terrain, meaning the water depth points varied by over 1 m. At Bomporto and Bastiglia focus areas, some points were located within short distance of 30-40 m, which was far denser than the resolution of the underlying terrains (50-100 m). Therefore, HEC-RAS on 1 m subgrid performed the best due to its ability to operate with highly-detailed terrain compared to other configurations with coarse subgrids (both, LISFLOOD-FP and HEC-RAS).

The differences in terms of computation time outlined in the Results section are crucial for instance for calibration and running Monte Carlo simulation scenarios, especially, if we intend to extrapolate this performance parameter to the larger-scale studies. Therefore, we may draw a suggestion, that flood mapping for geographically large areas can still be performed with the coarser grids (50 or 100 m) and produce reasonable results to identify the flood risk hotspots (areas with an increased flood risk compared to other areas in the region). Such hotspots can be then analysed using high-resolution datasets. In HEC-RAS configurations the use of high-resolution (1 m) subgrid outperforms those of the same resolution as size of the mesh (25, 50, 100 m). However, the computational costs for 1 m subgrid increases. The modeller should select among the two options in relation to the mesh size, when the mesh size is small (25 m) the difference in computation time is significant. On the other hand, when the mesh size is larger, the difference in terms of computation time among two becomes smaller. 1 m subgrid becomes more beneficial to be used in terms of computation time, as it additionally shows high performance.

Nevertheless, speaking of large-scale simulations, we expect that smaller areas complicated by highly heterogeneous terrain but with the potential for large socio-economic impacts (as it is in Bomporto) will still be misrepresented and wrongly estimated. As shown in the example of this study, the resolution of the topographic description is not the only key factor; another element of paramount importance is the ability of the model mesh/grid to correctly capture critical terrain features which determine the flood wave propagation. This aspect becomes particularly crucial when simulating floods over heavily anthropogenically altered floodplains, as it was the case in our study.

The solution of the problem can be assisted by performing a bottom up assessment, where the most vulnerable and susceptible areas are initially considered in hazard

modelling, such as was done in the current study. As it was known which areas were impacted the most, we particularly focused on the model behaviour in these regions. It helped us to attain better performance based on the study of Carisi et al. (2018) for the January 2014 event. In probabilistic assessment, these areas can be particularly outlined by intentionally focusing on the locations with high concentration of population/assets, meaning, more attention should be given to analyse flood characteristics in the calibration stage. By doing this, we may reduce uncertainties related to the identification of hotspots.

### 2.5.2. Limitations

One of the main issues for the HEC-RAS applications is the way in which the model distributes the water within a mesh cell. The volume-elevation curve drawn for each cell-face while pre-processing does not recognise the exact location of the higher/lower ground of the subgrid terrain. In case of rectangular mesh, when the cell faces are not aligned with the elevated linear features, they are not captured into the property tables. We may therefore observe a leaking effect (see Figure 19), or the opposite way when the model would not recognise the obstacles for the flow and route it further onto a neighbouring cell. This is a known limitation, previously observed in the used version of HEC-RAS 5.0 (Goodell 2015). In our case, we noticed that there is a certain amount of hydraulically disconnected flooded areas. Moreover, this effect is particularly obvious in the simulations with coarser subgrid terrains. Some areas (see Figure 19) simulated as flooded are, however disconnected from the main inundated area. This might be a limitation in the calculations of the flood extent and, in some cases, the distribution of local water depth values. This problem is normally solved by refining the mesh with the breaklines, reducing the mesh sizes along such linear irregularities, however, as explained above, the current study did not look into such property.

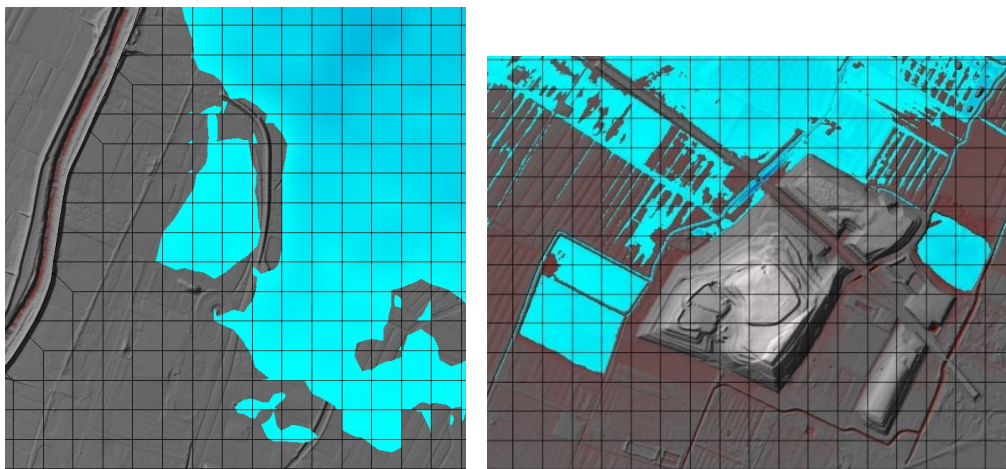


Figure 19. Leakage effect of HEC-RAS subgrid mesh examples of HR100\_100 (left), HR25\_1 (right). Larger ponds of water in both images are disconnected from the inundation extent.

Inundation boundaries produced by LISFLOOD-FP should be also taken with great care, as the model operates with a raster grid, and the water is distributed equally across the whole cell. For coarse grid resolutions (i.e. pixel size equal or larger than 100 m) it might thus misestimate the flood extent. In areas with complex topography, it is necessary to include important terrain features into the model. Due to the fact that LISFLOOD-FP simulates 4 directional water propagation at each cell face (i.e., D4 routing), the linear irregularities captured by L25 configuration (see Figure 20) would actually be sufficient to limit the flood propagation over such an elevation distribution. We suggest that this simplification of LISFLOOD-FP in case of high-elevation fine linear terrain features (i.e. levees, embankments, see Figure 20 light green cells) could help to route the water in the right direction and not to “leak” through the embankments. Nevertheless, the same peculiarity would restrain the water propagation in lower-elevation fine linear terrain features (i.e. rivers, canals, drainage networks) (blue cells in Figure 20, area near Bomporto). The same point applies to structured grid of HEC-RAS.



Figure 20. 25 m resolution DEM. Dark blue - canal, light green – levee.

By having 25 m mesh cell size (smallest in this case) it is not always possible to capture important local topographical features, such as embankments, small channels, etc., especially, when the linear features are significantly narrower than the model resolution. The known and widely used practice to include the actual terrain heights (levees, embankments, etc.) by “burning” them into the coarser terrain enables capturing such features, even when their width is smaller than the terrain resolution and mesh size. We intentionally avoided such option to see how the models would respond to the simplified approach of terrain pre-processing. Supposedly, on the geographically larger scale such manipulation when the complex and dense network of narrow levees in a specific area are ‘burnt’ into the terrain, may not be always feasible and/or effective. Especially, in cases when such modifications would greatly affect the storage volume of floodplains (i.e. when 100x100 m raster cell is given the height of the much narrower feature of 10 m breadth).

Moreover, this is certainly a challenging task for the areas, which are not covered with LiDAR data acquisition and areas with poor data availability and quality in general.

## 2.6. Conclusions

Due to the specific nature of the event described in this study and the growing use of fully 2D codes for flood modelling, we evaluated and compared the performance of the well-known HEC-RAS and LISLOOD-FP models for a floodplain with a complex and highly anthropogenically altered topography. The aim of the study was to see how the models of different complexity with given terrain resolution reproduce the flooding event and how accurate the results are. The resolutions were rather coarse for the given study area as our main goal was to identify the potential of the codes and mesh dimensions to simulate events over large regions.

One of the conclusions from the study is that 50 m resolution for describing terrain with complex linear features is a reasonable compromise between output accuracy and computation time for LISFLOOD-FP model, while HEC-RAS optimum solution would be the configuration of 1 m subgrid terrain and 100 m mesh size. This experience may contribute to simulations performed at catchment scales designed to capture large-scale system behaviour. Specific floodplain morphology may serve as water storage areas during flooding events and hence, lower the risks in the downstream part of the catchment.

Another point is the complexity of the modelling schemes. Raster-based LISFLOOD-FP was more efficient at representing overall flood extent and water depth at water marks, while HEC-RAS performed better at representing spatial distribution details (i.e. inundation boundary) considering given terrain (due to its high-resolution subgrid feature). Therefore, a selection of the modelling scheme and resolution should be carefully considered depending on the purpose of each given case study.

Finally, a topical issue in 2D code usage for large-scale simulations using high-resolution datasets is computational cost. As mentioned above, this can be significantly advanced by using GPU version of the codes. In this study we highlight the computational advantage of the inertial formulation of the shallow water LISFLOOD-FP model compared to diffusion wave HEC-RAS. This study shows that codes with simplified physics are a necessary tool for probabilistic/preliminary flood risk assessment. Moreover, by including high-resolution subgrid (HEC-RAS with 1 m terrain) we obtain more detailed hazard maps even for large meshes (i.e. 25, 50, 100), however, sacrificing the computational time. When comparing the overall performance of L25 and HR100\_1, the latter one is two times faster, however L25 showed somewhat better results in flood extent and water depth representation.

Nevertheless, we suggest that more complex tools (i.e. full momentum shallow water codes) have their place in local-scale studies to provide hyper-detailed

hydrodynamic modelling. Moreover, future work should consider the cases when the channel flow simulation is included in the model. Such advances will shed more light on the application of 2D models of different complexity.



# **Chapter 3. Large-scale high-resolution simulations using 2D raster-based model. The Po River case study**

## **3.1. Introduction**

There has been a limited amount of studies done on highly-detailed large-scale flood modelling using fully 2D codes. The limiting factor here is the common unavailability of LiDAR datasets for geographically large areas and insufficient computational power. Nevertheless, it is being changing nowadays, as there is trend in increasing of the computation capacity and wider access to high-resolution terrain data. As has been shown above, the application of 2D models gives an additional and valuable insight on the spatial distribution of the flooding extent, water depth and flow velocities. In order to meet the modern tendencies and look up into the upcoming years we evaluate the efficiency and accuracy of 2D large-scale simulations based on high-resolution LiDAR terrain data. Moreover, it is known that simulating a flood event based on a shorter river reach may bring an array of limitations, as certain hydrodynamic processes can be caught only considering upstream and downstream conditions on the whole catchment area (i.e. river system behaviour) (Vorogushyn et al. 2018). This issue becomes especially burning when it comes to the river basins with an intensive human interaction. Complex embankment networks greatly impact the hydrodynamics (Afshari et al. 2018; Shustikova et al. 2019). Particularly, we focus on the mid-lower portion of the Po River, which is described in the

subsequent paragraphs in detail. The main objective of this Chapter is to analyse the potential of a raster-based 2D model (i.e. LISFLOOD-FP) to simulate inundations across geographically large areas characterized by heavily anthropogenically modified terrain and discuss the impact of the data resolutions and pre-processing on results' accuracy. First we outline the study area with its characteristics and peculiarities. Then, we present most relevant modelling studies done on the investigation area, their limitations and gaps. And finally we present an advancement of our research by describing methods and discussing its results.

### 3.1.1. Study area

Po River is longest river in Italy (about 650 km) and located in the northern part of the country, 5% of the river basin in the upstream parts are shared between Switzerland and France (Figure 21). It flows from west to east and discharges into the Adriatic Sea, forming Po delta. From north and south, the river basin is surrounded by the Alps and Apennine mountains, respectively. The Po river flows across alluvial floodplain (Po valley), which is also known as *Pianura Padana*. The river slopes eastwards to the river mouth, where the source is at 2100 m a.s.l. (Cottian Alps) and downstream parts (Po Delta and Polesine regions) are up to 4 m below the sea level. The riverbed slopes gradually, from 0.35% in the upstream parts to 0.14% in the downstream. Due to orogenic formations, the valley slopes from northern and from southern mountain chains (Marchetti 2002). The overall area of the river basin is about 74000 km<sup>2</sup>, from which about 29000 km<sup>2</sup> are plain (Raggi et al. 2007).

There are 141 tributaries that contribute into the river flow, some of the largest are: Maira, Tanaro, Ticino, Lambro, Trebbia, Adda, Taro, Parma, Enza, Oglio, Secchia, Panaro (Montanari 2012). The area contains about 450 lakes, from which only several are large. Apart from tributaries, the flow input comes from numerous artificial irrigation and reclamation channels. The basin is split into 28 principal sub-basins, where each of them has different discharge characteristics.

The climate of the area varies from mountains (alpine) to floodplains to the delta (continental). The annual precipitation amount spatially changes in respect to the altitude. As can be seen from Figure 22, most rainfall is measured in the mountainous areas of Alps and Apennines (1200-1800 mm/year), whereas in plain parts of the Po Valley, it ranges between 800-1200 mm/year. Some parts (Po Delta and Northern parts of Emilia-Romagna and some regions upstream) are rather drier, with the mean annual rainfall amount of 400-800 mm/year.

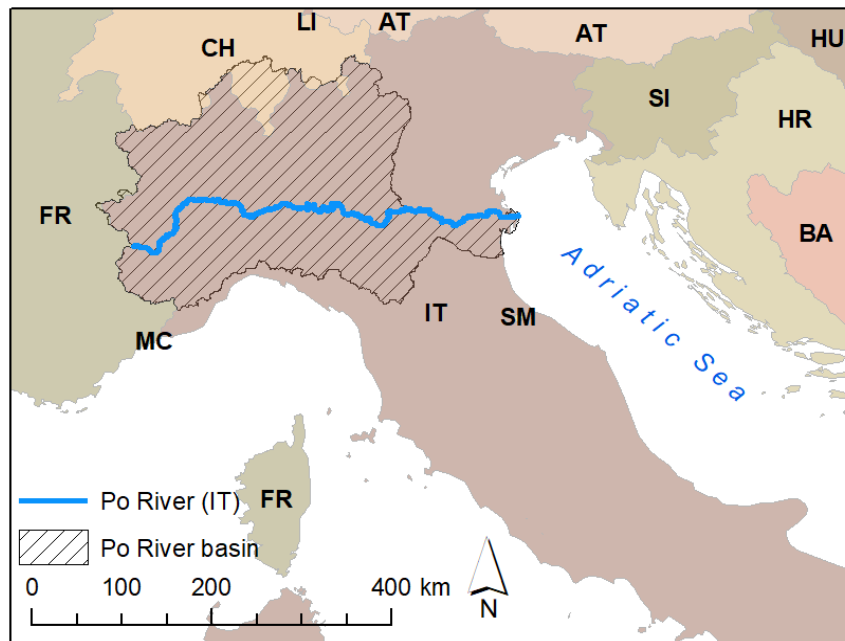


Figure 21. Location of the Po river basin within Italy.

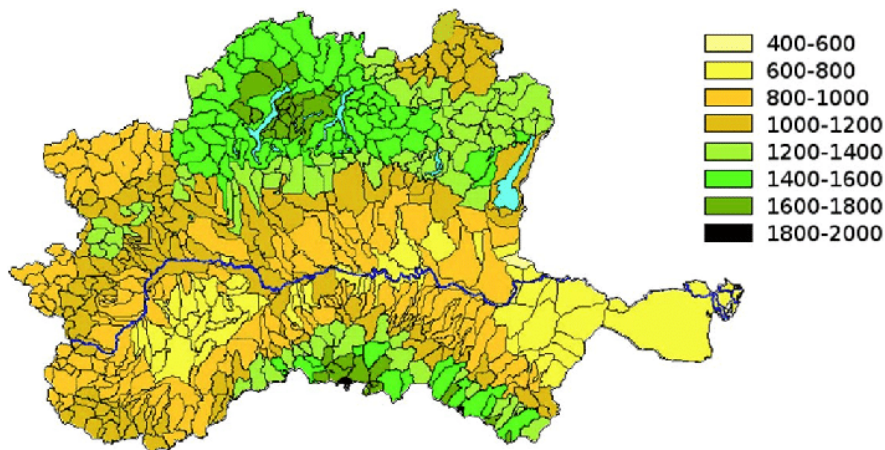


Figure 22. Mean annual rainfall over the Po River basin (mm/year). Taken from (Autorit`a di Bacino del Fiume Po 2006).

From socio-economic point of view, the floodplain is characterized by a variety of productive activities and infrastructure, it represents a nerve centre of national economy, and it is also densely populated: local population is 17 million people (Musolino et al. 2017). It covers 7 administrative regions of Italy, Piedmont, Valle d'Aosta, Lombardy, Veneto, Liguria, Emilia-Romagna, and Tuscany and autonomous province of Trento. This area contributes 34% of GNP; with 29% of national industry developed there. 41% of agricultural productivity comes from the basin surroundings, and 48% of national electrical consumption (Musolino et al. 2017). Because of fertile alluvial soils, lower regions of alluvial Po Valley have experienced a significant agricultural development; this was especially intensified after the Second World War. Various economic activities of the area consume a

large amount of fresh water from the river and from the groundwater sources. For instance, the agricultural production along, which considerably relies on water resources, takes about 17 billion m<sup>3</sup> per year. Additionally, the production sites, agriculture and high dense population have increased demands of electricity supplies; for this reason, 46% of national hydroelectric power is produced in the Po river Basin. One of the largest dams in the river is located near Isola Serafini, with the potential to produce 300 GWh per year on average (Collegio Ingegneri Venezia 2018). Additionally, the Po River floodplain is remarkably valuable in terms of touristic activities: there are more than 60 natural parks, natural reserves, sports and navigation sites. Some of the largest cities are Turin, Ferrara, Piacenza, Parma, Alessandria, Modena and Milan.

There has been a series of floods of different magnitude occurring on the history of human record. Analysis of such records allow us to assume that 22 flooding events occurred in the 16<sup>th</sup> century, 14 events in the 17<sup>th</sup> century and 18 floods occurred in the 18<sup>th</sup> century. Some of the most severe floods in the 19<sup>th</sup> century were recorded in 1801, 1839, 1846, 1857, 1868 and 1872. In the 20<sup>th</sup> century some most impacting floods occurred in 1926, 1928, 1949, 1951, 1953, 1957, 1968, 1994 and 2000. The event of 1951 was particularly catastrophic, as it involved multiple levee breaches near Ferrara on the left bank of the main channel. Vast floodplains were inundated for many months, which caused immense damages and human losses. The socio-economic recovery of the affected communities after 1951 flood lasted decades (Montanari 2012). Naturally, the local population was trying to reduce the risks related to flooding, so the first levees were surrounding agriculture regions and settlements. In the past centuries, the levee height and width has significantly changed (Di Baldassare et al. 2009a).

High heterogeneity in terms of climatic, eco-hydrological and geomorphological patterns makes the Po river basin a very complex interconnected system. Nowadays, in order to establish national policies and develop flood management plans, the following bodies are responsible for different aspects of controlling, monitoring and mitigation: the Interregional Agency of the Po River (AIPO; [www.agenziainterregionalepo.it](http://www.agenziainterregionalepo.it)) and the Po River Basin Authority (AdB-Po).

The subject area of the current research covers about 350 km-long reach between Isola Sant'Antonio to Pontelagoscuro (Figure 23). The area is characterised by an extensive system of main and minor embankments with different design return period, which makes it challenging for the flood managers to make decision based on the simplified or outdated flood maps.

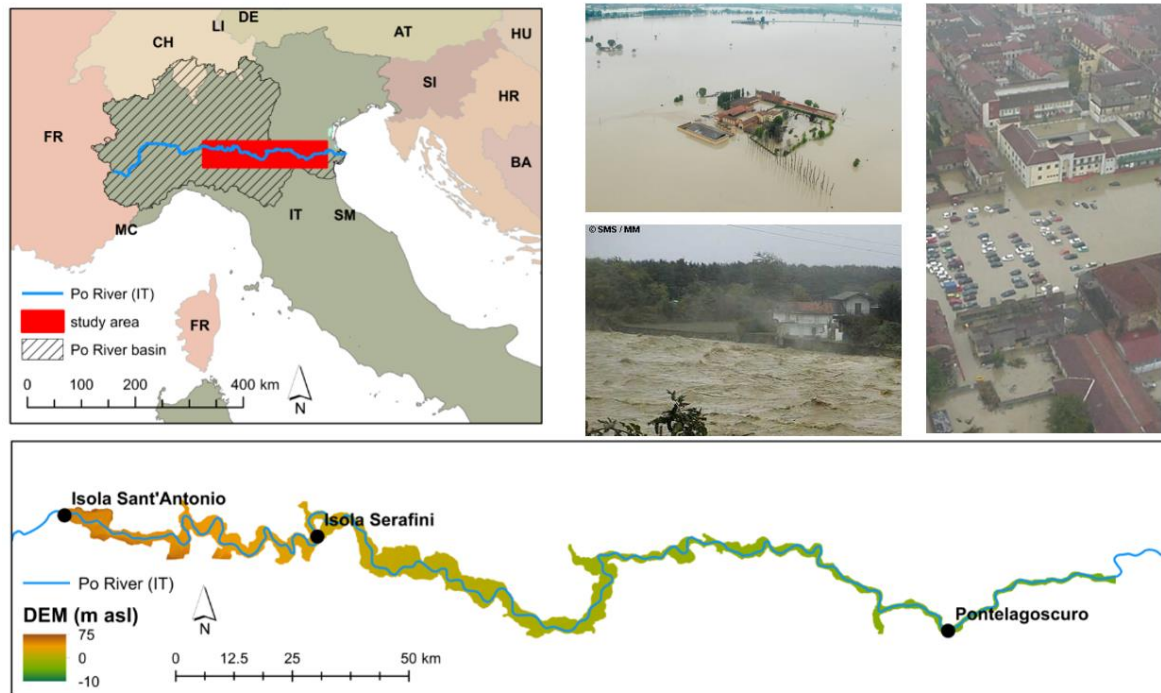


Figure 23. Study area extent and images from 2000 flood. Images in the upper right panel are taken from (Meteolive.it 2016; nimbus.it).

In particular, the floodplain is divided into certain buffer zones, so-called compartments (*fascia* in Italian). There are 3 compartment levels, depending on the configuration of embankments. Minor embankment has a design return period of 50 years, meaning it is likely to be overtopped when the flood event would be considered as 1 in 50 years or more. The zone between minor embankments is a so-called “Compartment A”. The main embankment (red line in Figure 24), was designed to protect against 1 in 200 years flood and corresponds to “Compartment B”. The schematic representation of the embankments can be seen in Figure 25. The floodplain behind main embankment is called “Compartment C”. It is activated once the main embankment is overtopped, or there is a breach. There is no strictly delineated boundary of the Compartment C, as it depends on the magnitude of the events and location of possible breaches. Meeting the EU Floods Directive requirements in flood mapping for extreme event, Po River Basin Authority considers 500 years event.

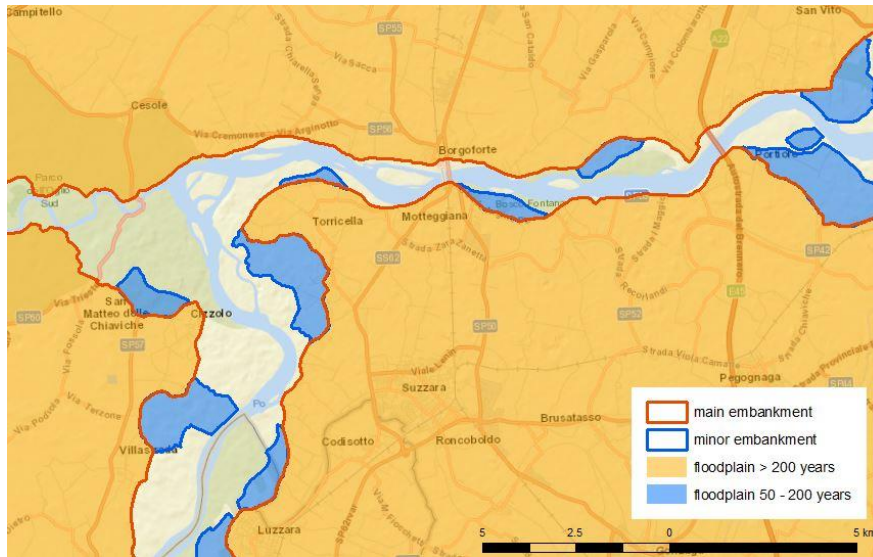


Figure 24. Spatial distribution of the main and minor embankments along a portion of the upstream part of the river with associated design return periods.

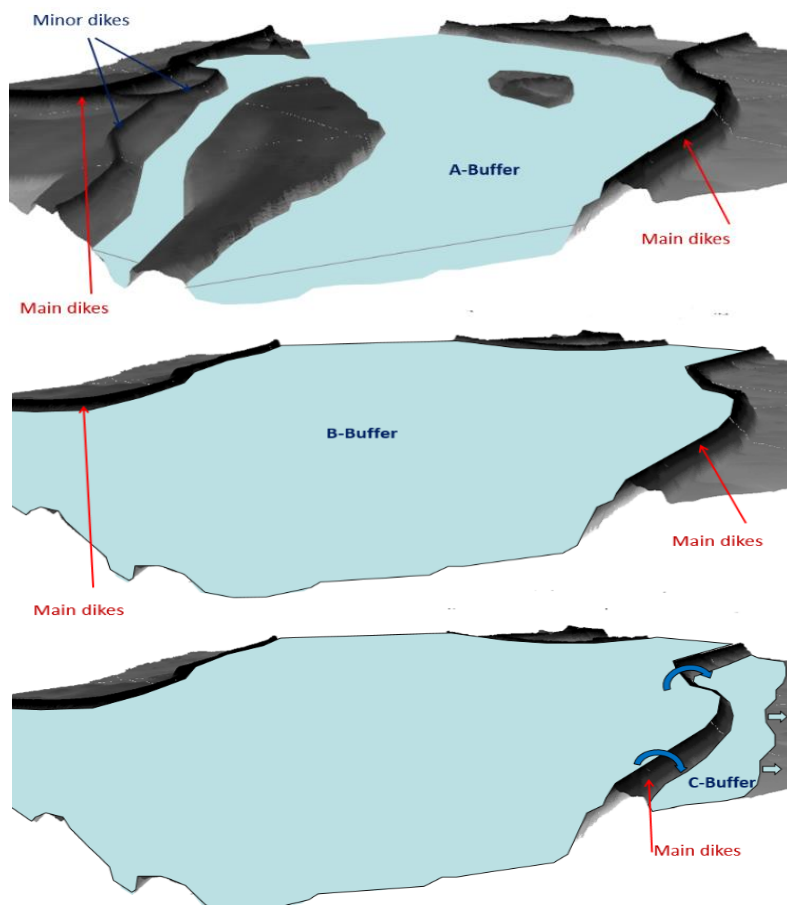


Figure 25. Schematic representation of the spread of inundation extent regarding the design return period of the main and minor embankment.

### 3.1.2. Flood modelling on the mid-lower portion of the Po River. Review of existing research

As one of the main aims of this thesis is to further deepen understanding of the flow behaviour on the Po River using 2D modelling techniques, the review of existing key studies done on the same study area using modelling tools of various complexity is crucial. There has been a series of researches, which aimed at investigating flood hazard evolution and flood management strategies on the mid-lower portion of the Po River by the means of flood models. Below, we would like to present most relevant studies, pointing on the modelling methods used, the river reach and main outcome of their work. Building on this review we expect to outline main advances, gaps and challenges in large-scale flood modelling on the Po River.

In the past 200 years, the geometry of embankments has significantly changed, it increased in height and width (Di Baldassare et al. 2009a). In Figure 26 we can see that near Pontelagoscuro, between 1878 and 2005, the embankment was elevated to more than 6 meters at certain places and got significantly wider.

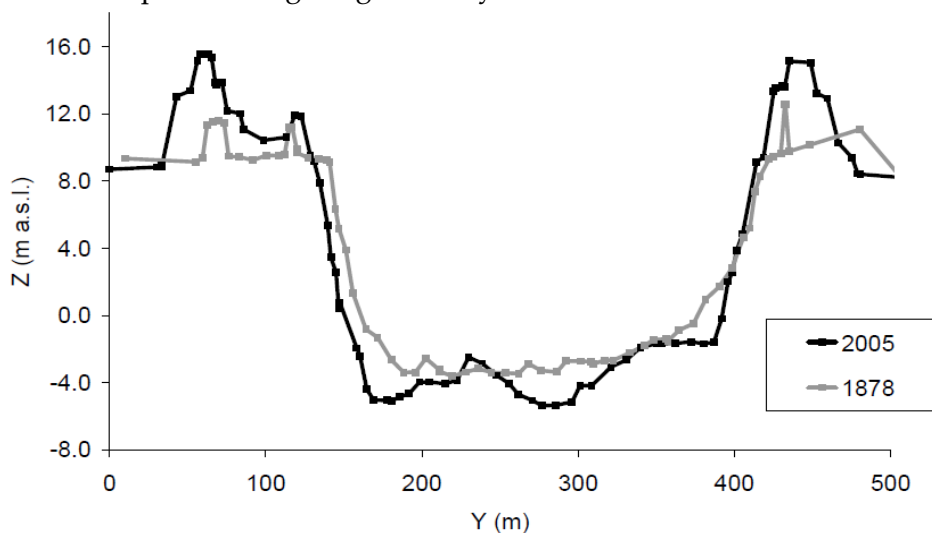


Figure 26. An example of the Po river cross-section showing the elevation of the embankment in 1878 and 2005 near the Pontelagoscuro gauging station. Taken from (Di Baldassare et al. 2009a).

Within the past decades the enhancement and upgrading of existing dikes posed additional issues causing so-called “levee effect”, when high-intensity low-frequency events may cause devastating effect on the growing socio-economic activities behind the dikes.

Di Baldassare et al. (2009a) investigated the impact of the levee changes over time on flood wave propagation on a mid-lower part of the Po River between 1878 and 2005 on 190-km reach of the Po River. They reconstructed the 1879 flooding event and evaluated the role of human activities in flood wave propagation by applying two coupled models: 1D channel flow run in HEC-RAS and 2D floodplain was simulated using TELEMAC-2D.

The authors highlight, that the increased levee height lowered the inundation frequency of the protected floodplains. Meanwhile, the levees decrease flood attenuation and cause the increase of the discharges downstream (Di Baldassare et al. 2009a). This study specifically points on the importance of the more detailed investigation of the flow dynamics and changes in the levee-height. Authors suggest that modern configuration of the levee-heights may result in multiple breaches in case of an extreme event (i.e. 500-year flood). Moreover, this study outlines the benefits of controlled flooding, rather than continuous levee-heightening for future flood risk management on the Po River.

A study by Castellarin et al. (2011a) aimed at identification of the effects of the changes in minor embankment elevations as an elaboration of risk mitigation strategies. Castellarin et al. (2011a) used combined 1D/2D scheme of HEC-RAS model in order to simulate different flooding scenarios on the mid-lower portion of the Po River (about 350 km long). The geometry was outlined in a way that the main channel was represented as 1D component and 2D flooded areas (Compartments B and C), which were connected by the means of lateral links (weirs), represented as the minor levee height. They performed a series of simulations in order to investigate an effect of the embankments height on the flooding dynamics reproducing a large-scale flooding event, which occurred on the Po River in October 2000. Additionally, they considered two synthetic hydrographs, both representing an event with recurrence interval greater than 200 years. The geometry configurations were set as following: (i) the minor embankment height retrieved from available LiDAR data (acquisition of 2005), (ii) the minor embankment elevated to maximum possible level according to the Po River Basin Authority normative, which is approximately 1 m lower than the height of the main embankment, (iii) minor embankment system is entirely removed from the DEM. Castellarin et al. (2011a) concluded that the floodplains that are protected by minor levees play a key role in peak discharge attenuation for extreme events (200 years flood). This complex system of flood defences greatly improves the capacity of the river to retain a certain amount of flood water. Moreover, the modified embankment height to maximum level (1 m below the height of the main embankment) would have even larger effect on flood peak attenuation. The authors suggest that in light of the finding presented in (Castellarin et al. 2011a) the existing management strategies developed by the AIPO should be revised and adapted. However, their study was based on the simulation performed by combined 1D/2D, which lacked the backwater effects that can be better captured with the fully 2D approach.

Castellarin et al. (2011b) applied combined 1D/2D model HEC-RAS on the 350 km river reach from Isola Sant'Antonio to Pontelagoscuro. By simulating a 500 years flood and evaluating different geometry of main embankments. Particularly, the model was set up in a way to simulate no overtopping of main embankment; overtopping and levee breaching at pre-defined locations by the mean of lateral structures; overtopping without levee breaching. The water volumes of the overflows and breach outflows were estimated and

compared under each scenario. Among main findings is that, in the light of the high uncertainty associated with the levee breach location and timing, the residual risks behind the main embankment are significant. Additionally, the controlled flooding is an efficient solution in case of the mid-lower portion of the Po River and should be further investigated.

Domeneghetti et al. (2013) looked into different uncertainty sources in flood modelling such as upstream and downstream boundary conditions and dike failure probabilities simulating probabilistic flooding on the Po River using 1D/2D model with a levee-breaching link (IHAM) (Vorogushyn et al. 2010). The authors advanced an understanding of the uncertainty role of the rating curve as a downstream boundary condition in probabilistic flood mapping. Brandimarte and Di Baldassarre (2012) by the means of 1D model deepened the research in the probabilistic framework for the flood defences design and uncertainties by simulating October 2000 flood on the Po River portion between Cremona and Borgoforte. Particularly, the standard freeboard used in the construction of the defence structures (as defined to be 1 m above estimated 200 years event) appears to underestimate the uncertainty associated with water levels. Alternatively, the authors suggest applying a pragmatic method, derived from the uncertain flood profile (Brandimarte and Di Baldassarre 2012).

The study area has been a subject of several continental and global flood models at coarse resolution (pixel size 100 m or larger) using various flood mapping methods. Among them are Alfieri et al. (2014) and Tavares da Costa et al. (2019). Despite having a complete extent of the study area, the performance of the continental-scale models usually does not allow for a detailed processing of the terrain, so the main and minor embankments are not particularly considered. This might bring misleading results in specific parts of the Po River. Therefore, showing the inundation in the Compartment C, even for events lower than 1-in-200-years event. This is a significant limitation for the production of the flood hazard and risk maps, as required by the Floods Directive 2007/60/EC. Table 5 shows a summary for some of the previous research done on the study area, the geographical extent covered and specific problem considered.

Table 5. Selected studies done on flood modelling on the mid-lower portion of the Po River.

Study	Model used	Domain	Study scope
Di Baldassare et al. 2009a	1D HEC-RAS 2D TELEMAC	Cremona to Pontelagoscuro (190 km long reach)	evaluation of the levee heightening in the past 140 years and its impact on the flow dynamics
Di Baldassare et al. 2009b	1D HEC-RAS 2D TELEMAC	Reno river, Po tributary	probability-weighted hazard maps

**Chapter 3. Large-scale high-resolution simulations using 2D raster-based model. The Po River case study**

Schumann et al. 2010	1D/2D HEC-RAS	between the two gaging stations of Cremona and Borgoforte	near real time space-born approximating using freely available data
Castellarin et al. 2011a	1D/2D HEC-RAS	Isola S. Antonio to Pontelagoscuro (350 km long reach)	attenuation of the peak discharge under the effect of different geometries of breach to reflect advantages of the controlled flooding
Castellarin et al. 2011b	1D/2D HEC-RAS	Isola S. Antonio to Pontelagoscuro (350 km long reach)	simulation of 500 years flood under different geometries of the main embankment considering the overtopping of the main embankment
Brandimarte and Di Baldassarre 2012	1D HEC-RAS	between Cremona and Borgoforte	probabilistic framework for the flood defences design and uncertainties
Domeneghetti et al. 2012	1D/2D HEC-RAS	river reach along Cremona	uncertainty related to rating curve and its effect on hydraulic model calibration
Domeneghetti et al. 2013	IHAM framework, 1D channel representation/2D raster based model	between the gauges at Piacenza and Cremona	uncertainty sources in flood modelling
Alfieri et al. 2014	1D/2D LISFLOOD-FP	continental	contentedly flood mapping of a 100 year event
Mazzoleni et al. 2014	1D HEC-RAS 2D LISFLOOD-FP	between the two gaging stations of Cremona and Borgoforte	probabilistic flood hazard mapping under levee breaching scenarios.
Tavares da Costa et al. 2019	GFI index	continental	DEM-based web application to derive flood-prone areas based on GFI index

From Table 5 we can see that the majority of the studies were done on a certain portion of the River using 1D or combined 1D/2D hydrodynamic models. However, some

of the study covered the whole area of current interest. Such as from modelling point of view, the study of Castellarin et al. (2011a) and (2011b) simulated the flood water volume entering the levee protected floodplains, so the 2D part did not include the underlying terrain data, but was simulated using spilling and filling method. Therefore, this method does not allow for representation of the spatial distribution of the water depth, velocities and inundation extent within the channel and inundated floodplains. In all abovementioned cases the entire interaction channel-floodplain-channel was never investigated on a detailed 2D level, which poses a significant limitation for the large-scale flood risk mapping, which would consider local distribution of flow velocities and water depth. Moreover, few studies that investigated the levee stability always applied the analysis adopting simple representation of the channel and protected floodplain, using combined 1D/2D models (Domeneghetti et al. 2013; Mazzoleni et al. 2017). Detailed flood hazard parameters are crucial for the flood risk maps, e.g. risk to life and direct damage assessment are calculated using the product of depth and velocities.

### 3.1.3. Research objectives

Previous research done on the study area utilised combined 1D/2D codes, where the flow within the channel was reproduced using 1D codes only. As mentioned above, such codes allow for a faster computation times and possibility to cover much larger areas. However, 1D representation of the river bed does not allow for the detailed spatial distribution of flow parameters. Among such flow parameters are water depth, velocities, arrival time, which are greatly beneficial for production of flood risk maps for the areas within and outside the embankments and as required by the EU Floods Directive. Flow details are function to better hazard evaluation, since they might be useful for breach failure investigations, protection structure design, etc. Therefore, it is important to consider the levee stabilities, whereas 1D models applied so far fail in providing accurate hydraulic load for the embankment. Growing availability of high-resolution data together with the increasing computational capacity of the working stations makes it possible to perform the simulations on the large-scale using high-resolution LiDAR data provided by Po River Basin authority (AdB-Po, [www.adbpo.it](http://www.adbpo.it)) using 2D codes. Different studies, which researched the topic on the large-scale flood modelling, would cover areas from 2000 km<sup>2</sup> Falter et al. (2013) to 170,000 km<sup>2</sup> Schumann et al. (2013) or cover the whole continent Wing et al. (2017). The definition of the “large-scale” highly dependent on the tools used and the context behind each particular study. Due to the complexity of the 2D codes, amount of computation cells, data availability and computation time, it is largely challenging to perform global or continental scale studies using fully 2D models. Global 2D simulations have been applied with a compromise in terms of DEM resolution, which in case of the study of Dottori et al. (2016) was 1 km. In this light, we suggest that the fully 2D codes allow flood modelling on the areas larger than several thousand square kilometres and can

be viewed as large-scale studies. Therefore, we stress that the suggested approach will greatly improve the representation of crucial elements (i.e. spatial distribution of flow parameters) on the given study area. As outlined above, it is important to investigate the system behaviour, which requires flood modelling on the large scale in order to track the catchment response. Thus, we would like to advance previous studies done on the mentioned geographical area and apply fully 2D inundation model. We would like to stress, that to the best knowledge of authors, this is the first fully 2D high-resolution study done on the mid-lower portion of the Po River. Moreover, we additionally test different configurations of DEM in order to better represent the complex network of embankments.

In this chapter, we would like to introduce and analyse the influence of the DEMs with different configuration (with and without embankments) on flood propagation on large scale. Our analysis is performed using high-resolution LiDAR data, which includes the bathymetric data of the mid-lower portion of the Po River. Such approach is performed using well-known LISFLOOD-FP code (see detailed description above) in fully 2D mode. By doing this, we would like to show to which extent the detailed data affects the model outcomes and how different resolutions and embankments inclusion contributes to flood mapping and further risk assessment. An additional, yet compelling advancement of this work is to show the potential of such models to simulate a series of flooding scenarios, regarding their computational efficiency.

More specifically, we simulated the flood of October 2000 on the mid-lower portion of the Po River (350 km river reach) using fully 2D LISFLOOD-FP model. We apply the model with a set of resolutions 30, 50 and 100 m and their configurations with the real embankment height included in aggregated DEM and without the manual adding of embankment height (simple DEM aggregation).

## 3.2. Methods and data

### 3.2.1. Study event and data

The domain includes compartments A and B, main embankment and 100 m buffer area outside the embankment (Figure 23). The DEM LiDAR data was provided by AdB-Po, its horizontal resolution is 2 m. The data acquisition took place in years 2004-2005 using two laser scanners mounted on aircrafts. The bathymetric data was collected using multi-beam sonars during approximately same period (Castellarin et al. 2011a). DEM used in the study represents bare earth terrain, cleared from trees and buildings with vertical accuracy of the data of about  $\pm 0.15$  m. The model domain has an overall area of over 6675 km<sup>2</sup>.

Most aggregation techniques used in flood modelling tend to produce various errors when it comes to representation of the fine linear features, which are finer than the resulting resolution. In such areas as Po River basin, to capture a complex embankment

system is a challenging, yet crucial task for flood modellers. We suggest that most of the coarse models would misestimate flow parameters due to this issue (Shustikova et al. 2019). In this study, our goal is to show to which extent a fully 2D model at different resolutions can correctly capture flood dynamic inside the floodplains, therefore we produced a set of configurations. First, we aggregated 2 m LiDAR data using the mean value of the pixel into 30, 50 and 100 m. The aggregation of LiDAR DEM means that the representation of topography is rather smooth, however contains some errors due to vertical averaging. Such errors are inevitable in large-scale studies when the DEM data is being resampled, this especially becomes evident when global datasets are utilised in flood modelling. In order to reduce such errors and include linear terrain irregularities (e.g. levees) we produced two sets of the DEM and compared the outcomes to highlight the importance of the levee in the flood dynamics. Based on resulted DEMs we produced another set of the configurations, where we manually ‘burnt’ in the actual height of embankments into the simply aggregated DEMs (Table 6 and Figure 27).

An important point here is that LISFLOOD-FP is a raster-based model, which operates with the rectangular mesh of the same cell size as input data (detailed model description can be found in Chapter 2.2.2). Therefore, different configurations will have an impact on the storage capacity of the floodplain. As can be seen from Figure 27 (two lower images), the resolution of the terrain data plays the greatest role. The modified DEM at each resolution (upper image) clearly identifies the location and the approximate height of the main and minor levees; however, the lower resolution (100 m) remarkably reduces the floodplain storage capacity (lower image, red line). Regular rectangular mesh is unable to represent fine linear terrain features, such as roads, levees or embankments. Therefore, here we analyse which configuration and which resolution, among those investigated here (Table 6 and Figure 27), is the most suitable.

Table 6. Names of configurations tested.

<b>DEM Resolution (m)</b>	<b>Aggregated LiDAR</b>	<b>Aggregated LiDAR with 'burnt' in embankments</b>
<b>30</b>	30m_noembank	30m_embank
<b>50</b>	50m_noembank	50m_embank
<b>100</b>	100m_noembank	100m_embank

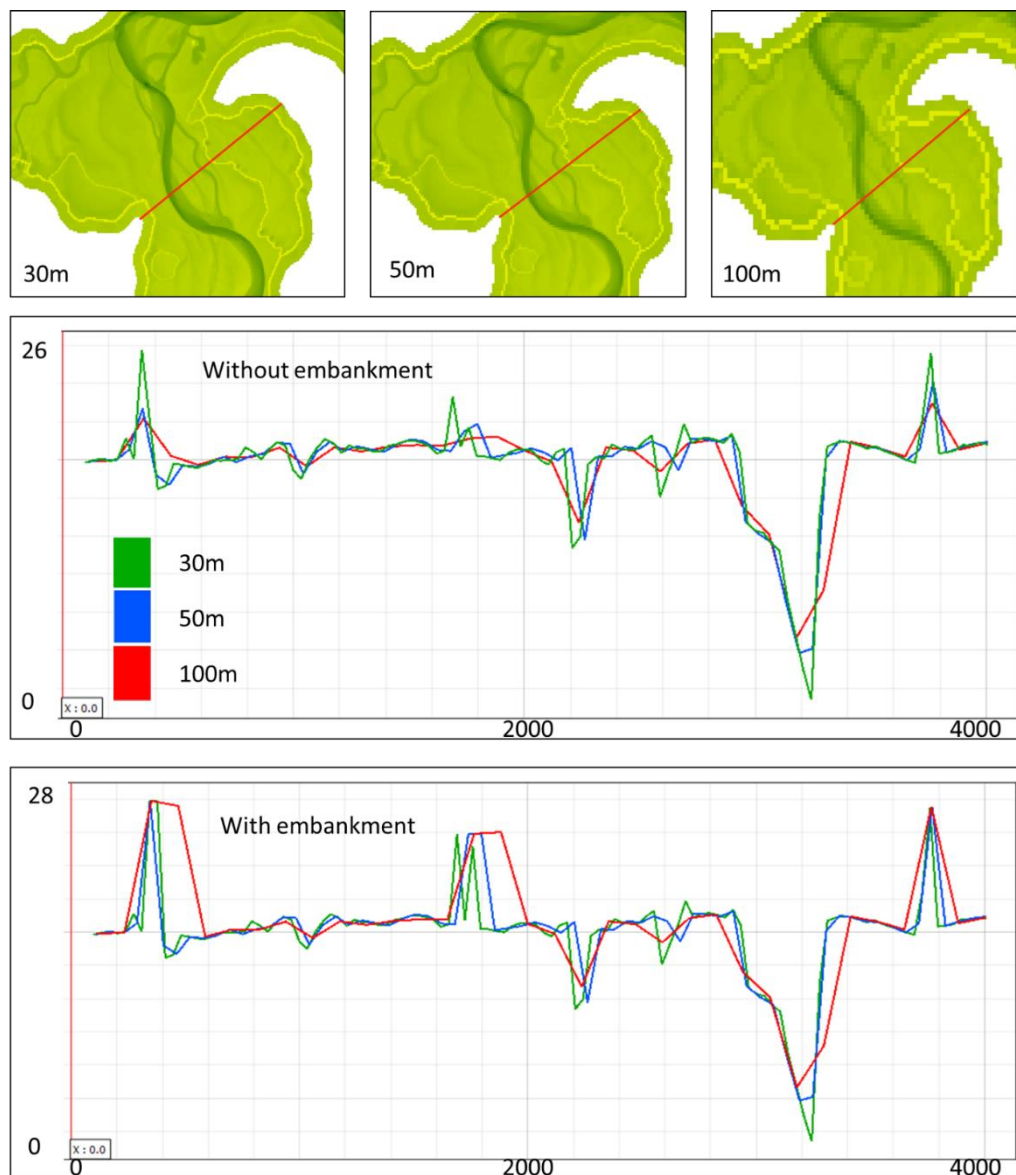


Figure 27. Cross-section profile location and DEM resolutions (upper). Profile without embankment (middle). Profile with embankment (lower).

To perform such investigation we refer to well-documented flooding event, which occurred on the Po River in October 2000. The flood of October 2000 is considered as one of most severe in the recent decades. Some of the rivers in the Po basin experienced 200 years return period discharges (Cassardo et al. 2001). Uncommonly heavy rainfalls extended all over the upstream part of the basin, where larges area of the mountainous settlements got damaged, as well as parts of Turin city. The strongest rainfalls were recorded on the tributaries of Po in Northern and Western parts of Piedmont region. Several gauges recorded historical maximum, such as it happened in Turin (2350 m<sup>3</sup>/s). Moreover, maximum water levels along the reach stayed for unusually long time (8-10 hours

continuously). The graph below shows the discharges at upstream part of the river, as well as the discharge at some tributaries (see Figure 28).

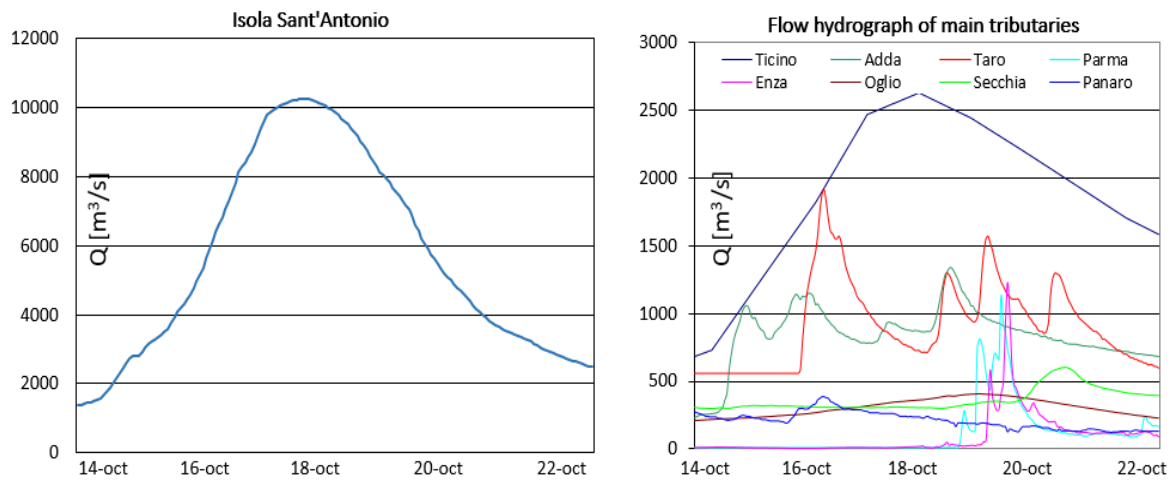


Figure 28. Left: observed discharge at upstream boundary. Right: inflow of the major tributaries.

The flood caused several deaths and severe damages in the affected areas (Cassardo et al. 2001). Maximum water levels along the reach are taken from the official report delivered by the Po River Basin Authority. The vertical errors in such measurements are known to be up to 0.5 m (Horritt et al. 2010a).

In mid-lower portion of the basin the flood behaved in a way that the water levels did not reach the crest height of the main embankments, so the inundation boundaries are clearly outlined by main embankment contour. This makes it a perfect case study to evaluate performance of the hydrodynamic model and influence of terrain modifications and resolutions on the accuracy of results. In order to evaluate efficiency of the large-scale 2D modelling, we specify the computation time of different resolutions. The simulations were performed on a server with 2 CPUs (20 real cores and hyperthreading 40 cores) and 64 GB RAM.

### 3.2.2. Model set up and calibration

We apply LISFLOOD-FP in fully 2D mode (no 1D or subgrid component is considered for channel flow calculation) to see how well the flow parameters can be represented with six selected configurations (Table 6) to simulate the October 2000 event. The upstream boundary condition was set at near Isola Sant'Antonio (at Ticino-Po confluence) main reach and tributaries: Trebbia, Lambro, Taro and Adda. The hydrograph from the inflows were taken from the river gauges measurements. The free downstream boundary condition was set 50 km downstream from Pontelagoscuro gauging station (Figure 23), the place where the main channel splits into two branches and forms the Po Delta. The simulation was set to 191 h with input hourly hydrograph data.

The spatially variable roughness coefficients were initially distributed in two main classes: channel and floodplain. LISLOOFD-FP is known to be sensitive to change in roughness parameters for 2D calculations. In order to obtain best results, we calibrated the model by varying roughness coefficients Manning's  $n$  ( $m^{-1/3}s$ ) at 30 m DEM. As the area is rather large and 2D simulations normally take many hours to run we did not consider running Monte Carlo simulations. Instead, we implemented trial and error method, where the distribution of initial values were taken from the work done by Domeneghetti et al. (2015). In order to achieve best results we manually modified values based on simulated and observed maximum water surface elevations by means of Root Mean Square Error. Altogether, there was data of 171 water mark records. Because the flooding extent was outlined by the main embankments, we additionally visually inspected the levees on subject of overflows. If some overflows (more than in 1-2 spots) were noticed during the simulation, we would disqualify the configuration. Due to the computation time length (around 4 h for one simulation) and amount of manual parameter tuning, the calibration of other 5 configurations would require enormous amount of time and effort, therefore we adopted the results of 30 m DEM for 50 and 100 m configurations.

### 3.3. Results and discussion

By performing the calibration, we identified the DEM resolutions and configurations, which were unable to maintain the flood within the main embankments. In case of "30m\_noembank", "50m\_noembank", "100m\_noembank" and "100m\_embank" the levee was always overtopped in multiple locations. The simple mean aggregation of 2 m LiDAR resulted in underestimations of the critical linear feature heights. The two remaining configurations "30m\_embank" and "50m\_embank" resulted in comparatively better results with maximum of 1-2 overtops along the whole reach and are further discussed.

Additionally, to have a profound insight into different parts of the selected domains, we looked into the performance of configurations in the upstream and downstream parts of the reach. Figure 29 shows the results for the water depth and flood extent for all six configurations and two focus areas (upstream and downstream the reach). The left column of panels "A" and "B" represents the results with manually enhanced embankments, while the right one shows the performance of the configurations without such enhancement. From Figure 29 (panel "A"), which represents the upstream part, where the floodplain between the main embankments is relatively wide and the height of the embankments is lower than downstream, we can see that the only configurations, where the main levee was not overtopped are the ones with manually added embankment with 30 and 50 m resolution, while the rest got overtopped in numerous places (blue pixels outside the red line in Figure 29). While, in the downstream part, all configurations (30, 50, 100 m) with

manually enhanced embankments performed considerably well, having no overtops. It can be justified by the fact that the embankments are higher than in upstream part, which allows for larger storage volume. Moreover, because of river system behaviour, the water that propagates to the floodplain behind the main embankment due to overtop in the upstream part reduce the discharges downstream.

As we can see from Figure 29 the role of the inclusion of both minor (panel “B”, green box) and main embankments is significant, as our simulation shows, they fully control the flow within the embankments. Clear distinction of Compartments A and B within the geometry of the configuration plays crucial role in the results accuracy. Because of the raster-based principle of the LISFLOOD-FP model, that was used in the simulations, the minimum width of the embankment equals to the input raster resolution. Despite the fact, that the height of the embankments from 100 m DEM was correctly represented, such inclusion sacrificed the volume of the Compartment B (compartment between main embankments). The capacity of the floodplain between the main embankments was reduced to the extent that the water spilled out from the floodplains in multiple locations. Altogether, 4 configurations (“30m\_noembank”, “50m\_noembank”, “100m\_noembank” and “100m\_embank”) were disqualified from the further analysis. Therefore, it is important to look at the model performance along the whole reach. As can be seen, the two configurations which perform consistently well in upstream and downstream parts are “30m\_embank” (0.34 m RMSE) and “50m\_embank” (0.39 m RMSE) and are further discussed in more details. RMSEs presented above lie within the range of the data observation errors, which can be up to 0.5 m (Horritt et al. 2010a).

. Since in this study we aimed at exploring the resolutions compared using calibration for highest resolution only (30 m), it is rather difficult to speculate if the results were different if we separately calibrated each configuration. Such assumption would not be straightforward due to the spatial extent of the study and rather different result we got during calibration.

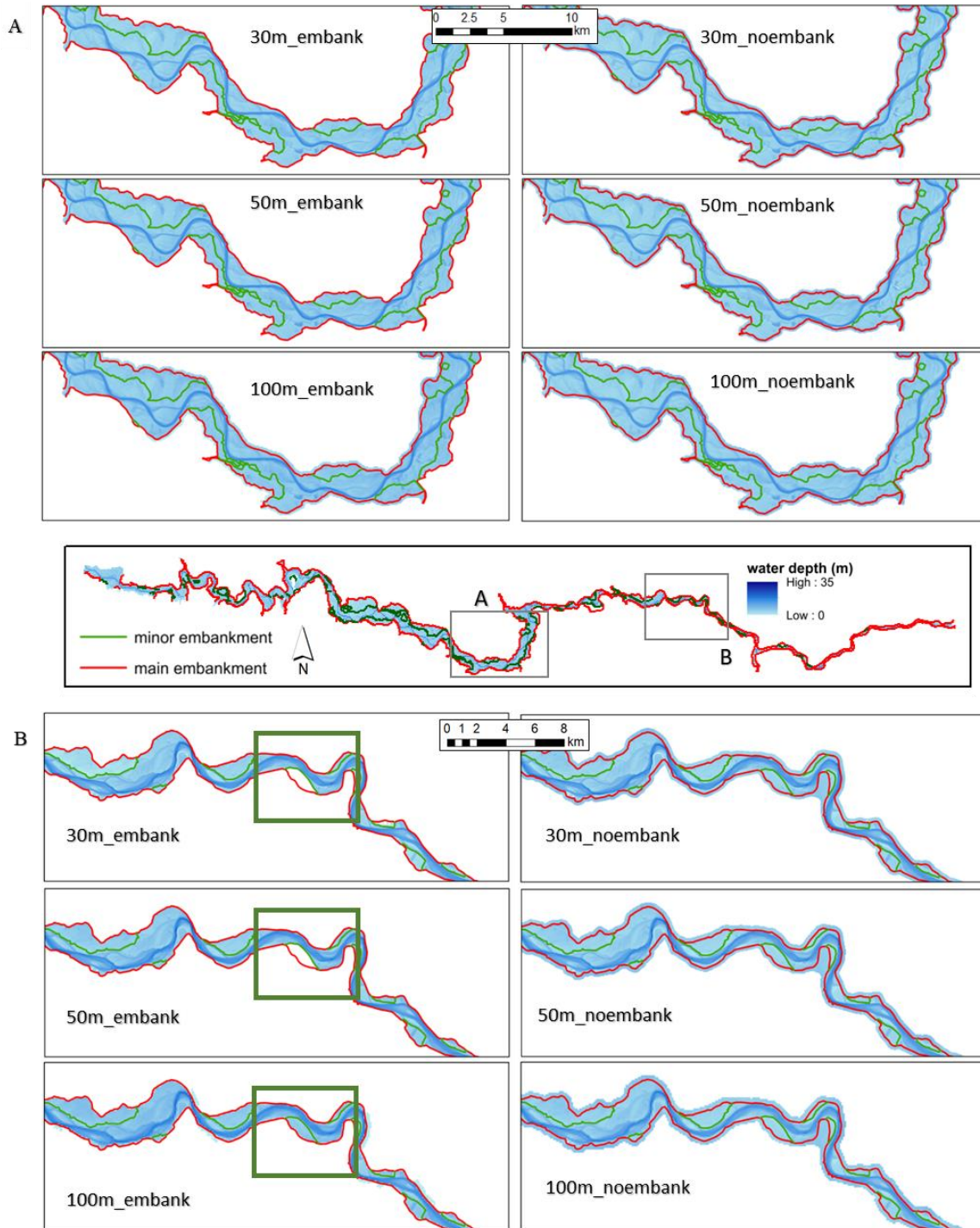


Figure 29. Distribution of local water depth. The middle panel shows overall representation of water depth for “30m\_embank” configuration with localised focus areas. The upper panel represent the results for six configurations in the upstream part (A). The lower panel represent the results for six configurations in the downstream part (B). Green boxes are used to point the differences between resolutions. Left columns shows configurations with embankments. Right columns shows configurations without embankments.

We looked at the hourly discharge at the gauging station of Cremona (15 km downstream from Isola Serafini, see Figure 21), which is located in the upstream part of the

study area. We compare it with the observed hourly discharge, where the Mean Error shows that the model overestimates the discharge (-311 and -272 m<sup>3</sup>/s for 30 and 50 m resolutions correspondingly, where the peak is 12,000 m<sup>3</sup>/s). Meanwhile R-squared is 0.98 for both resolutions. Concerning the peak flow, the maximum discharge is reached almost simultaneously considering the overall length of the simulation (191 h); for 30 m configuration the maximum was registered 4 h earlier and for 50 m – 2 h earlier compared to observations (Figure 30). The peak discharge for both configurations was less than 1% lower than observed.

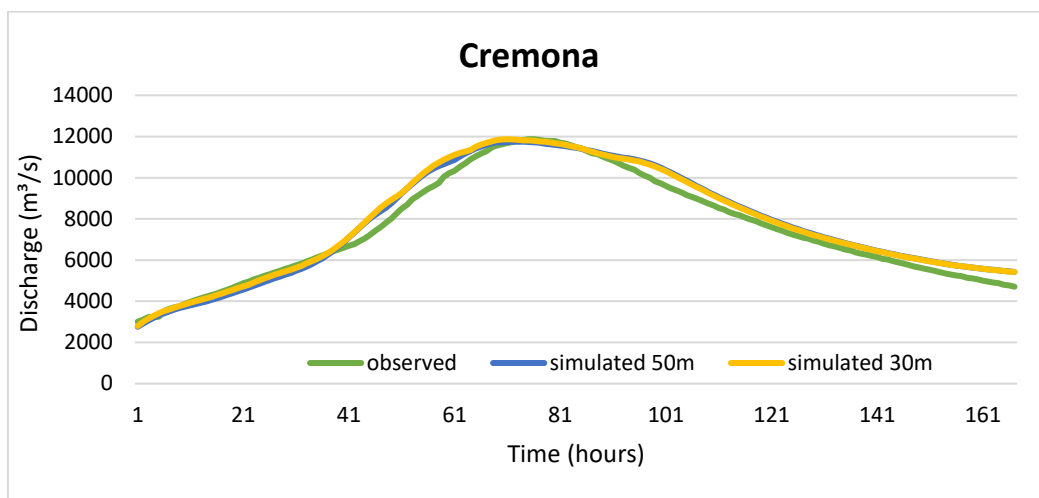


Figure 30. Observed vs. simulated (30 and 50 m DEM with embankment) flow hydrograph at Cremona gauging station.

Looking at the distribution of flow velocities for the two configurations, both of them produce quite similar results, where the difference between 30 and 50 m is about  $\pm 0.5$  m/s. However, their local distribution is an important parameter to consider while evaluating the proximity to the embankments, as it can be of use for the identification of places susceptible to higher erosion/piping rates and hence stability of the levees (Wang et al. 2014; Semar et al. 2011). In Figure 31 we can see that there are some distinctive areas at the main embankment line (in green), where the velocities are the highest (pixels in dark purple and dark blue). Most of such places are located at the outside bend of meanders, where the erosion is expected to be the highest. This provides an indication on potential places where the breaches may occur and the water may propagate into the protected floodplain. The 2D representation of velocity fields brings additional value to 2D modelling of the channel flow, since previously, with 1D models such information was obtained fragmentally (i.e. the velocities captured at 1D cross-sections). Moreover, the velocity values are averaged for each 1D cross-section, therefore there is a risk of underestimating velocities at some critical parts which are either averaged or not captured within the cross-section. Potentially, 2D approach may provide the river management authorities with the tool to develop risk management plans, such as more detailed studies, localised ground

surveys and levee reinforcement at certain places, increase preparedness in the floodplains behind potentially vulnerable portions of the main embankment. For this, the information taken from the large-scale studies can be later used for the smaller-scale investigations, to model the hotspots with the larger amount of details and include morphodynamic component to the set up.

Regarding the computation time, “30m\_embank” (7,441,830 cells) would take about 4 hours to compute, while “50m\_embank” (2,669,920 cells) would be about 1.5 h on average. The simulation time was 191 h and the maximum time step 10 sec.

From all the points mentioned above, we might suggest that using 50 m resolution is a fair compromise between the accuracy (water surface elevations, discharge at Cremona gauging station) and computation time.

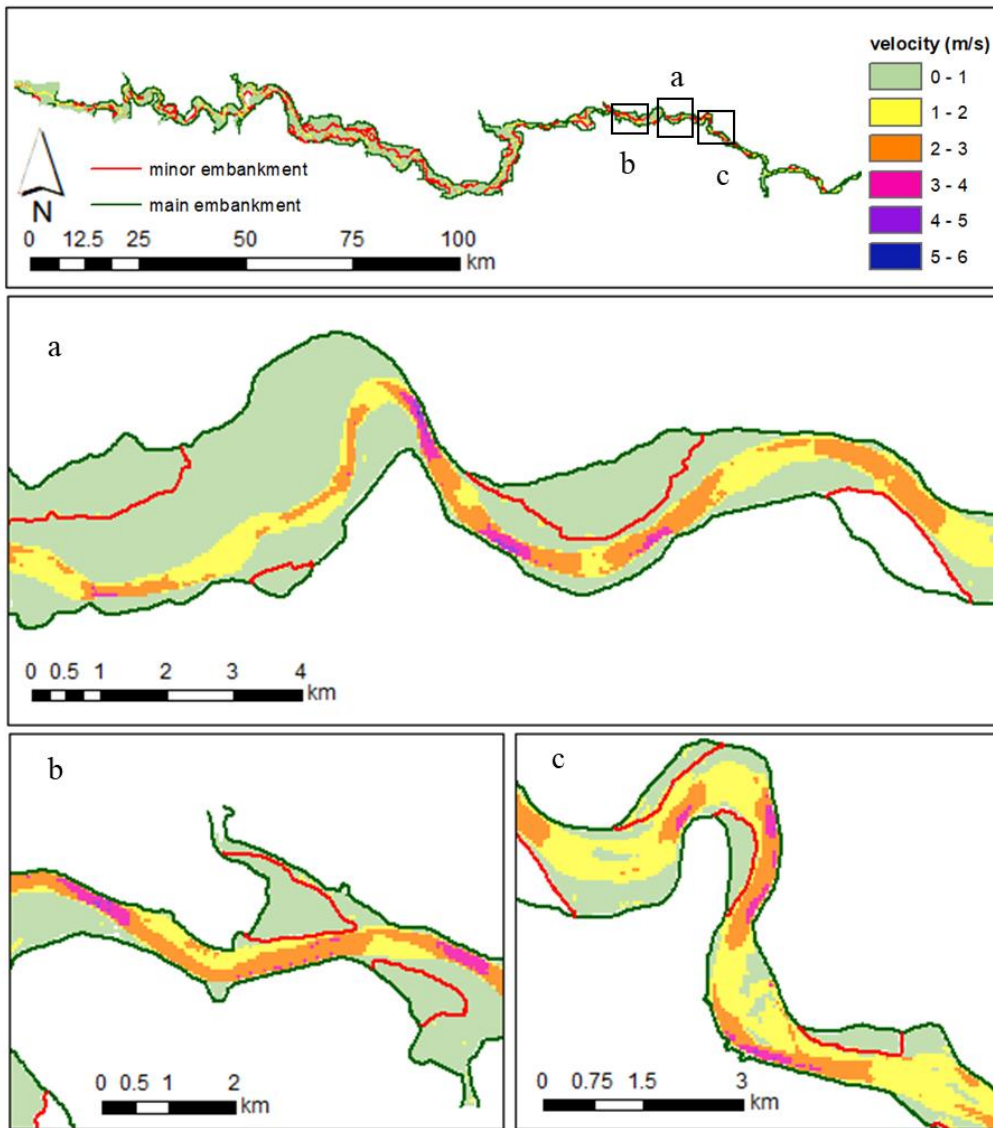


Figure 31. Distribution of local velocities. Zoomed in (a, b, c) examples represent the results of “50m\_embank” configuration.

### 3.4. Conclusion

The review of the previous research (for more details see Chapter 3.1.2) done on the mid-lower portion of the Po River shows that fully 2D inundation modelling has never been implemented earlier and therefore we would like to point out its' advantages. As expected, high-resolution data together with fully 2D model gives favourable results in terms of the flood extent. The analysis of the DEMs of different resolution (30, 50 and 100 m) and configurations (with and without manually added embankment) showed that the performance of the grids with the manually added embankment heights displayed better results in terms of water surface elevations for 30 m and 50 m. Meanwhile, other configurations were disqualified due to incorrect representation of the geometry of the flooded compartment. The inclusion of the actual levee height into the working grids shows the potential of LISFLOOD-FP to perform fully 2D simulations on the mid-lower portion of the Po River and other rivers with largely modified terrain. Moreover, we suggest that regarding the computation time and the accuracy of the results the optimal solution for the large-scale simulations on the mid-lower portion of Po River would be 2D simulations using 50 m resolution terrain data, which includes the actual embankment height. The research showed that the model run on 30 and 50 m resolution DEM produced very similar results in terms of maximum water surface elevations (the RMSE difference was 5 cm between 30 and 50 m resolutions), discharge at control gauging station and distribution of local velocities fields with much higher computation time advantage of 50 m resolution model.

It must be noted, that the results of this study should be taken with a great care, since the model calibration and resolutions used aimed at the specific terrain of the Po River. Despite of the outcome in terms of resolutions (30 m or 50 m), the study clearly showed the role of linear elements (embankments), and the limitations that one has to consider in case of not reproducing the embankments and the real behaviour of the interaction between floodplains of different return period. Therefore, regarding complex terrains and 2D raster-based models, there is a great potential of this approach to be applied on other river catchments with the additional investigation of the terrain configuration and resolutions for each case study. Moreover, 2D modelling provides a spatially complete outlook on the flood hazard parameters (water depth, local flow velocities) within river channel and floodplains, which of a specific interest for river system behaviour studies and flood management plans. The identification of the hotspots made in one simulation can provide a solid basis for the upgrade of the flood risk maps as required by the Floods Directive 2007/60/EC.

In addition, 2D modelling on the large-scale does not only allow for long-term plan development but also greatly benefit quick solutions needed in the emergency situation. Since LISFLOOD-FP model is fairly easy in its application and computationally very

efficient, as was proven by the current case study and numerous previous research, we suggest that this modelling approach is a step up in large-scale simulations on the Po River.

Further research on the Po River should consider investigating the distribution of the local hazard parameters (water depth, velocities) along the reach regarding different occurrence intervals of the flooding events (e.g. 100, 200, 500 years) and possible levee failure scenarios in order to estimate residual risks.

# Chapter 4. Levee Breaching: a New Extension to the LISFLOOD- FP Model

## 4.1. Introduction

Global warming under different socio-economic scenarios would lead to increasing flood risk in Europe and without further adaptation, flood defence structures will be breached more frequently in the future (Alfieri et al. 2017). Therefore, development of new strategies for flood risk reduction is crucial. As a primary element in this, flood hazard modelling encompasses reproduction of the hydraulic behaviour of flood water and its interaction with topographical features and engineering structures in the floodplain. Such structures may partially or entirely control the flood dynamics, which is especially evident in heavily modified terrain with complex networks of levees and embankments. Therefore, it is important to identify flooding patterns in case of possible levee breaches for both low- and high-intensity events.

Levee breaches may occur due to different mechanisms such as overtopping, geohydraulic failure or piping, and local and global static failure (Vorogushyn et al. 2009; Marijnissen et al. 2019). Such failures involve a complex pattern of possible consequences for river systems (van Mierlo et al. 2007; Bruijn et al. 2016). Protected floodplains remain vulnerable in case of embankment breaches, which is often termed the residual risk (Ludy and Kondolf 2012; Domeneghetti et al. 2015). For instance, the 1993 Mississippi flood, when the levees breached at numerous locations along a rather large reach of the river causing 32 deaths and \$15 billion in economic damage (Larson 1996). Alongside record events in terms of their magnitude, floods with much lower recurrence interval may cause significant

losses. For instance, a 5-year return period flood on the Secchia River (Northern Italy) in 2014 turned into a disaster, when the levee breached due to burrowing animals causing €400 million in monetary damages (Carisi et al. 2018). Together with severe damage, human losses and infrastructure disruptions due to sudden lowering of the embankment crests, levee breaches may reduce hydraulic loads upstream and downstream, and hence affect inundation patterns and the probability of failure elsewhere in the river system (van Mierlo et al. 2007; Vorogushyn et al. 2018)

Despite the obvious adverse effects of levee failures, there are other additional strategic aspects to consider. One flood management strategy is controlled flooding (activation of off-line floodplain storage) (Sanders et al. 2006). Therefore, it is important to have an understanding of how floods behave on a basin scale and which floodplains it is sensible to activate in a given flood scenario. For this it is important to jointly assess levee breach effects, both adverse and beneficial on the large scale (Vorogushyn et al. 2012).

There are numerous tools that offer a levee breach component to simulate floods (e.g., HEC-RAS, Delft3D, RFSM, Tuflow, TELEMAC2D, Sobek, BREACH, BASEMENT, 2DEF, PARFLOOD to name a few, see e.g. (Castellarin et al. 2011b; Viero et al. 2013; Wu 2011; Dazzi et al. 2019)). They allow for simulating the breach with a high level of detail and consider the breach evolution and forcing conditions in order to compute changes in the breach width and consequent flow entering the floodplain. Some associated uncertainties are flow conditions, geotechnical embankment properties and variability of external forces (Wu 2011; Dazzi et al. 2019). Moreover, other limitations related to the usage of those models, such as data availability, set up time and computational costs, pose a significant constraint. This especially becomes a critical burden when generating the levee breaching scenarios for large-scale studies. Some studies (Kamrath et al. 2006; Viero et al. 2013; Vorogushyn et al. 2010; Castellarin et al. 2011b) suggest using coupled 1D/2D interactions between the river channel and floodplain behind the embankment. Kamrath et al (2006) applied this method, where the river-floodplain interactions are limited to a straight river reach and two adjacent floodplains. The 1D/2D schematisation has obvious benefits over fully 2D codes, such as decreased computational time and accuracy. 1D/2D model set up and preparation is, however, is rather a time consuming task especially for large-scale studies.

The literature proposes several fully-2D models which allow for simulation of levee breaching (Wu 2011), however, to the best knowledge of the authors, the number of computationally efficient tools which allow for simplified levee breach at minimum setup/data/time costs, possibly over very large geographical areas, is rather limited (including the models mentioned above). With the increasing availability of high-resolution geodata (including bathymetry datasets) and improved computational performance, the use of 2D models to simulate events of different intensity becomes a real possibility for large-scale studies. Previous work has explored levee breaching using the well-known

LISFLOOD-FP model, which is known to be suitable for large scale studies and is computationally efficient. The study of Luke et al. (2015) discussed the river system behaviour and floodplain activation using the model, however the outputs were reached by performing coupled consequent simulations (i.e., modelling cascade; meaning, the model would be run before the breach, then another simulation with modified/"breached" DEM would be needed to mimic the breach). Another study, where the LISFLOOD-FP 2D module was used was Mazzoleni et al. (2014). In this study, the channel 1D flow and consequent levee breach were first simulated by the 1D HEC-RAS model and the floodplain propagation was then performed by the computationally efficient LISFLOOD-FP. HEC-RAS 1D simulation outputs in that study served as the inputs for the 2D computations. Such studies brought credible outcomes, however, would require additional time and effort to reproduce the whole chain of the levee failure. Since backflow from floodplain into the river channel was not considered, such a modelling cascade does not include the impact of backwater effects on system behaviour.

This study presents a newly developed extension to the LISFLOOD-FP model which allows levee-breach analysis on local or large scales (breach at one or multiple locations) in fully 2D mode. The approach permits flow dynamic tracking along the entire reach performed in one single simulation thereby giving the possibility to capture backwater effects and account for the effect of hydraulic interactions. Unlike most codes, where the links between the channel and floodplain are typically described by 1D/2D hybrid model, the new sub-routine represents these links in fully 2D mode. 2D representation would be particularly beneficial in the case when levees are located away from the river banks, which is a limitation for certain 1D/2D codes. If the levee course shows sudden contractions or widening, which is described by the 1D cross-sections, this adversely impacts 1D model stability. Moreover, the LISFLOOD-FP model is known for its computational efficiency and accuracy in representing flow parameters, which is particularly relevant for geographically large domains (Bates et al. 2010). Whilst implemented in LISFLOOD-FP, the approach is generic and could be used in any 2D structured grid model.

The objective of this Chapter is therefore to illustrate the newly developed levee breaching extension and its performance potential for the large-scale studies. We deliberately investigate the model behaviour on synthetic test cases and two historical events. We test on synthetic cases and compare them against identical setups of well-known HEC-RAS 2D model. The first historical event is a small-scale flood which occurred on the Secchia River. It is used to test the model sensitivity to its parameters and input data. The second historical event is a large-scale high-magnitude catastrophic inundation, which took place in 1951 in a large levee-protected floodplain of the lower reach of the Po River. These data are used to assess the model potential to perform geographically large-scale simulations. In this light, we assess the computational efficiency of the new tool and discuss possible limitations and broad areas of application.

## 4.2. Methods

### 4.2.1. Levee breach module

LISFLOOD-FP is a simplified hydrodynamic model based on the local inertial formulation of the shallow-water equation (Bates et al., 2010). For further details see Chapter 2.2.2. The model has been extensively validated for gradually varying flow problems on floodplains (Neal et al. 2012b) and includes basic structures such as weirs and 1D channel models.

In this study we propose a new levee breach module, which simulates outflow discharge into the protected floodplain subject to levee failures. The levee breach module is directly implemented within the LISFLOOD-FP code and is consistent with the raster-based model structure. The levee breach module is designed to simulate levee failures triggered by overtopping, however, the parameters can be set up in a way that the module may enable the “manual” levee breaching (when the water level is lower than the levee crest). Our main goal was to make the pre-processing simple, yet sufficient to represent the required levee failure triggers. The possible breach locations are pre-defined by the modeller at the setup stage.

The computational sub-routine evaluates two simple breaching conditions: (i) water levels exceed threshold height and (ii) water levels stay above threshold for a defined amount of time. The procedure of breach initialization and subsequent water flow simulation is schematically shown in Figure 32:

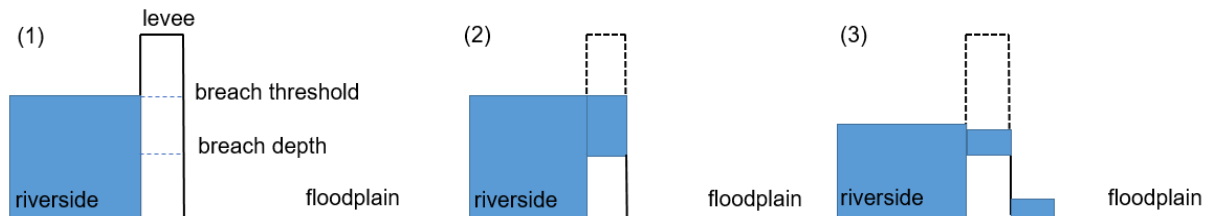


Figure 32. Orthogonal cross-sections of the levee and breach schematics: (1) water level in the river reaches the breach threshold (user defined); (2) the breach is fully formed reaching the breach depth (user defined); (3) outflow from the breach starts inundating the floodplain (equations (14) or (15)).

The following parameters need to be specified for the initiation of a breach: breach location, breach threshold, duration threshold and breach depth relative to the crest height. These parameters are further discussed in more details.

- Breach location is specified by x and y coordinates of a grid cell where breach may occur. For this, the levee needs to be explicitly represented in the input DEM with the corresponding location and height.
- Threshold level is the water level in meters which needs to be exceeded for breach initiation.

- Duration threshold is the time in seconds during which the threshold water level at the levee is exceeded.
- Breach depth is the depth in meters in relation to the levee crest height assigned upon the breach initiation. The levee breaches instantaneously, i.e. once the breach conditions are met, the breach depth is set to the pre-defined value.

If the breach conditions are fulfilled, the levee breach at the pre-defined location is simulated. The outflow discharge is calculated using the broad-crested weir equation:

$$Q = C * L * H^{1.5} \quad (14)$$

Where,  $C$  is a weir flow coefficient,  $L$  is levee breach width (m) and  $H$  is the energy head upstream (m) (Chow 1959). In a simplified form, the water depth above weir crest upstream of the breach is considered instead of energy head. The numerical stability of the sub-routine is mainly controlled by the modular limit (user-defined value), which automatically switches between the free flow over a broad-crested weir (Eq. 14) and the drowned weir flow (Eq. 15):

$$Q = C * L * hu * \sqrt{\frac{hu-hd}{M}} \quad (15)$$

Where  $hu$  and  $hd$  are water depths above the weir crest upstream and downstream from the breach, respectively, while  $M$  is modular limit. The value of  $M$  is selected by the user and is constant for the course of simulation. The typical range depends on the head upstream (water height relative to the bed elevation) and the final elevation of the breached embankment (White et al. 2000).

Weir equation (Eq. 14) is the most common approach to simulate flow through dike breaches (Wu and Li 2017). This approach is mass conservative, but no momentum transfer from the channel into the floodplain is considered.

The minimum breach width for one grid cell is equal to the input DEM cell width. In case, the specified breach width is larger than the input DEM resolution, the required amount of neighbouring cells must be specified as potential breach cells including both threshold parameters and breach depth.

The current configuration uses a simple set of conditions with which failure due to various breach mechanisms can be mimicked. For instance, in case of overtopping, the user can specify the breach threshold height at the levee crest. Further, the duration threshold of overtopping flow can be set. Once a failure occurs, the breach depth defined by the user is reached instantaneously. Failure due to piping/erosion (“manual” failure) can be mimicked by adjusting the breach threshold height and duration. For the reconstruction of historical events, if the time between the start of the piping process and the collapse of a levee is known, the duration threshold can be set accordingly.

We assume that the ultimate breach width has a larger impact on hazard characteristics than the width development rate, in particular for large-scale studies; this is a common assumption that has been adopted elsewhere, e.g. Vorogushyn et al. (2010).

### 4.2.2. Synthetic test description

In order to evaluate the performance of the levee breaching module, we set up a series of synthetic tests. As the reference for these tests, we perform simulations with the 2D model set up using HEC-RAS (version 5.0.3, Brunner 2016). It uses either the full momentum shallow water equation or a diffusive wave approximation; for our tests we selected the first approach as recommended in Brunner (2016). HEC-RAS has proved to be a reliable tool to simulate hydraulic processes within river channels and floodplains (water surface elevations, velocities, arrival time, etc.), including representation of various hydraulic structures (dams, levees, bridges, culverts, etc.). It allows flow parameters to be obtained with a high level of accuracy and detail (Brunner 2016; Shustikova et al. 2019). Levee breach simulation with HEC-RAS was undertaken in numerous studies (Mazzoleni et al. 2014; D’Oria et al. 2015; Castellarin et al. 2011b). The flow through the breach is calculated using a broad-crested weir equation (same as used in the presented module) (Brunner 2016). The 2D breaching link is represented as a lateral structure which connects both 2D areas, riverside and floodplain. For this, we specify a synthetic terrain model, inflow discharges and downstream boundary conditions (Figure 33 and Figure 34). Another relevant distinction is that HEC-RAS simulations were found up to 20 times slower than LISFLOOD-FP runs using the same resolution and domain size (Shustikova et al. 2019).

Synthetic tests for HEC-RAS and LISFLOOD-FP models were built to compare the breach outflow on a simple terrain. The synthetic DEM was designed to include a river channel with an adjacent floodplain, a levee (5 m crest height) and the floodplain behind the levee (Figure 33).

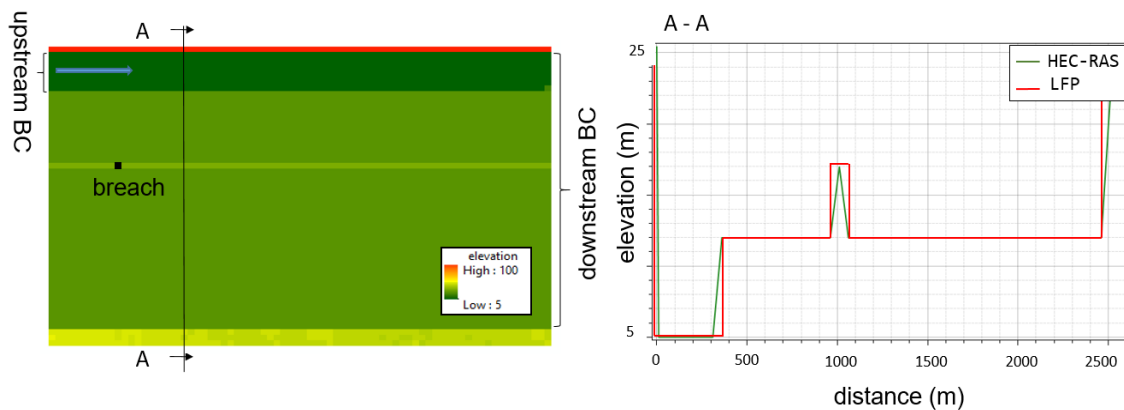


Figure 33. Synthetic DEM with boundary conditions (BC) used in both models (left); terrain cross-sections as reproduced by HEC-RAS and LISFLOOD-FP (LFP) from north to south (right).

While LISFLOOD-FP operates with a spatially uniform square mesh, which is at the same resolution as input raster grid, HEC-RAS internally processes terrain data into a Triangulated Irregular Network (TIN) file thus making slopes smoother. Therefore, the terrain profiles look different (See Figure 33) and this may influence the flow propagation. The parameterization of the breach module is set as follows: breach threshold is set to 2 m below the levee crest height, duration threshold equals to 10 seconds, breach depth was set to 2 meters, and the modular limit equals 0.5.

Several simulation runs using different roughness coefficients in the range 0.03 - 0.1  $\text{s/m}^{1/3}$ , with sampling step of 0.01  $\text{s/m}^{1/3}$  were performed. The model inflow hydrograph (Figure 34) was generated in such a way that in the absence of a breach the flood waters would not overtop the levee. The simulation time was set to 35 h with 3 s time step.

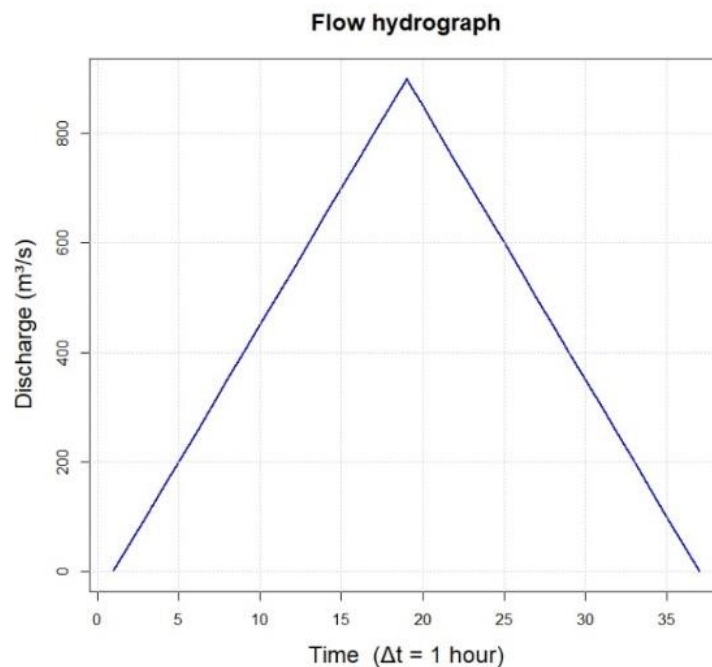


Figure 34. Flow hydrograph used as an upstream boundary condition for the synthetic tests.

We compared LISFLOOD-FP and HEC-RAS performance in terms of the breach outflow i.e. hydrograph shape and the peak flow differences. To improve model stability, the maximum Froude number was set to 1 for LISFLOOD-FP simulations, meaning the model is limited to subcritical and critical flows in this and all subsequent cases.

### 4.2.3. Secchia inundation

In addition to synthetic test, we used the new LISFLOOD-FP module to simulate a historical flood event that occurred on the Secchia River (right bank tributary of the Po River) in January 2014. This case study was selected to test the sensitivity of the model parameters. During this event, approximately 50 km<sup>2</sup> of the protected floodplain was

inundated as a consequence of a levee breach, causing a damage in excess of 400 million Euro and 2 fatalities. The water level at the levee did not exceed the design return period, so the levee was not overtopped. Post-event surveys concluded that the levee failed due to the lack of maintenance and burrowing animal activity, which resulted in erosive processes and followed by a lowering of the crest (Orlandini et al. 2015). The final breach depth reached the ground level. The full breach evolved within 9 hours and reached 80 m in width (Figure 35). The total outflow volume was estimated around 39 million m<sup>3</sup> (Vacondio et al. 2016).

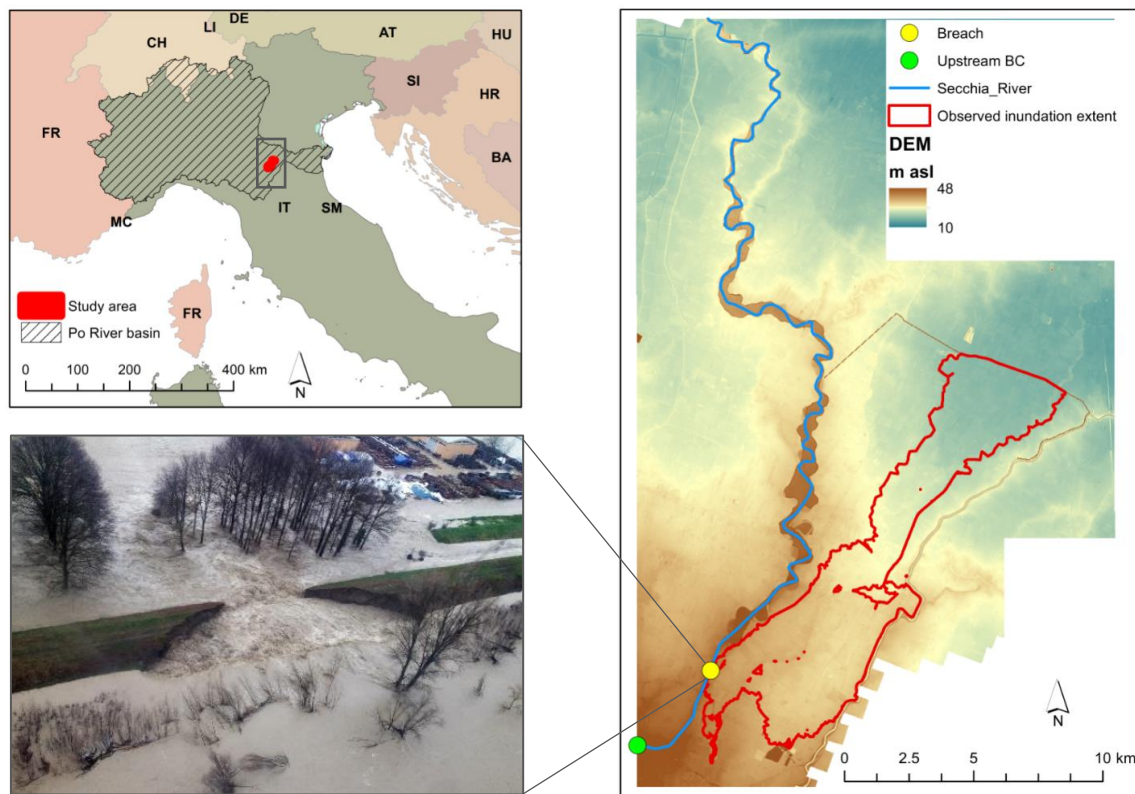


Figure 35. Study area of the Secchia flood: the location of upstream boundary condition (BC), the river channel, breach and floodplain (upper left and right panels). The photograph of the breach during the event (down left) (taken from Vacondio et al. 2016).

In this test we aim to reproduce the 2D flow within the Secchia River channel, breach and consequent inundation of the initially dry floodplain (Figure 35). We use a LiDAR DEM of 1 m resolution which represents the bare earth terrain with buildings and vegetation removed. It includes the bathymetry of the river bed and levees with a vertical accuracy of  $\pm 0.15$  m. We aggregate the DEM to 25 m horizontal resolution, using the mean value of the 1 m pixels. The levee is represented by ‘burning’ it into the 25 m DEM, i.e. the actual levee crest elevation is assigned from the 1 m LiDAR data to respective cells of the aggregated DEM. The resulting number of raster cells in the model domain was about 888,000. Additionally, we ‘burnt’ in an embankment downstream from the breach (northern part of

the domain) into the DEM, where the flood accumulated due to the elevated ground, as was reported by the post-event survey (D'Alpaos et al. 2014). The relief of the study area is characterised by highly heterogeneous terrain with a complex network of irrigation canals and embankments.

The upstream boundary condition for the Secchia River is assigned ca. 5.5 km upstream from the breach, where a gauging station is located (Figure 35). The input hydrograph at this location was obtained from Vacondio et al. (2016). The event simulation time was 100 hours with a maximum time step of 5 seconds. Downstream boundary condition was set where the Secchia River conflues with the Po River and set as a free boundary.

We identified the breach location from the post-event surveys and assigned corresponding three cells in the LISFLOOD-FP meaning the breadth equalled to 75 m (observed width was 80 m). The breach depth was assigned to reach the ground level. Because the breach was caused by an erosive processes, not overtopping, we adjusted the flood breach time manually according to historical observations. The levee failure extension was settled in order to reproduce the failure when the hydraulic condition (i.e. water level) within the river was equal to observations.

We investigated the sensitivity of the LISFLOOD-FP model to different modular limits. Additionally, we looked into the interaction between different values of the modular limit and the floodplain roughness coefficient in the area immediately behind the breach. Altogether we ran 135 simulations of all possible configurations of modular limit (0.1, 0.2... 0.9 s/m<sup>1/3</sup>) and floodplain roughness coefficients (0.03, 0.035, 0.4 ... 0.1 s/m<sup>1/3</sup>).

The performance of the model simulation was assessed by comparing the simulated and previously estimated outflow discharge by Vacondio et al. (2016) using the Nash-Sutcliffe model efficiency coefficient (NSE):

$$NSE = 1 - \frac{\sum_{t=1}^T (Q_m^t - Q_o^t)^2}{\sum_{t=1}^T (Q_o^t - \bar{Q}_o)^2} \quad (16)$$

Where,  $Q_m^t$  is simulated outflow,  $Q_o^t$  estimated outflow and  $\bar{Q}_o$  is the sample mean of estimated outflow at each time step. The river bed was assigned a calibrated Manning's n value of 0.015 s/m<sup>1/3</sup>.

Another aspect of model performance that we tested once the model was calibrated was the ability to reproduce the inundation boundary and water depth in the floodplain behind the breached levee. For this purpose, we looked into previous research and post-event surveys done to describe and analyse this event. In particular, we referred to the flood extent estimated in Carisi et al. (2018). Carisi et al. (2018) reconstructed the event reaching 90% Critical Success Index (CSI, see eq. (13)). This data was used as a benchmark to evaluate the simulated inundation extent. We selected the CSI (Eq. 13) to assess the match of the simulated and observed inundation extent.

Additionally, we looked into the spatial distribution of water depth at available control points, which were obtained from the field surveys done by the local municipalities and publicly available photographs of the water and wreck marks. Such measurements are known to be prone to errors, which could reach up to 0.5 m (Horritt et al. 2010a). All together there were 46 such control points, which are mostly located within the towns of Bastiglia and Bomporto. We analysed the ability of the models to predict these water elevations using Root Mean Square Error (RMSE). These and all consequent simulations were performed on a server with 2 CPUs having 20 real cores and hyperthreading 40 cores.

### 4.2.4. November 1951 Polesine catastrophic flood of the Po River

In order to test the LISFLOOD-FP model on more extreme events for geographically larger areas and evaluate its computational efficiency and accuracy, we simulated the catastrophic Polesine riverine flood, which occurred in November 1951 on the Po River (Northern Italy). During this event, an unusually massive rainfall generated extreme discharges in the Po river reaches (Viero et al. 2019). About 50 km upstream from the river mouth (at the Pontelagoscuro gauging station, see Figure 36), the left levee of the main channel was overtopped and then eventually breached at 3 different locations. The ultimate breach width reached the width between 200 and 300 m (See Figure 36).

The flood waters inundated over 1000 km<sup>2</sup> of protected floodplain, eventually reaching the shore of the Adriatic Sea. The event caused 114 deaths, long lasting population displacement, about \$7.8 billion monetary losses (in 2018 dollar values) and catastrophic impact on local ecosystems (Viero et al. 2019). Recent studies by Masoero et al. (2013) and Viero et al. (2019) together with historical reports provide an overview of the event. For the LISFLOOD-FP model setup, the upstream boundary condition was generated based on the report by SIMPO (1982), while some of the breaching parameters were retrieved from Masoero et al. (2013), who specified the location of the three breaches and their final width. The latter values were 220, 204 and 312 m, which in our set up were represented as breaches of 250, 200 and 300 m wide respectively. The reconstruction of the terrain data corresponding to the state of 1951 is challenging given that anthropogenic changes in the years after the event have triggered land subsidence of up to 3 meters in the coastal part of the model domain (Viero et al. 2019). However, the study of Carisi et al. (2018) pointed out that manmade alterations that mostly influence flood hazard over large floodplains are generally linear infrastructures. Viero et al. (2019) reports that some of the embankments were raised and new embankments were constructed in the aftermath of the event. We use terrain data from 2004 (river channel bathymetry) and 2011 (floodplain) survey (both datasets are provided by the Po River Basin Authority, [www.adbpo.it](http://www.adbpo.it)). We resampled 2 m resolution LiDAR data to 50 m resolution DEM and imposed the actual height of the embankments taken from LiDAR survey onto the resampled DEM.

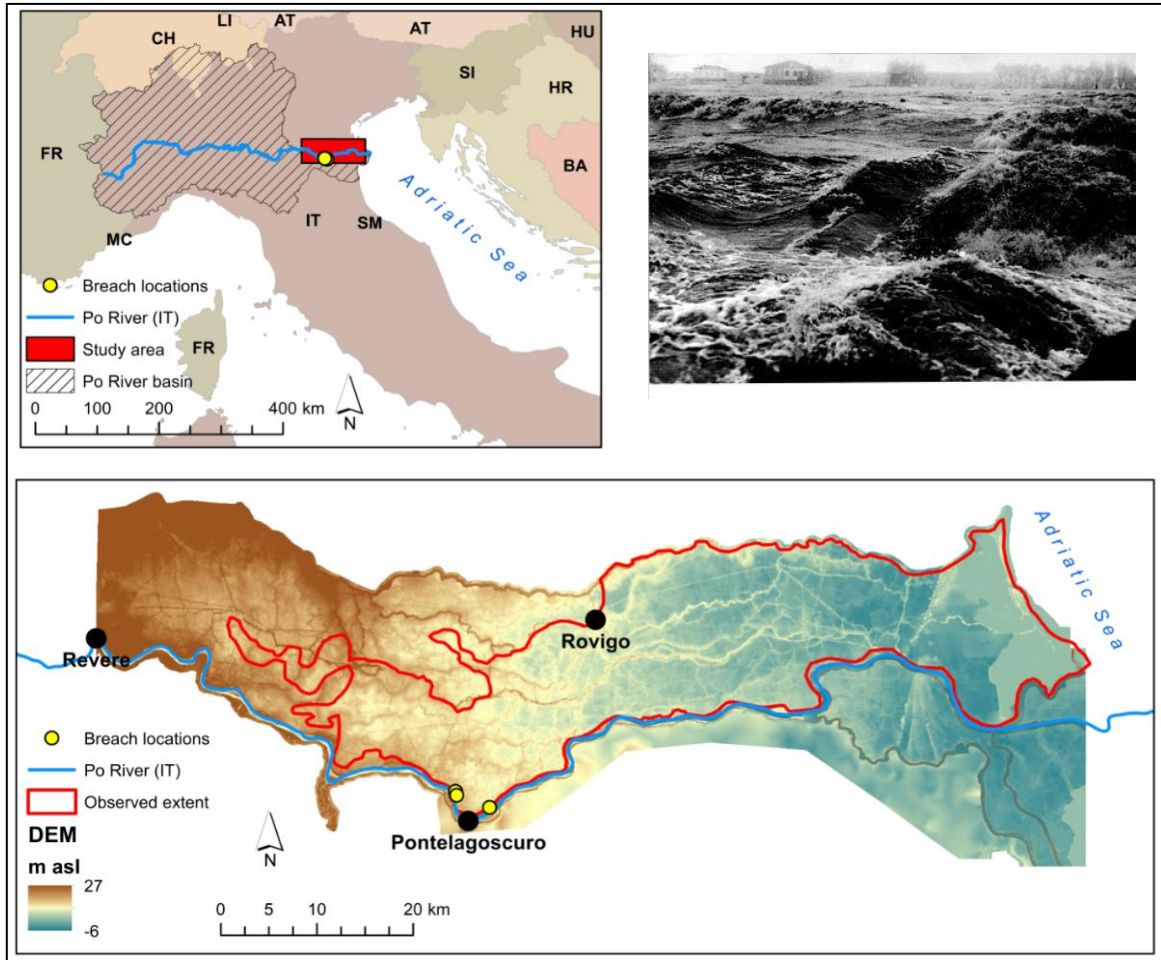


Figure 36. Polesine flood study area (upper left). Photograph of the flow through one of the breaches during the event (upper right). Study area extent and the outline of the surveyed flood extent (lower).

In this approach, the effect of the linear structures (embankments) on the flow propagation within the main channel is explicitly considered. Since we use the terrain data including levee locations which do not exactly correspond to the state of 1951, we expect certain dissimilarities, especially in the areas around newly built embankments. Because the exact levee geometry could not be reproduced due to differences in terrain between the event occurrence (1951) and data acquisition (2011), we set up the model according to the current elevations (2011). This means that the crest height, the breach depth relative to crest height and adjacent bathymetry were as of 2004/2011. We simulate the Polesine flood event in the fully 2D mode on the domain of over 4000 km<sup>2</sup>. Same as for the Secchia event study, we model the whole chain of the event including the 2D river flow, levee breaching, weir overflow and subsequent floodplain inundation. The upstream boundary condition is set up at the Revere gauging station (Figure 36), while downstream was at the Adriatic Sea. First, we calibrated the model against the reported discharge values at the Pontelagoscuro gauging station (SIMPO 1982) using a spatially uniform channel roughness coefficient where the breaches are not considered in the simulation. Afterwards, we set up the

breaching locations and widths as reported in Masoero et al. (2013). The threshold height is set to the levee crest height and the failure occurs instantaneously. The breach time was adjusted to allow simultaneous breach at all 3 locations. The floodplain was given a uniform roughness coefficient of  $0.05 \text{ s/m}^{1/3}$ . The simulation duration was set to 348 hours, of which first 61 hours were a warm-up with a maximum time step of 5 s. The breaching depth was set to 7 m at all locations and the modular limit of 0.5 was selected by trial and error in order to let the simultaneous breach at all indicated locations. The approximate extent of the flood is known from the previous studies of Viero et al. (2019), which is reported to have 88% accuracy (CSI). This data is used here to evaluate the model performance using CSI (Eq. 13).

### 4.3. Results

#### 4.3.1. Synthetic tests

In the synthetic tests, the breach occurred for simulations where the roughness coefficient of the floodplain was more than  $0.05 \text{ s/m}^{1/3}$ . For lower roughness coefficients the breach was not activated because the triggering hydraulic conditions were not met. The shape of the outflow hydrographs is similar for both models for all roughness coefficients (Figure 37). In LISFLOOD-FP simulations the breach occurs about 1 hour later than in HEC-RAS. The absolute difference in the discharge peaks is rather insignificant, considering the inflow discharge. For  $n = 0.05$  and  $0.06$  the LISFLOOD-FP peak is 7% lower than HEC-RAS, whereas for  $0.07$ ,  $0.08$ ,  $0.09$  and  $0.1$  both models perform identically for this parameter (difference is less than 1%). The computation time for LISFLOOD-FP simulations was 9 times faster than for identical setup of HEC-RAS.

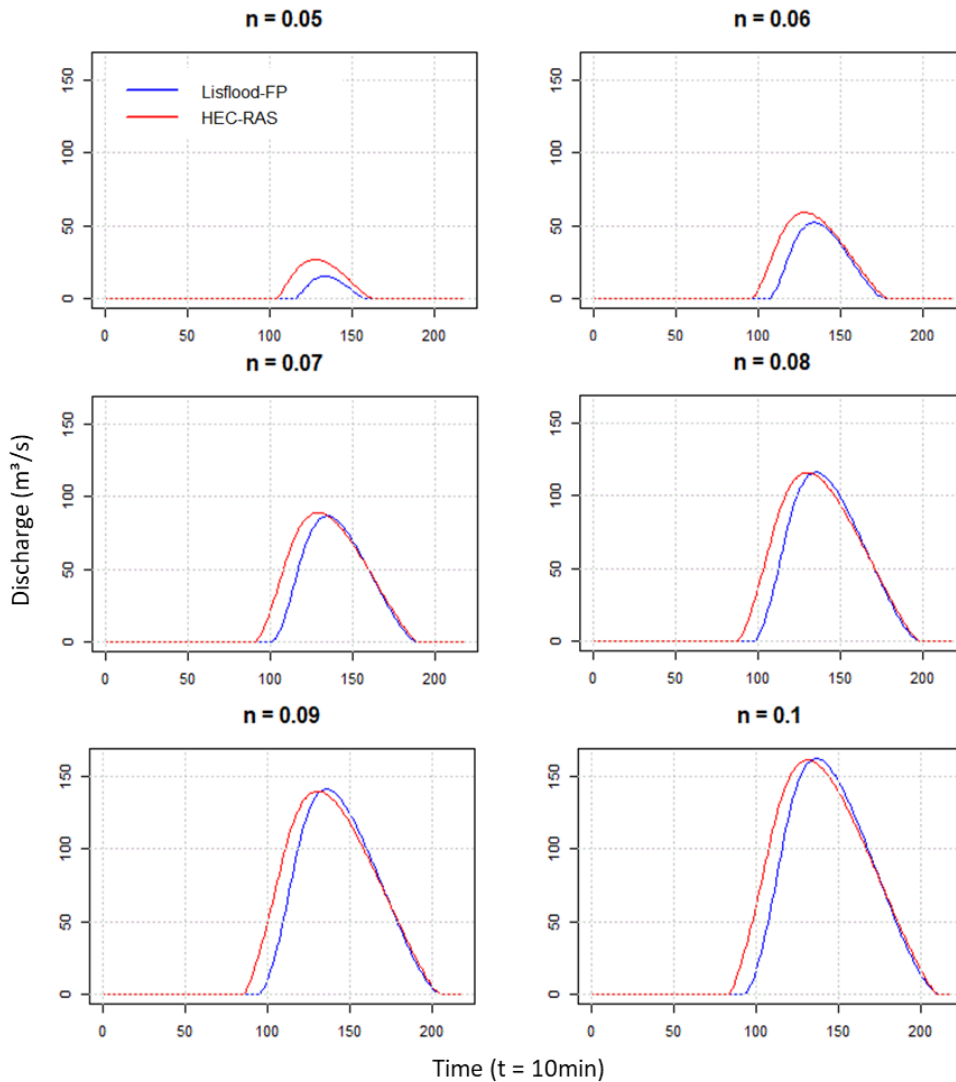


Figure 37. Flow through the breach simulated by HEC-RAS and LISFLOOD-FP, unsteady boundary conditions.

### 4.3.2. Secchia inundation

As outlined in the Methods section (Chapter 4.2.), the aim of this case study was to analyse the performance of the breach module on a complex terrain for a historic event and explore the sensitivity to various model parameters. In Figure 38 the performance with regards to the simulated outflow is evaluated depending on the roughness coefficient and modular limit. The outflow discharge is more sensitive to variations in the roughness parameters compared to variations in the modular limit. The difference between NSE values obtained for the set of modular limits within each roughness coefficient (i.e. modular limits 0.1 – 0.9 run with 0.03 s/m<sup>1/3</sup>) are in range of 0.05-0.07. Whereas, the variation of NSE for different roughness coefficients and same modular limit is in range of 0.32 (as a

maximum value). The NSE slightly increases for lower Manning values, becoming nearly stable at  $<0.025 \text{ s/m}^{1/3}$ . For lower roughness values ( $<0.015 \text{ s/m}^{1/3}$ ) LISFLOOD-FP becomes numerically unstable in calculating the flow leaving. As can be seen from Figure 38, there is a pattern change when the modular limit is 0.1 for most of the roughness coefficients.

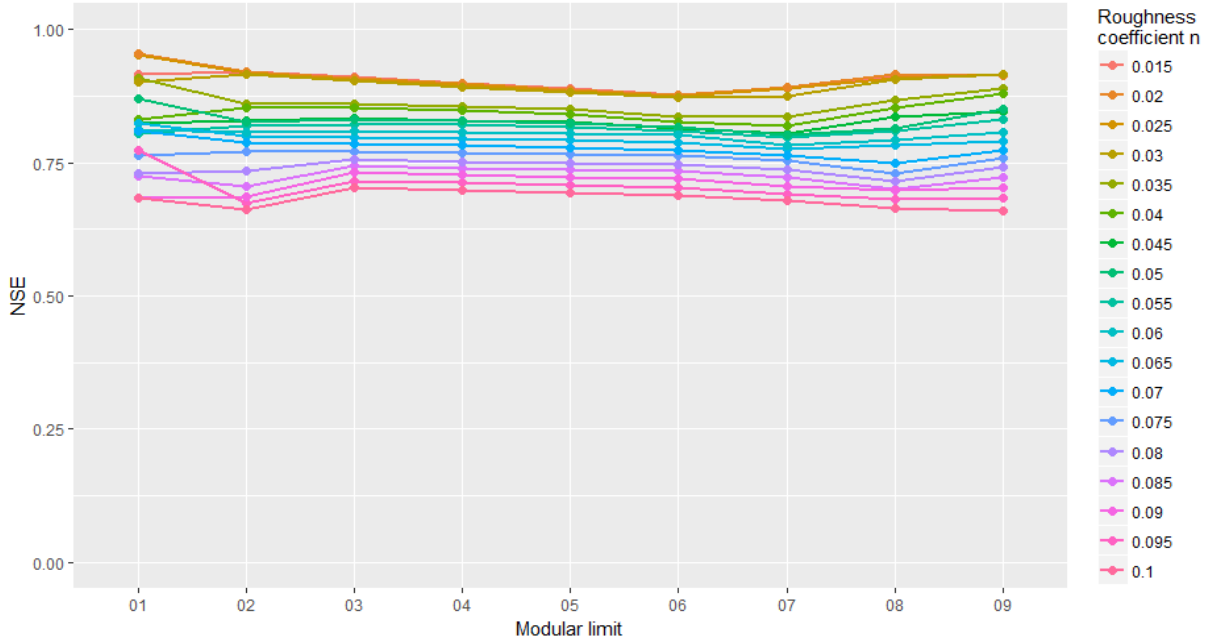


Figure 38. NSE values for each configuration of modular limit and roughness coefficient  $n$ .

Among all simulations the best NSE value was obtained from the configuration where the modular limit was set to 0.1 and floodplain Manning value  $n = 0.025 \text{ s/m}^{1/3}$  (See Figure 38). For this combination, the NSE coefficient reaches 0.96. Because the modular limit value is constant in each simulation, this seemingly low value (0.1) compensates for effect of changes in the upstream head over the event. Therefore, we select this configuration for further analysis. The overall volume of water leaving the breach in the selected simulation run was about 7% higher than estimated (which is 42 and 39  $\text{m}^3/\text{s}$  correspondingly). The CSI value for the best calibrated run was 64%, which shows the ability to reproduce the inundation extent (See Figure 39).

The RMSE values of observed and simulated water depths at 46 points is 0.84 m (See Figure 39). Horritt et al. (2010a) reports that post-event surveys of flood water marks might have up to 0.5 m vertical error. The resulting RMSE is close to the observational error. Concerning the computation time, it took a little over 3 minutes to run one simulation (on a server with 2 CPUs having 20 real cores and hyperthreading 40 cores).

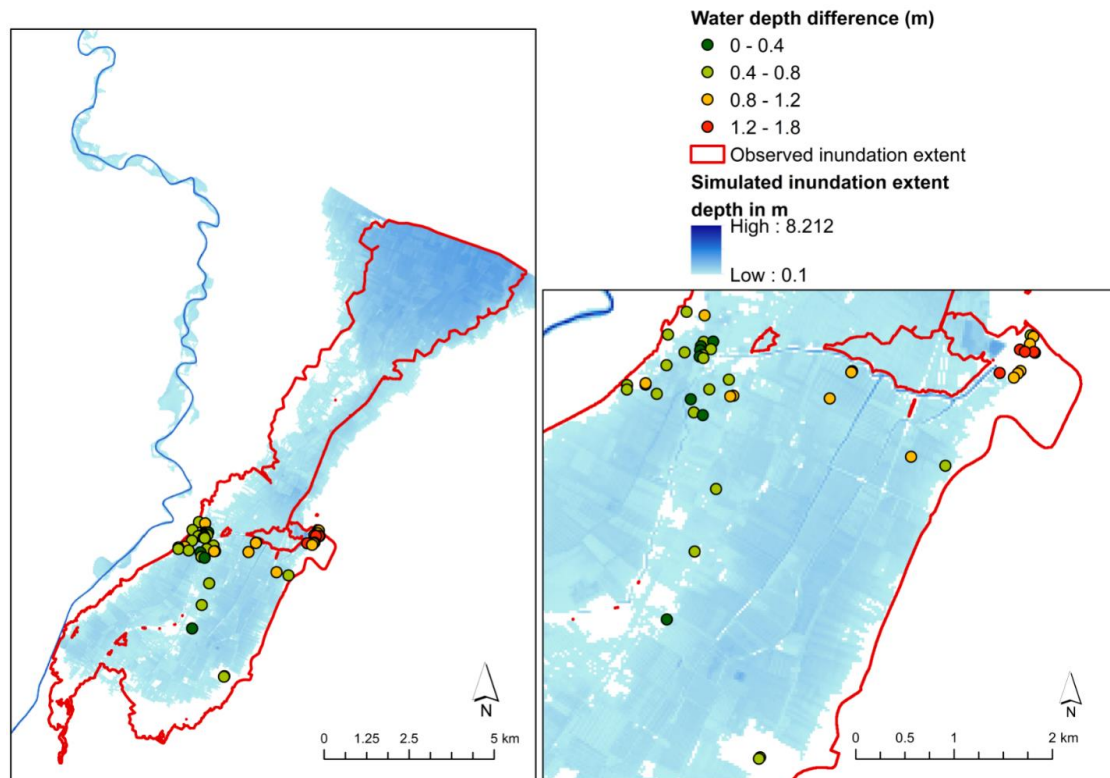


Figure 39. Simulated (blue) and observed (red) inundation extent

### 4.3.3. November 1951 Polesine catastrophic flood, Po River

The simulations of the Polesine flood on the Po river showed that the model is able to correctly simulate the simultaneous breach of all 3 locations at the time reported by Viero et al. (2019). Due to the lack of the data on the flow leaving through the breach into the floodplain and the shape of the outflow hydrograph, we evaluated the model performance based on the inundation extent, for which more studies (i.e. Masoero et al. 2013; Viero et al. 2019) are available. As can be seen from Figure 40, the propagation of the flood water eastwards is correctly captured by the model, which resulted in 83% accuracy in terms of the CSI for the overall flood extent compared to the surveys.

The computational time of one simulation of 348 hours and over 1,620,000 cells of the input domain with a maximum time step of 5 s was about 50 minutes.

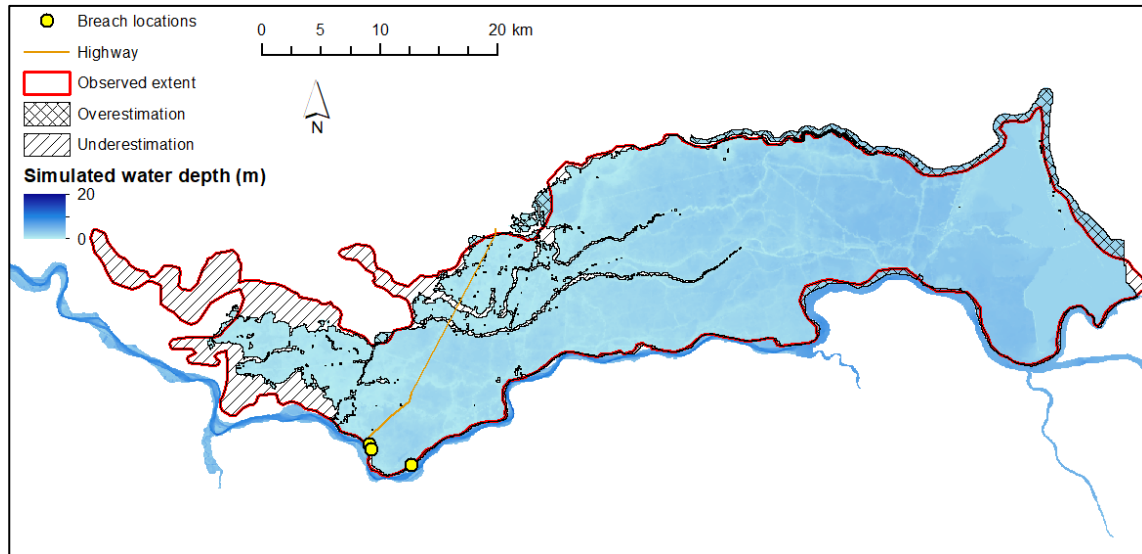


Figure 40. Results of the Polesine flood simulation. Maximum water depth at each cell and surveyed flood extent.

## 4.4. Discussion

The new levee breaching sub-routine of LISFLOOD-FP was tested on a number of synthetic and real case scenarios.

### 4.4.1. Synthetic cases

First, we have identified that our subroutine behaves similarly to the breach module of the HEC-RAS 5.0.3 model under synthetic conditions. Outflow hydrographs using various roughness values had similar patterns in the two models. The peak flow differences were less than 1% for most of simulations. Largely because the same equation is used to calculate the flow leaving through the breach (see Methods section, Chapter 4.2.). The slight differences between the two models might be explained by their rather different formulations used to calculate floodplain flow (inertial formulation of the shallow-water equation in LISFLOOD-FP and full momentum equation in HEC-RAS) and correspondingly different peak flow in the hydrograph in main channel.

For unsteady flow simulations (triangular hydrograph, Figure 34) we obtained a definite pattern, where under identical set ups and breaching conditions, the levee fails about an hour later for all simulations in LISFLOOD-FP compared to HEC-RAS. This is due to the differences in channel and floodplain flow to the breach location, which, as mentioned above, is computed using different terms. For lower roughness coefficients ( $< 0.6 \text{ s/m}^{1/3}$ ) the difference in the peak flow is the largest, while for the higher ones the peak flow is virtually identical. Also, the roughness coefficient controls the water level in the river channel and the adjacent floodplain and thus the water height above the levee toe.

Higher water levels at higher roughness conditions lead to a stronger breach outflow discharge.

The tests demonstrated reliability of the new breach module in LISFLOOD-FP under different conditions on simplified terrain and also shows the potential to calibrate the models to obtain identical results. Moreover, the computation time difference showed an obvious advantage of LISFLOOD-FP over HEC-RAS. Computation time plays a crucial role in large-scale flood modelling and is rather a remarkable burden in 2D large-scale simulations particularly.

### 4.4.2. Historic events simulations

Concerning more complex configurations, we looked at the embankment failure that occurred on the Secchia River. There we aimed at simulating the whole chain of the flood event starting from the flow ca. 5.5 km upstream of the breach, the failure and the floodplain inundation using the new module of LISFLOOD-FP. Notwithstanding the heterogeneity of the terrain in the area, which potentially might have become a source of inaccuracies, LISFLOOD-FP produced credible outcomes. Moreover, a raster-based model with 25 m resolution would not be able to include fine linear features of the terrain such as embankments and canals, which are in some cases not more than 5 m wide. We suggest that in order to address these points additional calibration of the floodplain roughness coefficients should substantially improve the flood extent fit, however this was not the goal of the sensitivity analysis. This study was not deliberately assessing the uncertainties related to the input data, nevertheless, it is worth mentioning that there are possible ambiguities related to the DEM vertical accuracy and likely errors in the water evaluation control points.

In some simulations low modular limits of 0.1 provided numerically unstable calculations of the flow leaving the breach with the large portion of backwater effect at the time point when it is not supposed to occur. The tests have shown that such instabilities can be solved by the change of modular limit. Based on sensitivity analysis and synthetic tests we found that modular limit values between 0.2 and 0.8 produce numerically stable simulations. Moreover, very low Manning roughness coefficients ( $< 0.015$ ) used in the area adjacent to the breach should be avoided due to instability issues.

Concerning the test of the Polesine flood of 1951, due to the lack of detailed bathymetry and terrain data from 1951, the model was set up according to modern geometries (breach depth and width). LISFLOOD-FP reached sufficient accuracy in simulating the whole chain of the event: extreme water levels within the channel, simultaneous breach at multiple pre-defined locations and consequent inundation of the floodplain. Investigating the floodplain flow propagation, we gained substantial accuracy of 83%. Viero et al. (2019) in their study attained 86-88% accuracy by using a DEM which does not contain anthropogenic changes imposed since 1951. However, the model was not

able to simulate inundation in the western part of the domain. This was expected due to the terrain topography which lowers to the east, closer to the vicinity of the sea coast. The changes in terrain elevation between 1951 and 2004/2011 are rather prominent in the western part of the model domain (Viero et al. 2019). As mentioned above, some of the embankments were built after 1951; one of them crossing from north to south and acted in our simulation as a flood boundary (see brown line in Figure 40). We suspect that this could explain the underprediction of inundation in the western part of the domain.

It is, however, important to specify that the reference inundation extent used to compute CSI is likely subject to biases, as it was reconstructed based on historical data and post-event field surveys (Viero et al. 2019). From this test we could see that the sub-routine is numerically stable for a geographically large simulation with multiple breaches and was able to produce reasonable outcomes.

### 4.4.3. Assumption and limitation of the levee failure extension

Alongside the module flexibility and rather simple setup, there are certain aspects of the newly developed routine that are worth highlighting. First and foremost, the input DEM has to include important elements, such as the levee location and crest height. In many instances the levee height and location data can be unavailable. However there are options being developed to extract levee locations and height from the remotely sensed images, available geodata (OpenStreetMap (Contributors OSM 2012)) cadastral data. Some methods would include DEM-based algorithms (Sofia et al. 2014; Krüger 2010; Wing et al. 2019). The increasing availability of LiDAR surveys should make levee extraction more feasible for flood modellers in the future.

Another important aspect is that the assumed breach shape is rectangular and expressed as a multiple of the raster resolution. For large-scale modelling which sometimes run at the 100 m resolution and coarser, the minimum breach width might be an overestimation. Numerous studies on the breach modelling have shown the importance of a detailed description of the geometry of the breach, which in most cases is either rectangular or trapezoidal (Viero et al. 2013; Wu and Li 2017). In our study, we assume that for large-scale studies, where the breach width would range from 25 m up to hundreds of meters, such complication for the model is negligible. The levee thickness is defined by the terrain resolution, meaning, if the input DEM resolution is 50 m, the levee is 50 m wide.

An important point to consider is that breach occurs instantaneously, meaning, the breach width starts developing as soon as the breaching conditions are met. For long-term simulations on large scale we might neglect the breach evolution over time (Di Baldassare et al. 2009b).

Moreover, the model does not account for sediment transport and rapid changes in the river bed due to morphodynamic processes. Therefore, in cases where the flow is expected to be largely impacted by the above mentioned factors, the breaching module of

LISFLOOD-FP should be replaced by a morphodynamic model. The tool is not meant for detailed engineering studies of the breaching phenomenon and should be used for regional and large-scale hazard and risk assessments. However, in case when supercritical flow is expected, full-momentum models should be applied.

### 4.5. Conclusion

This Chapter presents a new levee-breaching extension within the widely-used model LISFLOOD-FP for simulating flood breaching scenarios over geographically small and large areas, which extends the array of possible applications of the LISFLOOD-FP model. Levee breaching is a useful component for hydrodynamic models to replicate the complex interaction between the river channel and floodplains in 2D mode. The tests shown above prove that the extension is capable to reasonably simulate historical flooding events. The tests on various domain sizes and different magnitudes of hydrological forcing proved that the module is able to capture the flow leaving the breach and reproduce the interactions between the river channel and protected floodplains. Given the computation time of the Secchia river flood simulations (about 3 minutes) and the rather large amount of computational cells (880,000) we suggest that levee breaching in fully 2D mode with LISFLOOD-FP can be performed in Monte Carlo simulations for the probabilistic flood mapping. The same conclusion also applies for larger study areas as demonstrated by the Polesine flood simulations. Compared to already existing tool (i.e. HEC-RAS), which allows levee-breaching in fully 2D mode, LISFLOOD-FP is much more computationally faster. The ability to quickly yet efficiently simulate levee failure and consequent inundation of the protected floodplain in 2D mode may be of great use for flood risk modellers and decision-makers, as the calculation of the residual risks is a crucial component for flood management. Such efficiency can benefit near-real time simulations and support flood management solutions in emergency cases.

Further studies should be aimed at running more tests of the tool in more diverse conditions, setups and scales, in detail investigate backwater effects. By accepting certain assumptions and performing numerous tests, we suggest that the LISFLOOD-FP breaching extension is an effective tool which will allow for levee breaching simulations on the local, regional and large scales with the minimum setup and computation effort.



# Synthesis

The Thesis aimed at investigating new approaches to simulate inundations and flooding across large geographical scales, considering the possibility for levee systems to breach, adopting a fully 2D modelling scheme. In order to tackle this general goal, we addressed the following research questions (RQs):

1. How do two-dimensional hydrodynamic models with different complexity contribute to flood hazard mapping with a specific focus on areas with complex topography? What is their potential relative to large-scale studies?
2. What is the potential of raster-based 2D models for simulating inundations across large geographical areas characterized by heavily anthropogenically modified terrain? What is the impact of terrain pre-processing and resolution under such circumstances?
3. Concerning a new levee breaching extension for LISFLOOD-FP<sup>1</sup> model, what are its main advantages and potential?

Below we would like to present the conclusion drawn for each RQ.

*How do two-dimensional hydrodynamic models with different complexity contribute to flood hazard mapping with a specific focus on areas with complex topography? What is their potential relative to large-scale studies?*

---

<sup>1</sup> Bates, P.; Horritt, M. S.; Fewtrell, T. J. (2010): A simple inertial formulation of the shallow water equations for efficient two-dimensional flood inundation modelling. In *Journal of Hydrology* 387 (1-2), pp. 33–45. DOI: 10.1016/j.jhydrol.2010.03.027.

The aim of first RQ was to see how two models (LISFLOOD-FP and HEC-RAS 2D<sup>2</sup>) of different complexity (in terms of the governing equation used and the mesh representation) with given terrain resolution reproduce the flooding event of January 2014 that occurred on Secchia River and how accurate the results are. We adopted rather coarse resolutions for the Secchia River study area, as our main goal was to identify the potential of the codes and mesh dimensions to simulate events over large regions; therefore, we resampled LiDAR DEM to obtain 25, 50 and 100 m resolution datasets. First, it was concluded that 25 m resolution for describing terrain with complex linear features is a reasonable compromise between output accuracy and computational time for LISFLOOD-FP model (8 minutes on the 4 cores with the Intel Core i7 3.60 GHz CPU, 64 GB RAM), while for HEC-RAS it would be the configuration of 1 m subgrid terrain and 100 m mesh size (4 minutes on the same hardware). The other resolutions performed comparably to the best performing ones in terms of the overall flood extent (77-78% compared to best result of 81%), however a more detailed look showed, that in the focus areas (small urbanised settlements, which experienced most damages during the January 2014 Secchia River flooding event) the models tended to underestimate the observed flooding parameters (water depth and flood extent). This brought us to the conclusion, that despite overall satisfying performance (77-81%), the focus areas with potential to have large socio-economic losses remain poorly predicted. This issue is suggested to be solved by focusing on such areas initially, by giving additional attention to such areas in the model set up and calibration. Another crucial factor in flood hazard modelling is computation time. To investigate this aspect we analysed the run time in light of the obtained results accuracy. We found out that best performing configurations of LISFLOOD-FP with 25 m resolution was two times slower than HEC-RAS (8 minutes and 4 minutes, correspondingly). It is worth pointing out, that the HEC-RAS configuration which showed a good balance between results accuracy (78% inundation extent accuracy) and computation time (4 minutes) required the usage of the LiDAR terrain data with 1 m resolution as an input file, which is available in very limited number of river basins around the globe. While, 25-30 m DEM is more available globally (e.g., SRTM DEM has 30 m resolution).

Second, the investigation provided useful insights regarding the complexity of the modelling schemes and mesh representation. Our study highlights the computational advantage of the inertial formulation of the shallow water equations LISFLOOD-FP model compared to diffusion wave HEC-RAS. Comparing the duration of one simulation for the same mesh sizes and time step of the two models, LISFLOOD-FP was up to 20 times faster (for 50 m LISFLOOD-FP and 50 m HEC-RAS mesh with 1 m subgrid terrain). This study

---

<sup>2</sup> Brunner, G. W. (2016): HEC-RAS River Analysis System. Hydraulic Reference Manual. Version 5.0. HYDROLOGIC ENGINEERING CENTER DAVIS CA.

showed that such codes and setup can potentially be used for probabilistic/preliminary flood risk assessment.

*What is the potential of raster-based 2D models for simulating inundations across large geographical areas characterized by heavily anthropogenically modified terrain? What is the impact of terrain pre-processing and resolution under such circumstances?*

To address this question we considered large-scale simulations on the River Po (study domain of over 6675 km<sup>2</sup>). A fully 2D model implemented by referring to detailed topographic data may produce spatially complete results in terms of the inundated extent, water depths and velocities. We looked into the mid-lower portion of the Po River, from near Isola Sant'Antonio to Po River delta (overall length of the river stretch: 350 km). This river reach is extremely complex in terms of morphology and terrain, i.e. there is an extensive network of main and minor embankments that protect the floodplains from the events of different recurrence interval. We analysed 6 sets of topographical configurations, which represented different resolution (30, 50 and 100m) and levee representation (simple LiDAR aggregation and LiDAR aggregation with precise manual incorporation of the levee height and location).

We simulated a historic event that occurred on the Po River in October 2000 using LISLFOOD-FP fully 2D model. Our results showed that in such complex system, as in the current case study, a careful manual incorporation of the actual levee location and height is the most crucial element for controlling the accuracy of the simulation. The inclusion of the actual levee height into the working grids enabled us to look into the hydraulic process in detail. By performing an exhaustive calibration of the model, we identified that 30 and 50 m resolution provided favourable results in terms of maximum water surface elevations at the 171 investigated river cross-section by means of RMSE. With the second configuration (50 m resolution with manually added levees) we gained better performance in relation to the computation time, which was over two times longer for 30 m resolution with only a few centimetres improvement for the water surface elevation RMSE (0.34 m for 30 m resolution and 0.39 for 50 m resolution). The comparison between observed and simulated discharges at Cremona gauging station (upstream part of the reach) showed that the model slightly overestimates the discharge (Mean Error 311 m<sup>3</sup>/s and -272 m<sup>3</sup>/s for 30 m and 50 m resolutions correspondingly, where the peak is 12,000 m<sup>3</sup>/s). Moreover, the peak discharge for both configurations was less than 1% lower than observed. The behaviour of the 30 m and 50 m resolutions in terms of the distribution of local velocities was very similar, the average difference was within  $\pm 0.5$  m/s. Maximum velocities were observed at the outer side of meanders near the embankment, which gives valuable input for the investigation of the embankment stability and breach probability.

Such an approach (2D) advances previous studies (1D, combined 1D/2D simulations) done on the same study area. This leads to an assumption that 2D raster-based model can be used for even larger areas, than those presented above and cover i.e. the whole Po River basin. Furthermore, we suggest that it makes it possible to consider the levee breaching simulations for large-scale studies.

*Concerning a new levee breaching extension for LISFLOOD-FP model, what are its main advantages and potential?*

Analysing two previous objectives, it was concluded that with this given configuration and current data availability it is possible to further deepen the understanding of the channel-floodplain interactions on the large-scale. Such understanding will greatly contribute to the studies on the river system behaviour and flow dynamics upstream and downstream from a possible breach. Controlled flooding or activation of protected floodplain may reduce breaching risk downstream. On the basis of these encouraging outcomes, we specifically developed a new extension for the widely used and well-known model LISFLOOD-FP. The new LISFLOOD-FP extension enables the user to simulate levee-breaching scenarios over geographically small and large areas, which extends the array of possible applications of the model itself. The extension is based on a set of breaching conditions written into the original code of LISFLOOD-FP, where the breach is activated when a user-defined breaching criteria are met (e.g. water levels from the riverside are higher than a certain value for a set duration of time), while the breach location and depth are also set by the user.

Since LISFLOOD-FP is a raster-based model that operates with rectangular structured mesh of the same size as input raster, the minimal breach width equals to the input raster resolution. Such simplified set of parameters is particularly useful for large-scale simulations, when multiple breaches are considered for levee systems consisting of several thousand kilometres of levee and embankments. In order to test the new extension, we applied an analysis of different flow conditions and topographic settings. It showed that the results are in good agreement with those obtained from full-momentum 2D modelling scheme (i.e. HEC-RAS 2D) and historical records. The simple tests on synthetic terrain and hydrograph and comparison with HEC-RAS 2D proved the ability of the new LISFLOOD-FP model to accurately reproduce the outcomes of state-of-the-art numerical schemes in terms of the flow leaving. The two other events analysed are January 2014 Secchia River flood and a catastrophic flooding of 1951 in Polesine.

The Secchia inundation case was run in fully 2D mode, where the river flow, the breaching link and consequent floodplain inundation was run in one single setup. The analysed discharge through the breach showed that the model is more sensitive to variations in the roughness parameters (at the areas at and near to the breaching location)

compared to variations in the modular limit. The accuracy of LISFLOOD-FP in simulating floodplain inundation was 64% (Critical Success Index, which measures the spatial fit of the model compared to observations, it considers over- and underestimations). Given the complexity of the study area (numerous embankments and irrigation canals which were not possible to capture with the 25 m DEM resolution) such result is considered as sufficient.

The simulations of the Polesine flood on the Po river (extreme inundation event impacting over 1000 km<sup>2</sup>), showed that the model is capable of correctly simulating the concurrent activation of three breaches at three different locations, as reported in historical records. This setup allowed the overtopping of the levee and consequent breach to be well captured and to be in line with the reports. The propagation of the flood water eastwards was correctly captured by the model, which resulted in 83% accuracy in terms of the Critical Success Index value for overall flood extent compared to the surveys.

The flexibility of the new module allows levee breaching simulations not only on the case studies shown above, but it can be applied in various geographical regions. The current configuration is designed to activate a previously located breach for user-specified criteria, therefore it does not enable the user to perform detailed studies of the breaching mechanisms nor of the morphological evolution of the breach, which are very common in the areas with high rates of sediment movement and levee erosion. Nevertheless, the levee-breaching module is a useful tool for preliminary flood risk assessment and probabilistic flood mapping. A fast solution to map levee breaches and flood propagation behind the levees is crucial for the development of flood management strategies, and this tool is specifically designed to tackle this objective and track river system behaviour and can be used on small and large-scale studies globally.

The runtime for the Polesine flood simulation, with c.a. 1,620,000-cell mesh (over 4000 km<sup>2</sup>) and overall duration of the event of 348 hours, was about 50 minutes on a server (with 2 CPUs -20 real cores and hyperthreading 40 cores- and 64 GB RAM). Given the efficient computation time, various flooding scenarios with different breach configurations and hydraulic conditions can be run on a batch mode and produce a set of flood hazard maps. Based on the performance of the tool we suggest that the tool can be applied on much larger areas than presented in the thesis, i.e. longer river reaches, large basin studies. Moreover, because of its setup efficiency, the new module may greatly contribute to the flood mapping during an event and in emergency situations, when decisions need to be made within a few hours. For instance, in reaches where the monitoring system registers higher water stages and discharges, which in turn may cause overtopping and possible breaches in highly vulnerable areas, it is possible to provide a quick assessment of flooding dynamics for different hypothetical failures and assess in advance the effects of artificial levee opening at a given location (i.e. controlled flooding) for preventing from higher flood losses downstream. In contrast to somewhat faster options, such as 1D/2D models, fully 2D

models allow representation of a scope of hazard parameters (water depth, flow velocities, arrival time) and the behaviour of the flow upstream and downstream of the breach, which can not be fully captured by 1D/2D models. This advances existing strategies in numerous governmental and non-governmental bodies which are responsible for flood management and emergency management. For instance, Civil Protection Agencies, Basin Authorities, land-use and urban planners, infrastructure and building agencies and so on. Such flood maps can be used to plan an intentional and controlled levee opening elsewhere upstream (controlled flooding), to prepare evacuation and rescue schemes, facilitate the installing of soft and hard flood defences.

It has been shown that 2D models regardless of their complexity and mesh representation provide valuable input in terms of the representation of the flooding parameters (water depth, flood extent, etc.). While HEC-RAS has a significant advantage in terms of the possibility to include high-resolution subgrid (1 m) and compute very detailed flood maps, raster-based LISFLOOD-FP achieved similar results while using coarser data (25 m) on complex terrain. In case of the Po River and its topographically complex mid-lower portion (network of minor and main embankments of different design return period along the whole reach), the use of 2D model may greatly improve already existing flood maps, which are now rather basic and schematic. As controlled flooding is recognised as one of the flood management solutions and applied in numerous countries, we suggest that development of the spatially complete hazard maps in terms of water depth and velocities may greatly facilitate for flood management and mitigation. The array of flooding scenarios can be expanded with a set of probabilistic flood maps with various breaching configurations along main embankment in order to account for different flood magnitude and breaching locations. As was shown by the January 2014 flood event on the Secchia River, even recurrent floods, that is 1 in 5 or 1 in 10-year floods, may cause immense damages and life losses. Therefore, we suggest that flood maps of different magnitude and breaching scenarios should be available to the responsible authorities. With the new levee-breaching extension of the computationally efficient LISFLOOD-FP, the development and simulations of breaching scenarios on local and large-scales has proved to be an accurate, efficient and easy-to-apply tool.

Further work on this matter should address uncertainties associated with 2D modelling on large scale considering levee breaches. The improvements should be made to aid the flood risk assessment on the basin scale and account for the numerous uncertainties associated with the breaching parameters. One of the ways to improve production of the levee breaching scenarios is by including fragility curves, which are highly informative tools for the identification of the location of the breach, based on the flood event characteristics (e.g. freeboard, duration, local velocity, hydraulic head, etc.).

Finally, we suggest that given the ever-growing computation power of the working stations and availability of high-resolution data, there will be a large attention given to various 2D models applied on large-scale studies. This study has shown that 2D modelling using raster-based code is a feasible exercise even on very large domains. Moreover, the deliberate representation of the terrain with a complex network of linear features, as it was demonstrated here, greatly improves the quality and content of outputs compared to those obtained from local studies and coarse continental models available now. Detailed 2D models are a necessary step in providing spatially complete flood maps to contribute to the EU Floods Directive objectives, hence flood risk mitigation and preparedness.



# List of Figures

Figure 1. Number of affected people (million) by disaster type: 2018 compared to 2008-2017 annual average. Taken from (CRED 2019b).....	1
Figure 2. Share of affected people (%) by continent (million). Taken from (CRED 2019b)...	2
Figure 3. Flood extent delineation on airborne SAR images at four different dates during one event. Taken from (Schumann and Moller 2015).....	12
Figure 4. Schematics of the steps commonly used in flood mapping when hydraulic models are applied. Based on Hoch and Trigg (2019) and Caribbean handbook of Risk Information Management .....	15
Figure 5. Example of 1D geometry and boundary conditions. Upper right panel is a top view on the channel and cross-sections, where yellow arrows point on the upstream and downstream boundary conditions, which in this case are represented as the relevant cross-section, located on the edges of the domain. The lower images graphically show the geometry of the cross-sections and associated water levels. Taken from (Caribbean handbook of Risk Information Management). .....	17
Figure 6. Different meshes used in 2D modelling: a) structured mesh; b) unstructured mesh; c) flexible mesh. Taken from (Teng et al. 2017).....	19
Figure 7. Schematic representation of 1D (cross-sections, green lines) and 2D (floodplain, green polygon with mesh) areas and lateral link between them (black line at left top corner in the image).....	20
Figure 8. Schematics of the raster-based model representation. Taken from (Bates 2009-2019) .....	22
Figure 9. RasMapper representation of 2 m subgrid DEM and 25 m mesh cell size of HEC-RAS 2D (adapted from Brunner (2016)). .....	30

## List of Figures

---

Figure 10. Cell face terrain data (left) and schematic representation of A (area) – H (elevation) relationship reproduced with the Property Table (right) (adapted from Brunner (2016)).....	30
Figure 11. Breach location and flow direction during the event.....	33
Figure 12. Images of the January 2014 Secchia River flooding event. Upper left corner is the breach location. Upper right shows the inundated houses and fields in the affected area. Two lower images show the inundation in Bomporto. Taken from (Raggini 2016). .....	33
Figure 13. Outflowing discharge at the levee breach point over time (adopted from D’Alpaos et al. 2014).....	34
Figure 14. Observed flood extent, hotspot focus areas (red boxes) and water marks (control points). Left red box captures the inundation in Bastiglia; right red box shows the inundation extent in Bomporto.....	35
Figure 15. Overall simulated extent for all configurations (blue), compared to the observed extent (red outline) .....	39
Figure 16. LISFLOOD-FP and HEC-RAS flood extent for different configurations at Bomporto (right red box in Figure 14). Water depth difference (m) between predicted and observed at water mark points.....	40
Figure 17. LISFLOOD-FP and HEC-RAS flood extent for different configurations at Bastiglia (left red box in Figure 14). Water depth difference (m) between predicted and observed at water marks.....	41
Figure 18. Approximate computation time of HEC-RAS and LISFLOOD-FP configurations. .....	43
Figure 19. Leakage effect of HEC-RAS subgrid mesh examples of HR100_100 (left), HR25_1 (right). Larger ponds of water in both images are disconnected from the inundation extent. ....	46
Figure 20. 25 m resolution DEM. Dark blue - canal, light green – levee.....	47
Figure 21. Location of the Po river basin within Italy. ....	53
Figure 22. Mean annual rainfall over the Po River basin (mm/year). Taken from (Autorit`a di Bacino del Fiume Po 2006). ....	53
Figure 23. Study area extent and images from 2000 flood. Images in the upper right panel are taken from (Meteolive.it 2016; nimbus.it). ....	55
Figure 24. Spatial distribution of the main and minor embankments along a portion of the upstream part of the river with associated design return periods. ....	56

## List of Figures

---

Figure 25. Schematic representation of the spread of inundation extent regarding the design return period of the main and minor embankment.....	56
Figure 26. An example of the Po river cross-section showing the elevation of the embankment in 1878 and 2005 near the Pontelagoscuero gauging station. Taken from (Di Baldassare et al. 2009a). .....	57
Figure 27. Cross-section profile location and DEM resolutions (upper). Profile without embankment (middle). Profile with embankment (lower). .....	64
Figure 28. Left: observed discharge at upstream boundary. Right: inflow of the major tributaries. ....	65
Figure 29. Distribution of local water depth. The middle panel shows overall representation of water depth for “30m_embank” configuration with localised focus areas. The upper panel represent the results for six configurations in the upstream part (A). The lower panel represent the results for six configurations in the downstream part (B). Green boxes are used to point the differences between resolutions. Left columns shows configurations with embankments. Right columns shows configurations without embankments. ....	68
Figure 30. Observed vs. simulated (30 and 50 m DEM with embankment) flow hydrograph at Cremona gauging station. ....	69
Figure 31. Distribution of local velocities. Zoomed in (a, b, c) examples represent the results of “50m_embank” configuration. ....	70
Figure 32. Orthogonal cross-sections of the levee and breach schematics: (1) water level in the river reaches the breach threshold (user defined); (2) the breach is fully formed reaching the breach depth (user defined); (3) outflow from the breach starts inundating the floodplain (equations (14) or (15)). .....	76
Figure 33. Synthetic DEM with boundary conditions (BC) used in both models (left); terrain cross-sections as reproduced by HEC-RAS and LISFLOOD-FP (LFP) from north to south (right). ....	78
Figure 34. Flow hydrograph used as an upstream boundary condition for the synthetic tests. ....	79
Figure 35. Study area of the Secchia flood: the location of upstream boundary condition (BC), the river channel, breach and floodplain (upper left and right panels). The photograph of the breach during the event (down left) (taken from Vacondio et al. 2016). .....	80
Figure 36. Polesine flood study area (upper left). Photograph of the flow through one of the breaches during the event (upper right). Study area extent and the outline of the surveyed flood extent (lower). .....	83

## List of Figures

---

Figure 37. Flow through the breach simulated by HEC-RAS and LISFLOOD-FP, unsteady boundary conditions. ....	85
Figure 38. NSE values for each configuration of modular limit and roughness coefficient n. ....	86
Figure 39. Simulated (blue) and observed (red) inundation extent.....	87
Figure 40. Results of the Polesine flood simulation. Maximum water depth at each cell and surveyed flood extent.....	88

# List of Tables

Table 1. Some of most common 2D software used for river flood modelling.....	21
Table 2. Simulation configurations.....	37
Table 3. Critical Success Index (in %), inundation extent accuracy.....	39
Table 4. RMSE [m] of the water depth at water marks.....	42
Table 5. Selected studies done on flood modelling on the mid-lower portion of the Po River. .....	59
Table 6. Names of configurations tested.....	63



# Bibliography

- Afshari, Shahab; Tavakoly, Ahmad A.; Rajib, Mohammad Adnan; Zheng, Xing; Follum, Michael L.; Omranian, Ehsan; Fekete, Balázs M. (2018): Comparison of new generation low-complexity flood inundation mapping tools with a hydrodynamic model. In *Journal of Hydrology* 556, pp. 539–556. DOI: 10.1016/j.jhydrol.2017.11.036.
- Alfieri, L.; Bisselink, B.; Dottori, F.; Naumann, G.; Roo, A. de; Salamon, P. et al. (2017): Global projections of river flood risk in a warmer world. In *Earth's Future* 5 (2), pp. 171–182. DOI: 10.1002/2016EF000485.
- Alfieri, L.; Burek, P.; Feyen, L.; Forzieri, G. (2015): Global warming increases the frequency of river floods in Europe. In *Hydrol. Earth Syst. Sci.* 19 (5), pp. 2247–2260. DOI: 10.5194/hess-19-2247-2015.
- Alfieri, L.; Salamon, P.; Bianchi, A.; Neal, J.; Bates, P.; Feyen, L. (2014): Advances in pan-European flood hazard mapping. In *Hydrol. Process.* 28 (13), pp. 4067–4077. DOI: 10.1002/hyp.9947.
- Alfieri, Lorenzo; Dottori, Francesco; Betts, Richard; Salamon, Peter; Feyen, Luc (2018): Multi-Model Projections of River Flood Risk in Europe under Global Warming. In *Climate* 6 (1), p. 6. DOI: 10.3390/cli6010006.
- Almeida, Gustavo A. M. de; Bates, Paul (2013): Applicability of the local inertial approximation of the shallow water equations to flood modeling. In *Water Resour. Res.* 49 (8), pp. 4833–4844. DOI: 10.1002/wrcr.20366.
- Amarnath, G.; Umer, Y. M.; Alahacoon, N.; Inada, Y. (2015): Modelling the flood-risk extent using LISFLOOD-FP in a complex watershed. Case study of Mundeni Aru River Basin, Sri Lanka. In *Proc. IAHS* 370, pp. 131–138. DOI: 10.5194/piahs-370-131-2015.
- Andersen, Christine F. (2007): The New Orleans hurricane protection system. What went wrong and why. A report. Reston Va.: ASCE.

## Bibliography

---

- Apel, H.; Aronica, G. T.; Kreibich, H.; Thielen, A. H. (2009): Flood risk analyses—how detailed do we need to be? In *Nat Hazards* 49 (1), pp. 79–98. DOI: 10.1007/s11069-008-9277-8.
- Apel, Heiko; Thielen, Annegret H.; Merz, Bruno; Blöschl, Günter (2006): A Probabilistic Modelling System for Assessing Flood Risks. In *Nat Hazards* 38 (1-2), pp. 79–100. DOI: 10.1007/s11069-005-8603-7.
- Aronica, G.; Bates, P. D.; Horritt, M. S. (2002): Assessing the uncertainty in distributed model predictions using observed binary pattern information within GLUE. In *Hydrol. Process.* 16 (10), pp. 2001–2016. DOI: 10.1002/hyp.398.
- Autorità di Bacino del Fiume Po (2006): Behaviour of the Po River catchment and first investigation of the impact of human activities on water resources. in Italian.
- Bates, P. (2009-2019): LISFLOOD-FP. University of Bristol. Bristol. Available online at <http://www.bristol.ac.uk/geography/research/hydrology/models/lisflood/>, checked on 10/15/2019.
- Bates, P.; Horritt, M. S.; Fewtrell, T. J. (2010): A simple inertial formulation of the shallow water equations for efficient two-dimensional flood inundation modelling. In *Journal of Hydrology* 387 (1-2), pp. 33–45. DOI: 10.1016/j.jhydrol.2010.03.027.
- Bates, P.D; Roo, A.P.J de (2000): A simple raster-based model for flood inundation simulation. In *Journal of Hydrology* 236 (1-2), pp. 54–77. DOI: 10.1016/S0022-1694(00)00278-X.
- Biancamaria, Sylvain; Lettenmaier, Dennis P.; Pavelsky, Tamlin M. (2016): The SWOT Mission and Its Capabilities for Land Hydrology. In *Surv Geophys* 37 (2), pp. 307–337. DOI: 10.1007/s10712-015-9346-y.
- Bindlish, Rajat; Crow, Wade T.; Jackson, Thomas J. (2009): Role of Passive Microwave Remote Sensing in Improving Flood Forecasts. In *IEEE Geosci. Remote Sensing Lett.* 6 (1), pp. 112–116. DOI: 10.1109/LGRS.2008.2002754.
- Bradbrook, Kate (2006): JFLOW. A multiscale two-dimensional dynamic flood model. In *Water & Environment J* 20 (2), pp. 79–86. DOI: 10.1111/j.1747-6593.2005.00011.x.
- Brandimarte, Luigia; Di Baldassarre, Giuliano (2012): Uncertainty in design flood profiles derived by hydraulic modelling. In *Hydrology Research* 43 (6), pp. 753–761. DOI: 10.2166/nh.2011.086.
- Brivio, P. A.; Colombo, R.; Maggi, M.; Tomasoni, R. (2010): Integration of remote sensing data and GIS for accurate mapping of flooded areas. In *International Journal of Remote Sensing* 23 (3), pp. 429–441. DOI: 10.1080/01431160010014729.

## Bibliography

---

- Bruijn, K. de; Diermanse, F. L.; van der Doef, M.; & Klijn, F. (Eds.) (2016): Hydrodynamic system behaviour. Its analysis and implications for flood risk management. E3S Web of Conferences: EDP Sciences.
- Brunner, G. W. (2016): HEC-RAS River Analysis System. Hydraulic Reference Manual. Version 5.0. HYDROLOGIC ENGINEERING CENTER DAVIS CA.
- Bubeck, Philip; Dillenardt, Lisa; Alfieri, Lorenzo; Feyen, Luc; Thielen, Annegret H.; Kellermann, Patric (2019): Global warming to increase flood risk on European railways. In *Climatic Change* 155 (1), pp. 19–36. DOI: 10.1007/s10584-019-02434-5.
- Büchle, B.; Kreibich, H.; Kron, A.; Thielen, A.; Ihringer, J.; Oberle, P. et al. (2006): Flood-risk mapping. Contributions towards an enhanced assessment of extreme events and associated risks. In *Nat. Hazards Earth Syst. Sci.* 6 (4), pp. 485–503. DOI: 10.5194/nhess-6-485-2006.
- Calabresi, G. (Ed.) (1996): The use of ERS SAR for flood monitoring. An overall assessment. ERS Applications.
- Caribbean handbook of Risk Information Management: 3.4 Fluvial modelling. Edited by M. A. Trigg. Caribbean handbook of Risk Information Management. Available online at <http://www.charim.net/methodology/34>.
- Carisi, F.; Schröter, K.; Domeneghetti, A.; Kreibich, H.; Castellarin, A. (2018): Development and assessment of uni- and multivariable flood loss models for Emilia-Romagna (Italy). In *Nat. Hazards Earth Syst. Sci.* 18 (7), pp. 2057–2079. DOI: 10.5194/nhess-18-2057-2018.
- Cassardo, C.; Cremonini, R.; Gandini, D.; Paesano, G.; Pelosini, R.; Qian, M. W. (2001): Analysis of the severe flood of 13th-16th October 2000 in Piedmont (Italy). In *Cuadernos de Investigación Geográfica* 27 (0), p. 147. DOI: 10.18172/cig.1120.
- Castellarin, A.; Ceola, S.; Toth, E.; Montanari, A. (2014): Evolving water resources systems. Understanding, predicting and managing water - society interactions. Wallingford, Oxfordshire: International Association of Hydrological Sciences (IAHS) Press (IAHS publication, 0144-7815, 364).
- Castellarin, A.; Di Baldassare, G.; Brath, A. (2011a): Floodplain management strategies for flood attenuation in the river Po. In *River Res. Applic.* 27 (8), pp. 1037–1047. DOI: 10.1002/rra.1405.
- Castellarin, A.; Di Baldassarre, G.; Bates, P. D.; Brath, A. (2009): Optimal Cross-Sectional Spacing in Preissmann Scheme 1D Hydrodynamic Models. In *J. Hydraul. Eng.* 135 (2), pp. 96–105. DOI: 10.1061/(ASCE)0733-9429(2009)135:2(96).
- Castellarin, Attilio; Domeneghetti, Alessio; Brath, Armando (2011b): Identifying robust large-scale flood risk mitigation strategies. A quasi-2D hydraulic model as a tool for the

## Bibliography

---

- Po river. In *Physics and Chemistry of the Earth, Parts A/B/C* 36 (7-8), pp. 299–308. DOI: 10.1016/j.pce.2011.02.008.
- Collegio Ingegneri Venezia (2018): Visita Tecnica alla Centrale di Isola Serafini sul fiume Po. Available online at <https://www.collegioingegnerivenezia.it/eventi/301-visita-tecnica-alla-centrale-di-isola-serafini-sul-fiume-po.html>.
- Contributors OSM (2012): OpenStreetMap. Available online at [www.openstreetmap.org](http://www.openstreetmap.org).
- Coulthard, Tom J.; Neal, Jeff C.; Bates, Paul D.; Ramirez, Jorge; Almeida, Gustavo A. M. de; Hancock, Greg R. (2013): Integrating the LISFLOOD-FP 2D hydrodynamic model with the CAESAR model. Implications for modelling landscape evolution. In *Earth Surf. Process. Landforms* 38 (15), pp. 1897–1906. DOI: 10.1002/esp.3478.
- CRED (2019a): 2018 Review of disaster events. Supplementary Information. Centre for Research on the Epidemiology of Disasters. Available online at <http://www.emdat.be>.
- CRED (2019b): Natural Disasters 2018. Centre for Research on the Epidemiology of Disasters. Available online at [www.emdat.be](http://www.emdat.be).
- D’Alpaos, L.; Brath, A.; Fioravante, V.; Gottardi, G.; Mignosa, P.; Orlandini, S. (2014): Relazione tecnico-scientifica sulle cause del collasso dell’argine del fiume Secchia avvenuto il giorno 19 gennaio 2014 presso la frazione San Matteo: Regione Emilia-Romagna, Bologna.
- D’Oria, Marco; Mignosa, Paolo; Tanda, Maria Giovanna (2015): An inverse method to estimate the flow through a levee breach. In *Advances in Water Resources* 82, pp. 166–175. DOI: 10.1016/j.advwatres.2015.05.002.
- Dazzi, S.; Vacondio, R.; Mignosa, P. (2019): Integration of a Levee Breach Erosion Model in a GPU-Accelerated 2D Shallow Water Equations Code. In *Water Resour. Res.* 137 (12), p. 1549. DOI: 10.1029/2018WR023826.
- Dellepiane, S.; Angiati, E. (Eds.) (2012): Cosmo SkyMed in support of flood monitoring. 2012 IEEE International Geoscience and Remote Sensing Symposium: IEEE.
- Dewan, Ashraf M.; Islam, M. Monirul; Kumamoto, T.; Nishigaki, M. (2007): Evaluating Flood Hazard for Land-Use Planning in Greater Dhaka of Bangladesh Using Remote Sensing and GIS Techniques. In *Water Resour Manage* 21 (9), pp. 1601–1612. DOI: 10.1007/s11269-006-9116-1.
- Di Baldassare, G.; Castellarin, A.; Brath, A. (2009a): Analysis of the effects of levee heightening on flood propagation. Example of the River Po, Italy. In *Hydrological Sciences Journal* 54 (6), pp. 1007–1017. DOI: 10.1623/hysj.54.6.1007.

## Bibliography

---

- Di Baldassare, G.; Castellarin, A.; Molnar, P.; Brath, A. (2009b): Probability-weighted hazard maps for comparing different flood risk management strategies. A case study. In *Nat Hazards* 50 (3), pp. 479–496. DOI: 10.1007/s11069-009-9355-6.
- Di Baldassare, G.; Schumann, G. J.-P.; Bates, P. D.; Freer, J. E.; Beven, K. J. (2010): Flood-plain mapping. A critical discussion of deterministic and probabilistic approaches. In *Hydrological Sciences Journal* 55 (3), pp. 364–376. DOI: 10.1080/02626661003683389.
- Dimitriadis, P.; Tegos, A.; Oikonomou, A.; Pagana, V.; Koukouvinos, A.; Mamassis, N. et al. (2016): Comparative evaluation of 1D and quasi-2D hydraulic models based on benchmark and real-world applications for uncertainty assessment in flood mapping. In *Journal of Hydrology* 534, pp. 478–492. DOI: 10.1016/j.jhydrol.2016.01.020.
- Domeneghetti, A. (2014): Effects of minor drainage networks on flood hazard evaluation. In *Proc. IAHS* 364, pp. 192–197.
- Domeneghetti, A.; Carisi, F.; Castellarin, A.; Brath, A. (2015): Evolution of flood risk over large areas. Quantitative assessment for the Po river. In *Journal of Hydrology* 527, pp. 809–823. DOI: 10.1016/j.jhydrol.2015.05.043.
- Domeneghetti, A.; Castellarin, A.; Brath, A. (2012): Assessing rating-curve uncertainty and its effects on hydraulic model calibration. In *Hydrol. Earth Syst. Sci.* 16 (4), pp. 1191–1202. DOI: 10.5194/hess-16-1191-2012.
- Domeneghetti, A.; Vorogushyn, S.; Castellarin, A.; Merz, B.; Brath, A. (2013): Probabilistic flood hazard mapping. Effects of uncertain boundary conditions. In *Hydrol. Earth Syst. Sci.* 17 (8), pp. 3127–3140. DOI: 10.5194/hess-17-3127-2013.
- Dottori, Francesco; Salamon, Peter; Bianchi, Alessandra; Alfieri, Lorenzo; Hirpa, Feyera Aga; Feyen, Luc (2016): Development and evaluation of a framework for global flood hazard mapping. In *Advances in Water Resources* 94, pp. 87–102. DOI: 10.1016/j.advwatres.2016.05.002.
- Dottori, Francesco; Szewczyk, Wojciech; Ciscar, Juan-Carlos; Zhao, Fang; Alfieri, Lorenzo; Hirabayashi, Yukiko et al. (2018): Increased human and economic losses from river flooding with anthropogenic warming. In *Nat Clim Chang* 8 (9), pp. 781–786. DOI: 10.1038/s41558-018-0257-z.
- European Commission: The EU Floods Directive. Available online at [https://ec.europa.eu/environment/water/flood\\_risk/](https://ec.europa.eu/environment/water/flood_risk/).
- European Commission (2007): Directive 2007/60/EC of the European Parliament and of the Council of 23 October 2007 on the assessment and management of flood risks, Flood Directive, revised European Parliament and Council. In : Official Journal L 288.

## Bibliography

---

- European Environment Agency (2007): CLC2006 technical guidelines. Luxembourg: Publications Office (Technical report (European Environment Agency. Online), 17/2007).
- Falter, D.; Vorogushyn, S.; Lhomme, J.; Apel, H.; Gouldby, B.; Merz, B. (2013): Hydraulic model evaluation for large-scale flood risk assessments. In *Hydrol. Process.* 27 (9), pp. 1331–1340. DOI: 10.1002/hyp.9553.
- Fewtrell, T. J.; Bates, P. D.; Horritt, M.; Hunter, N. M. (2008): Evaluating the effect of scale in flood inundation modelling in urban environments. In *Hydrol. Process.* 22 (26), pp. 5107–5118. DOI: 10.1002/hyp.7148.
- Fewtrell, Timothy J.; Neal, Jeffrey C.; Bates, Paul D.; Harrison, Peter J. (2011): Geometric and structural river channel complexity and the prediction of urban inundation. In *Hydrol. Process.* 25 (20), pp. 3173–3186. DOI: 10.1002/hyp.8035.
- Geoportale Nazionale (2017): Progetto PST - Dati LiDAR. Available online at <http://www.pcn.minambiente.it/mattm/progetto-pst-dati-lidar/>.
- Goodell, C. (2015): The RAS Solution 2015. 2D Mesh “Leaking”. Available online at <http://hecrasmodel.blogspot.com/search/label/Leaking>.
- Gouldby, B.; Sayers, P.; Mulet-Marti, J.; Hassan, M. A. A. M.; Benwell, D. (2008): A methodology for regional-scale flood risk assessment. In *Proceedings of the Institution of Civil Engineers - Water Management* 161 (3), pp. 169–182. DOI: 10.1680/wama.2008.161.3.169.
- Grimaldi, Stefania; Li, Yuan; Pauwels, Valentijn R. N.; Walker, Jeffrey P. (2016): Remote Sensing-Derived Water Extent and Level to Constrain Hydraulic Flood Forecasting Models. Opportunities and Challenges. In *Surv Geophys* 37 (5), pp. 977–1034. DOI: 10.1007/s10712-016-9378-y.
- Groeve, Tom de (2010): Flood monitoring and mapping using passive microwave remote sensing in Namibia. In *Geomatics, Natural Hazards and Risk* 1 (1), pp. 19–35. DOI: 10.1080/19475701003648085.
- Hailemariam, F. M.; Brandimarte, L.; Dottori, F. (2014): Investigating the influence of minor hydraulic structures on modeling flood events in lowland areas. In *Hydrol. Process.* 28 (4), pp. 1742–1755. DOI: 10.1002/hyp.9717.
- Hallegatte, Stephane; Green, Colin; Nicholls, Robert J.; Corfee-Morlot, Jan (2013): Future flood losses in major coastal cities. In *Nature Climate Change* 3, 802 EP -. DOI: 10.1038/nclimate1979.
- Hawker, Laurence; Neal, Jeffrey; Bates, Paul (2019): Accuracy assessment of the TanDEM-X 90 Digital Elevation Model for selected floodplain sites. In *Remote Sensing of Environment* 232, p. 111319. DOI: 10.1016/j.rse.2019.111319.

## Bibliography

---

- Hess, L. L.; Melack, J. M.; Filoso, S.; Wang, Yong (1995): Delineation of inundated area and vegetation along the Amazon floodplain with the SIR-C synthetic aperture radar. In *IEEE Trans. Geosci. Remote Sensing* 33 (4), pp. 896–904. DOI: 10.1109/36.406675.
- Hoch, Jannis M.; Trigg, Mark A. (2019): Advancing global flood hazard simulations by improving comparability, benchmarking, and integration of global flood models. In *Environmental Research Letters* 14 (3), p. 34001. DOI: 10.1088/1748-9326/aaf3d3.
- Hoque, Roxana; Nakayama, Daichi; Matsuyama, Hiroshi; Matsumoto, Jun (2011): Flood monitoring, mapping and assessing capabilities using RADARSAT remote sensing, GIS and ground data for Bangladesh. In *Nat Hazards* 57 (2), pp. 525–548.
- Horritt, M. S.; Bates, P. D. (2002): Evaluation of 1D and 2D numerical models for predicting river flood inundation. In *Journal of Hydrology* 268 (1-4), pp. 87–99. DOI: 10.1016/S0022-1694(02)00121-X.
- Horritt, M. S.; Bates, P. D.; Fewtrell, T. J.; Mason, D. C.; Wilson, M. D. (2010a): Modelling the hydraulics of the Carlisle 2005 flood event. In *Proceedings of the Institution of Civil Engineers - Water Management* 163 (6), pp. 273–281. DOI: 10.1680/wama.2010.163.6.273.
- Horritt, M. S.; Mason, D. C.; Luckman, A. J. (2010b): Flood boundary delineation from Synthetic Aperture Radar imagery using a statistical active contour model. In *International Journal of Remote Sensing* 22 (13), pp. 2489–2507. DOI: 10.1080/01431160116902.
- Hunter, N. M.; Bates, P. D.; Neelz, S.; Pender, G.; Villanueva, I.; Wright, N. G. et al. (2008): Benchmarking 2D hydraulic models for urban flooding. In *Proceedings of the Institution of Civil Engineers - Water Management* 161 (1), pp. 13–30. DOI: 10.1680/wama.2008.161.1.13.
- IPCC (2014): Climate change 2014. Synthesis report. Contribution of Working Groups I, II and III to the Fifth Assessment Report of the Intergovernmental Panel on Climate Change. With assistance of Core Writing Team, R.K. Pachauri and L.A. Meyer (eds.). IPCC, Geneva, Switzerland.
- Jafarzadegan, Keighobad; Merwade, Venkatesh (2017): A DEM-based approach for large-scale floodplain mapping in ungauged watersheds. In *Journal of Hydrology* 550, pp. 650–662. DOI: 10.1016/j.jhydrol.2017.04.053.
- Johnson, J. Michael; Munasinghe, Dinuke; Eyelade, Damilola; Cohen, Sagy (2019): A Comprehensive Evaluation of the National Water Model (NWM) & Height Above Nearest Drainage (HAND) Flood Mapping Methodology. In *Nat. Hazards Earth Syst. Sci. Discuss.*, pp. 1–17. DOI: 10.5194/nhess-2019-82.
- Joyce, Karen E.; Belliss, Stella E.; Samsonov, Sergey V.; McNeill, Stephen J.; Glassey, Phil J. (2009): A review of the status of satellite remote sensing and image processing

## Bibliography

---

- techniques for mapping natural hazards and disasters. In *Progress in Physical Geography: Earth and Environment* 33 (2), pp. 183–207. DOI: 10.1177/0309133309339563.
- Kakar, Din Mohammad; Naeem, Ghazala; Usman, Abdullah; Hasan, Haider; Lohdi, Hira Ashfaq; Srinivasalu, Seshachalam et al. (2014): Elders Recall an Earlier Tsunami on Indian Ocean Shores. In *Eos Trans. AGU* 95 (51), pp. 485–486. DOI: 10.1002/2014EO510002.
- Kamrath, Paul; Disse, Markus; Hammer, Matthias; Köngeter, Jürgen (2006): Assessment of Discharge through a Dike Breach and Simulation of Flood Wave Propagation. In *Nat Hazards* 38 (1-2), pp. 63–78. DOI: 10.1007/s11069-005-8600-x.
- Khan, Sadiq I.; Hong, Yang; Wang, Jiahu; Yilmaz, Koray K.; Gourley, Jonathan J.; Adler, Robert F. et al. (2011): Satellite Remote Sensing and Hydrologic Modeling for Flood Inundation Mapping in Lake Victoria Basin. Implications for Hydrologic Prediction in Ungauged Basins. In *IEEE Trans. Geosci. Remote Sensing* 49 (1), pp. 85–95. DOI: 10.1109/TGRS.2010.2057513.
- Kienzler, S.; Pech, I.; Kreibich, H.; Müller, M.; Thielen, A. H. (2015): After the extreme flood in 2002. Changes in preparedness, response and recovery of flood-affected residents in Germany between 2005 and 2011. In *Nat. Hazards Earth Syst. Sci.* 15 (3), pp. 505–526. DOI: 10.5194/nhess-15-505-2015.
- Koks, E. E.; Thissen, M.; Alfieri, L.; Moel, H. de; Feyen, L.; Jongman, B.; Aerts, JCJH (2019): The macroeconomic impacts of future river flooding in Europe. In *Environmental Research Letters* 14 (8), p. 84042.
- Kreibich, Heidi; Seifert, Isabel; Thielen, Annegret H.; Lindquist, Eric; Wagner, Klaus; Merz, Bruno (2011): Recent changes in flood preparedness of private households and businesses in Germany. In *Regional Environmental Change* 11 (1), pp. 59–71. DOI: 10.1007/s10113-010-0119-3.
- Krüger, T. (2010): Algorithms for Detecting and Extracting Dikes from Digital Terrain Models. Geospatial Crossroads @ GI\_Forum -10 Proceedings of the Geoinformatics Forum Salzburg. Berlin, Offenbach: Wichmann: A. Car, G. Griesebner, J. Strobl (Eds.).
- Krupka, Martin; Wallis, Steve; Pender, Gareth; Neélz, Sylvain (2007): Some practical aspects of flood inundation modelling. In *Transport phenomena in hydraulics, Publications of the Institute of Geophysics, Polish Academy of Sciences. E-7 (401)*, pp. 129–135.
- Lacava, Teodosio; Brocca, Luca; Coviello, Irina; Faruolo, Mariapia; Pergola, Nicola; Tramutoli, Valerio (2015): Integration of optical and passive microwave satellite data for flooded area detection and monitoring. In : *Engineering Geology for Society and Territory-Volume 3*: Springer, pp. 631–635.

## Bibliography

---

- Lamb, R.; Crossley, M.; Waller, S. (2009): A fast two-dimensional floodplain inundation model. In *Proceedings of the Institution of Civil Engineers - Water Management* 162 (6), pp. 363–370. DOI: 10.1680/wama.2009.162.6.363.
- Lamovec, Peter; Veljanovski, Tatjana; Mikoš, Matjaž; Oštir, Krištof (2013): Detecting flooded areas with machine learning techniques. Case study of the Selška Sora river flash flood in September 2007. In *J. Appl. Remote Sens* 7 (1), p. 73564. DOI: 10.1117/1.JRS.7.073564.
- Larson, Lee W. (1996): The Great USA Flood of 1993. NOAA/National Weather Service. Available online at [https://www.nwrfc.noaa.gov/floods/papers/oh\\_2/great.htm](https://www.nwrfc.noaa.gov/floods/papers/oh_2/great.htm).
- Lee, Seung; Kim, Sooyoung; Kim, Moonil; Lim, Kyoung; Jung, Younghun (2014): The Effect of Hydraulic Characteristics on Algal Bloom in an Artificial Seawater Canal. A Case Study in Songdo City, South Korea. In *Water* 6 (2), pp. 399–413. DOI: 10.3390/w6020399.
- Lhomme, Julien; Sayers, Paul; Gouldby, Ben; Wills, Martin; Mulet-Marti, Jonatan (2009): Recent development and application of a rapid flood spreading method. In Paul Samuels (Ed.): *Flood risk management. Research and practice : proceedings of the European Conference on Flood Risk Management Research into Practice (FLOODrisk 2008)*, Oxford, UK, 30 September-2 October 2008 / editors, Paul Samuels ... [et al.]. Boca Raton: CRC Press, pp. 15–24.
- Li, Yuan; Grimaldi, Stefania; Walker, Jeffrey; Pauwels, Valentijn (2016): Application of Remote Sensing Data to Constrain Operational Rainfall-Driven Flood Forecasting. A Review. In *Remote Sensing* 8 (6), p. 456. DOI: 10.3390/rs8060456.
- Lim, Joongbin; Lee, Kyoo-seock (2018): Flood Mapping Using Multi-Source Remotely Sensed Data and Logistic Regression in the Heterogeneous Mountainous Regions in North Korea. In *Remote Sensing* 10 (7), p. 1036. DOI: 10.3390/rs10071036.
- Liu, Z.; Merwade, V.; Jafarzadegan, K. (2019): Investigating the role of model structure and surface roughness in generating flood inundation extents using one- and two-dimensional hydraulic models. In *Journal of Flood Risk Management* 12 (1), e12347. DOI: 10.1111/jfr3.12347.
- Liu Y., Pender G. (Ed.) (2010): A new rapid flood inundation model. proceedings of the first IAHR European Congress.
- Ludy, Jessica; Kondolf, G. Matt (2012): Flood risk perception in lands “protected” by 100-year levees. In *Nat Hazards* 61 (2), pp. 829–842. DOI: 10.1007/s11069-011-0072-6.
- Luke, Adam; Kaplan, Brad; Neal, Jeff; Lant, Jeremiah; Sanders, Brett; Bates, Paul; Alsdorf, Doug (2015): Hydraulic modeling of the 2011 New Madrid Floodway activation. A case study on floodway activation controls. In *Nat Hazards* 77 (3), pp. 1863–1887. DOI: 10.1007/s11069-015-1680-3.

## Bibliography

---

- Manfreda, Salvatore; Nardi, Fernando; Samela, Caterina; Grimaldi, Salvatore; Taramasso, Angela Celeste; Roth, Giorgio; Sole, Aurelia (2014): Investigation on the use of geomorphic approaches for the delineation of flood prone areas. In *Journal of Hydrology* 517, pp. 863–876. DOI: 10.1016/j.jhydrol.2014.06.009.
- Marchetti, Mauro (2002): Environmental changes in the central Po Plain (northern Italy) due to fluvial modifications and anthropogenic activities. In *Geomorphology* 44 (3-4), pp. 361–373. DOI: 10.1016/S0169-555X(01)00183-0.
- Marcus, W. Andrew; Fonstad, Mark A. (2008): Optical remote mapping of rivers at sub-meter resolutions and watershed extents. In *Earth Surf. Process. Landforms* 33 (1), pp. 4–24. DOI: 10.1002/esp.1637.
- Marijnissen, Richard; Kok, Matthijs; Kroeze, Carolien; van Loon-Steensma, Jantsje (2019): Re-evaluating safety risks of multifunctional dikes with a probabilistic risk framework (4).
- Masoero, Alessandro; Claps, Pierluigi; Asselman, Nathalie E. M.; Mosselman, Erik; Di Baldassarre, Giuliano (2013): Reconstruction and analysis of the Po River inundation of 1951. In *Hydrol. Process.* 27 (9), pp. 1341–1348. DOI: 10.1002/hyp.9558.
- Matgen, P.; Hostache, R.; Schumann, G.; Pfister, L.; Hoffmann, L.; Savenije, H.H.G. (2011): Towards an automated SAR-based flood monitoring system. Lessons learned from two case studies. In *Physics and Chemistry of the Earth, Parts A/B/C* 36 (7-8), pp. 241–252. DOI: 10.1016/j.pce.2010.12.009.
- Matgen, P.; Schumann, G.; Henry, J.-B.; Hoffmann, L.; Pfister, L. (2007): Integration of SAR-derived river inundation areas, high-precision topographic data and a river flow model toward near real-time flood management. In *International Journal of Applied Earth Observation and Geoinformation* 9 (3), pp. 247–263. DOI: 10.1016/j.jag.2006.03.003.
- Maugeri, Antonin (2012): Capabilities of a coupled 1D/2D model for flood inundation simulation. In *Columbia Water Center*.
- Mazzoleni, M.; Bacchi, B.; Barontini, S.; Di Baldassarre, G.; Pilotti, M.; Ranzi, R. (2014): Flooding Hazard Mapping in Floodplain Areas Affected by Piping Breaches in the Po River, Italy. In *J. Hydrol. Eng.* 19 (4), pp. 717–731. DOI: 10.1061/(ASCE)HE.1943-5584.0000840.
- Mazzoleni, Maurizio; Dottori, Francesco; Brandimarte, Luigia; Tekle, Shewandagn; Martina, Mario L. V. (2017): Effects of levee cover strength on flood mapping in the case of levee breach due to overtopping. In *Hydrological Sciences Journal* 62 (6), pp. 892–910. DOI: 10.1080/02626667.2016.1246800.

## Bibliography

---

- McGrath, Heather; Bourgon, Jean-François; Proulx-Bourque, Jean-Samuel; Nastev, Miroslav; El Ezz, Ahmad Abo (2018): A comparison of simplified conceptual models for rapid web-based flood inundation mapping. In *Nat Hazards* 93 (2), pp. 905–920.
- Meteolive.it (2016): Alluvione Piemonte e Valle d'Aosta del 13-16 ottobre 2000: 16 anni dopo! Available online at <http://www.meteolive.it/news/Amarcord/11/alluvione-piemonte-e-valle-d-aosta-del-13-16-ottobre-2000-16-anni-dopo-/55162/>.
- Moel, H. de; van Alphen, J.; Aerts, J. C. J. H. (2009a): Flood maps in Europe & methods, availability and use. In *Nat. Hazards Earth Syst. Sci.* 9 (2), pp. 289–301. DOI: 10.5194/nhess-9-289-2009.
- Moel, H. de; van Alphen, J.; Aerts, JCJH (2009b): Flood maps in Europe—methods, availability and use. In *Natural Hazards and Earth System Sciences* 9 (2), pp. 289–301.
- Montanari, A. (2012): Hydrology of the Po River. Looking for changing patterns in river discharge. In *Hydrol. Earth Syst. Sci.* 16 (10), pp. 3739–3747. DOI: 10.5194/hess-16-3739-2012.
- Morsy, M. M.; Goodall, J. L.; O'Neil, G. L.; Sadler, J. M.; Voce, D.; Hassan, G.; Huxley, C. (2018): A cloud-based flood warning system for forecasting impacts to transportation infrastructure systems. In *Environmental Modelling & Software* 107, pp. 231–244. DOI: 10.1016/j.envsoft.2018.05.007.
- Munich RE (2016): Costliest natural disasters (overall losses). Loss events worldwide 1980 – 2015. 10 costliest events ordered by overall losses. Munich, Germany.
- Musolino, Dario; Carli, Alessandro de; Massarutto, Antonio (2017): Evaluation of socio-economic impact of drought events. The case of Po river basin. In *European Countryside* 9 (1), pp. 163–176. DOI: 10.1515/euco-2017-0010.
- Nardi, Fernando; Vivoni, Enrique R.; Grimaldi, Salvatore (2006): Investigating a floodplain scaling relation using a hydrogeomorphic delineation method. In *Water Resour. Res.* 42 (9), p. 1441. DOI: 10.1029/2005WR004155.
- National Flood Relief Commission (1933): Report of the National Flood Relief Commission 1931-1932. Republic of China. Available online at <https://archive.org/details/reportofthenatio032042mbp/page/n5>.
- Neal, J.; Schumann, G.; Bates, P. (2012a): A subgrid channel model for simulating river hydraulics and floodplain inundation over large and data sparse areas. In *Water Resour. Res.* 48 (11), p. 619. DOI: 10.1029/2012WR012514.
- Neal, J.; Villanueva, I.; Wright, N.; Willis, T.; Fewtrell, T.; Bates, P. (2012b): How much physical complexity is needed to model flood inundation? In *Hydrol. Process.* 26 (15), pp. 2264–2282. DOI: 10.1002/hyp.8339.

## Bibliography

---

- Néelz, S.; Pender, G. (2009): Desktop review of 2D hydraulic modelling packages. Bristol: Environment Agency (Science project, SC080035/SR).
- Néelz S.; Pender G. (2013): Benchmarking the Latest Generation of 2D Hydraulic Flood Modelling Packages. Report SC120002. Environment Agency. Environment Agency, Horison House, Deanery Road,. Available online at <http://publications.environmentagency.gov.uk>, checked on 12/19/2018.
- nimbus.it: L'ALLUVIONE NEL NORD-OVEST DEL 13-16 OTTOBRE: CRONACA DI UNA TRAGEDIA. Available online at <http://www.nimbus.it/meteonews/alluvionenordovest.htm>.
- Nobre, Antonio Donato; Cuartas, Luz Adriana; Momo, Marcos Rodrigo; Severo, Dirceu Luís; Pinheiro, Adilson; Nobre, Carlos Afonso (2016): HAND contour. A new proxy predictor of inundation extent. In *Hydrol. Process.* 30 (2), pp. 320–333. DOI: 10.1002/hyp.10581.
- Nones, Michael (2017): Flood hazard maps in the European context. In *Water International* 42 (3), pp. 324–332. DOI: 10.1080/02508060.2016.1269282.
- Oberstadler, R.; Hönsch, H.; Huth, D. (1997): Assessment of the mapping capabilities of ERS-1 SAR data for flood mapping. A case study in Germany. In *Hydrol. Process.* 11 (10), pp. 1415–1425.
- Orlandini, S.; Moretti, G.; Albertson, J. D. (2015): Evidence of an emerging levee failure mechanism causing disastrous floods in Italy. In *Water Resour. Res.* 51 (10), pp. 7995–8011. DOI: 10.1002/2015WR017426.
- Patel, Dhruvesh P.; Srivastava, Prashant K. (2013): Flood hazards mitigation analysis using remote sensing and GIS. Correspondence with town planning scheme. In *Water Resour Manage* 27 (7), pp. 2353–2368.
- Pender, G.; Liu, Y. (2012): Rapid flood inundation modelling. Meta-Modelling of 2D hydrodynamic model using artificial intelligence techniques. FRMRC Research Report WP1. 3. Project Website: [www.floodrisk.org.uk](http://www.floodrisk.org.uk).
- Penning-Rowsell, E.; Floyd, P.; Ramsbottom, D.; Surendran, S. (2005): Estimating Injury and Loss of Life in Floods. A Deterministic Framework. In *Nat Hazards* 36 (1-2), pp. 43–64. DOI: 10.1007/s11069-004-4538-7.
- Popescu, Ioana; Cioaca, Eugenia; Pan, Quan; Jonoski, Andreja; Hanganu, Jenica (2015): Use of hydrodynamic models for the management of the Danube Delta wetlands. The case study of Sontea-Fortuna ecosystem. In *Environmental Science & Policy* 46, pp. 48–56. DOI: 10.1016/j.envsci.2014.01.012.
- Proud, Simon Richard; Fensholt, Rasmus; Rasmussen, Laura Vang; Sandholt, Inge (2011): Rapid response flood detection using the MSG geostationary satellite. In *International*

## Bibliography

---

- Journal of Applied Earth Observation and Geoinformation* 13 (4), pp. 536–544. DOI: 10.1016/j.jag.2011.02.002.
- Pulvirenti, L.; Pierdicca, N.; Chini, M.; Guerriero, L. (2011): An algorithm for operational flood mapping from Synthetic Aperture Radar (SAR) data using fuzzy logic. In *Nat. Hazards Earth Syst. Sci.* 11 (2), pp. 529–540. DOI: 10.5194/nhess-11-529-2011.
- Raggi, Meri; Davide Ronchi; Laura Sardonini; Davide Viaggi (2007): Po Basin Case study status report. AquaMoney.
- Raggini, A. (2016): Cede l'argine del Secchia, alluvione a Modena: succedeva 4 anni fa. Racconto e foto (in italian). Available online at <http://www.emiliaromagnameteo.com/cede-largine-del-secchia-alluvione-a-modena-succedeva-2-anni-fa-racconto-e-foto/>.
- Roo, A. de; van der Knijff, J.; Horritt, M.; Schmuck, G.; Jong, S. M. de (Eds.) (Eds.) (1999): Assessing flood damages of the 1997 Oder flood and the 1995 Meuse flood. Proceedings of the Second International ITC Symposium on Operationalization of Remote Sensing, Enschede. The Netherlands.
- Sampson, C. C.; Smith, A. M.; Bates, P.; Neal, J.; Alfieri, L.; Freer, J. E. (2015): A high-resolution global flood hazard model. In *Water resources research* 51 (9), pp. 7358–7381. DOI: 10.1002/2015WR016954.
- Sanders, Brett F.; Pau, John C.; Jaffe, David A. (2006): Passive and active control of diversions to an off-line reservoir for flood stage reduction. In *Advances in Water Resources* 29 (6), pp. 861–871. DOI: 10.1016/j.advwatres.2005.07.015.
- Sanders, Brett F.; Schubert, Jochen E. (2019): PRIMo. Parallel raster inundation model. In *Advances in Water Resources* 126, pp. 79–95. DOI: 10.1016/j.advwatres.2019.02.007.
- Sanyal, Joy; Lu, X. X. (2004): Application of Remote Sensing in Flood Management with Special Reference to Monsoon Asia. A Review. In *Nat Hazards* 33 (2), pp. 283–301. DOI: 10.1023/B:NHAZ.0000037035.65105.95.
- Savage, J. T. S.; Bates, P.; Freer, J. E.; Neal, J.; Aronica, G. (2016): When does spatial resolution become spurious in probabilistic flood inundation predictions? In *Hydrol. Process.* 30 (13), pp. 2014–2032. DOI: 10.1002/hyp.10749.
- Schnebele, E.; Cervone, G. (2013): Improving remote sensing flood assessment using volunteered geographical data. In *Nat. Hazards Earth Syst. Sci.* 13 (3), pp. 669–677. DOI: 10.5194/nhess-13-669-2013.
- Schumann, G.; Di Baldassarre, G.; Alsdorf, D.; Bates, P. D. (2010): Near real-time flood wave approximation on large rivers from space. Application to the River Po, Italy. In *Water Resour. Res.* 46 (5), p. 174. DOI: 10.1029/2008WR007672.

## Bibliography

---

- Schumann, G. J.-P.; Bates, P.; Horritt, M. S.; Matgen, P.; Pappenberger, F. (2009): Progress in integration of remote sensing–derived flood extent and stage data and hydraulic models. In *Rev. Geophys.* 47 (4), RG2002. DOI: 10.1029/2008RG000274.
- Schumann, G. J.-P.; Neal, J. C.; Voisin, N.; Andreadis, K. M.; Pappenberger, F.; Phanthuwongpakdee, N. et al. (2013): A first large-scale flood inundation forecasting model. In *Water Resour. Res.* 49 (10), pp. 6248–6257. DOI: 10.1002/wrcr.20521.
- Schumann, G. J.-P.; Stampoulis, D.; Smith, A. M.; Sampson, C. C.; Andreadis, K. M.; Neal, J.; Bates, P. (2016): Rethinking flood hazard at the global scale. In *Geophys. Res. Lett.* 43 (19), 10,249–10,256. DOI: 10.1002/2016GL070260.
- Schumann, Guy J.-P.; Moller, Delwyn K. (2015): Microwave remote sensing of flood inundation. In *Physics and Chemistry of the Earth, Parts A/B/C* 83-84, pp. 84–95. DOI: 10.1016/j.pce.2015.05.002.
- Semar, Olivier; Witt, Karl Josef; Fannin, R. Jonathan (2011): Suffusion Evaluation-Comparison of Current Approaches. In Susan E. Burns (Ed.): Scour and erosion. Proceedings of the fifth International Conference on Scour and Erosion, ICSE-5, November 7-10, 2010, San Francisco, California / sponsored by the Geo-Institute of the American Society of Civil Engineers, the Environmental and Water Resources Institute of the American Society of Civil Engineers ; edited by Susan E. Burns ... [et al.]. International Conference on Scour and Erosion (ICSE-5) 2010. San Francisco, California, United States, November 7-10, 2010. American Society of Civil Engineers. Geo-Institute; Environmental and Water Resources Institute. Reston, Va.: American Society of Civil Engineers (Geotechnical special publication, no. 210), pp. 251–262.
- Shustikova, I.; Domeneghetti, A.; Neal, J.; Bates, P.; Castellarin, A. (2019): Comparing 2D capabilities of HEC-RAS and LISFLOOD-FP on complex topography. In *Hydrological Science Journal*, pp. 1–14. DOI: 10.1080/02626667.2019.1671982.
- SIMPO (1982): Studio e progettazione di massima delle sistemazioni idrauliche dell'asta principale del Po, dalle sorgenti alla foce, finalizzata alla difesa ed alla conservazione del suolo e nella utilizzazione delle risorse idriche. Magistrato del Po: Parma.
- Singh, Yogesh; Ferrazzoli, Paolo; Rahmoune, Rachid (2013): Flood monitoring using microwave passive remote sensing (AMSR-E) in part of the Brahmaputra basin, India. In *International Journal of Remote Sensing* 34 (14), pp. 4967–4985. DOI: 10.1080/01431161.2013.786194.
- Smith, Laurence C. (1997): Satellite remote sensing of river inundation area, stage, and discharge. A review. In *Hydrol. Process.* 11 (10), pp. 1427–1439.

## Bibliography

---

- Sofia, Giulia; Fontana, Giancarlo Dalla; Tarolli, Paolo (2014): High-resolution topography and anthropogenic feature extraction. Testing geomorphometric parameters in floodplains. In *Hydrol. Process.* 28 (4), pp. 2046–2061.
- Sosa, Jeison; Sampson, Chris; Smith, Andy; Neal, Jeff; Bates, Paul (2019): A toolbox to quickly prepare flood inundation models for LISFLOOD-FP simulations. In *Environmental Modelling & Software*, p. 104561. DOI: 10.1016/j.envsoft.2019.104561.
- Sun, Donglian; Li, Sanmei; Zheng, Wei; Croitoru, Arie; Stefanidis, Anthony; Goldberg, Mitchell (2015): Mapping floods due to Hurricane Sandy using NPP VIIRS and ATMS data and geotagged Flickr imagery. In *International Journal of Digital Earth* 9 (5), pp. 427–441. DOI: 10.1080/17538947.2015.1040474.
- Syme, W. J. (2008): 9th National Conference on Hydraulics in Water Engineering. Hydraulics 2008. Barton, A.C.T.: Engineers Australia.
- Tavares da Costa, Ricardo; Manfreda, Salvatore; Luzzi, Valerio; Samela, Caterina; Mazzoli, Paolo; Castellarin, Attilio; Bagli, Stefano (2019): A web application for hydrogeomorphic flood hazard mapping. In *Environmental Modelling & Software* 118, pp. 172–186. DOI: 10.1016/j.envsoft.2019.04.010.
- Te Chow, Ven (1959): Open-channel hydraulics: McGraw-Hill New York.
- Temimi, Marouane; Lacava, Teodosio; Lakhankar, Tarendra; Tramutoli, Valerio; Ghedira, Hosni; Ata, Riadh; Khanbilvardi, Reza (2011): A multi-temporal analysis of AMSR-E data for flood and discharge monitoring during the 2008 flood in Iowa. In *Hydrol. Process.* 25 (16), pp. 2623–2634. DOI: 10.1002/hyp.8020.
- Temimi, Marouane; Leconte, Robert; Brissette, Francois; Chaouch, Naira (2005): Flood monitoring over the Mackenzie River Basin using passive microwave data. In *Remote Sensing of Environment* 98 (2-3), pp. 344–355. DOI: 10.1016/j.rse.2005.06.010.
- Teng, J.; Jakeman, A. J.; Vaze, J.; Croke, B.F.W.; Dutta, D.; Kim, S. (2017): Flood inundation modelling. A review of methods, recent advances and uncertainty analysis. In *Environmental Modelling & Software* 90, pp. 201–216. DOI: 10.1016/j.envsoft.2017.01.006.
- Townsend, Philip A.; Walsh, Stephen J. (1998): Modeling floodplain inundation using an integrated GIS with radar and optical remote sensing. In *Geomorphology* 21 (3-4), pp. 295–312. DOI: 10.1016/S0169-555X(97)00069-X.
- Twele, André; Cao, Wenxi; Plank, Simon; Martinis, Sandro (2016): Sentinel-1-based flood mapping. A fully automated processing chain. In *International Journal of Remote Sensing* 37 (13), pp. 2990–3004. DOI: 10.1080/01431161.2016.1192304.
- United Nations (2015): Paris Agreement. Available online at <https://unfccc.int/process-and-meetings/the-paris-agreement/the-paris-agreement>, checked on 10/23/2019.

## Bibliography

---

- Vacondio, R.; Aureli, F.; Ferrari, A.; Mignosa, P.; Dal Palù, A. (2016): Simulation of the January 2014 flood on the Secchia River using a fast and high-resolution 2D parallel shallow-water numerical scheme. In *Nat Hazards* 80 (1), pp. 103–125. DOI: 10.1007/s11069-015-1959-4.
- Vacondio, R.; Dal Palù, A.; Mignosa, P. (2014): GPU-enhanced Finite Volume Shallow Water solver for fast flood simulations. In *Environmental Modelling & Software* 57, pp. 60–75. DOI: 10.1016/j.envsoft.2014.02.003.
- van Ballegooyen, R.; Taljaard, S.; van Niekerk, L.; Huizinga, P. (2004): Using 3D modelling to predict physico-chemical responses to variation in river inflow in smaller, stratified estuaries typical of South Africa. In *Journal of Hydraulic Research* 42 (6), pp. 563–577. DOI: 10.1080/00221686.2004.9628311.
- van Mierlo, M.C.L.M.; Vrouwenvelder, A.C.W.M.; Calle, E.O.F.; Vrijling, J. K.; Jonkman, S. N.; Bruijn, K. M. de; Weerts, A. H. (2007): Assessment of flood risk accounting for river system behaviour. In *International Journal of River Basin Management* 5 (2), pp. 93–104. DOI: 10.1080/15715124.2007.9635309.
- van Staveren, Martijn F.; Warner, J. F.; Wester, P. (2017): Bringing in the floods. A comparative study on controlled flooding in the Dutch, Bangladesh and Vietnamese deltas. With assistance of J. P. M. Tatenhove. Wageningen: Wageningen University.
- Viero, Daniele P.; Roder, Giulia; Matticchio, Bruno; Defina, Andrea; Tarolli, Paolo (2019): Floods, landscape modifications and population dynamics in anthropogenic coastal lowlands. The Polesine (northern Italy) case study. In *The Science of the total environment* 651 (Pt 1), pp. 1435–1450. DOI: 10.1016/j.scitotenv.2018.09.121.
- Viero, Daniele Pietro; D’Alpaos, Andrea; Carniello, Luca; Defina, Andrea (2013): Mathematical modeling of flooding due to river bank failure. In *Advances in Water Resources* 59, pp. 82–94. DOI: 10.1016/j.advwatres.2013.05.011.
- Villaret, Catherine; Hervouet, Jean-Michel; Kopmann, Rebekka; Merkel, Uwe; Davies, Alan G. (2013): Morphodynamic modeling using the Telemac finite-element system. In *Computers & Geosciences* 53, pp. 105–113. DOI: 10.1016/j.cageo.2011.10.004.
- Vorogushyn, S.; Merz, B.; Apel, H. (2009): Development of dike fragility curves for piping and micro-instability breach mechanisms. In *Natural Hazards and Earth System Sciences* 9 (4), pp. 1383–1401.
- Vorogushyn, S.; Merz, B.; Lindenschmidt, K.-E.; Apel, H. (2010): A new methodology for flood hazard assessment considering dike breaches. In *Water Resour. Res.* 46 (8), p. 125. DOI: 10.1029/2009WR008475.

## Bibliography

---

- Vorogushyn, Sergiy; Bates, Paul D.; Bruijn, Karin de; Castellarin, Attilio; Kreibich, Heidi; Priest, Sally et al. (2018): Evolutionary leap in large-scale flood risk assessment needed. In *Wiley Interdisciplinary Reviews: Water* 5 (2), e1266.
- Vorogushyn, Sergiy; Lindenschmidt, Karl-Erich; Kreibich, Heidi; Apel, Heiko; Merz, Bruno (2012): Analysis of a detention basin impact on dike failure probabilities and flood risk for a channel-dike-floodplain system along the river Elbe, Germany. In *Journal of Hydrology* 436, pp. 120–131.
- Wang, Da-yu; Fu, Xu-dong; Jie, Yu-xin; Dong, Wei-jie; Hu, Die (2014): Simulation of pipe progression in a levee foundation with coupled seepage and pipe flow domains. In *Soils and Foundations* 54 (5), pp. 974–984. DOI: 10.1016/j.sandf.2014.09.003.
- Ward, D. P.; Petty, A.; Setterfield, S. A.; Douglas, M. M.; Ferdinands, K.; Hamilton, S. K.; Phinn, S. (2014): Floodplain inundation and vegetation dynamics in the Alligator Rivers region (Kakadu) of northern Australia assessed using optical and radar remote sensing. In *Remote Sensing of Environment* 147, pp. 43–55. DOI: 10.1016/j.rse.2014.02.009.
- Werner, M. G.F. (2004): A comparison of flood extent modelling approaches through constraining uncertainties on gauge data. In *Hydrology and Earth System Sciences Discussions* 8 (6), pp. 1141–1152.
- White, W. R.; Whitehead, E.; Forty, E. J. (2000): Extending the scope of standard specifications for open channel flow gauging structures.
- Wilson, Matthew; Bates, Paul; Alsdorf, Doug; Forsberg, Bruce; Horritt, Matthew; Melack, John et al. (2007): Modeling large-scale inundation of Amazonian seasonally flooded wetlands. In *Geophys. Res. Lett.* 34 (15), p. 54. DOI: 10.1029/2007GL030156.
- Wing, O.; Bates, P.; Neal, J.; Sampson, C.; Smith, A.; Quinn, N. et al. (2019): A new automated method for improved flood defence representation in large-scale hydraulic models. In *Water resources research*.
- Wing, Oliver E. J.; Bates, Paul D.; Sampson, Christopher C.; Smith, Andrew M.; Johnson, Kris A.; Erickson, Tyler A. (2017): Validation of a 30 m resolution flood hazard model of the conterminous United States. In *Water Resour. Res.* 53 (9), pp. 7968–7986. DOI: 10.1002/2017WR020917.
- Winsemius, Hessel C.; Aerts, Jeroen C. J. H.; van Beek, Ludovicus P. H.; Bierkens, Marc F. P.; Bouwman, Arno; Jongman, Brenden et al. (2016): Global drivers of future river flood risk. In *Nature Climate Change* 6 (4), pp. 381–385. DOI: 10.1038/nclimate2893.
- Wu, W. (2011): Earthen Embankment Breaching. In *J. Hydraul. Eng.* 137 (12), pp. 1549–1564. DOI: 10.1061/(ASCE)HY.1943-7900.0000498.

## Bibliography

---

- Wu, Weiming; Li, Honghai (2017): A simplified physically-based model for coastal dike and barrier breaching by overtopping flow and waves. In *Coastal Engineering* 130, pp. 1–13. DOI: 10.1016/j.coastaleng.2017.09.007.
- Yamazaki, Dai; Ikeshima, Daiki; Tawatari, Ryunosuke; Yamaguchi, Tomohiro; O'Loughlin, Fiachra; Neal, Jeffery C. et al. (2017): A high-accuracy map of global terrain elevations. In *Geophys. Res. Lett.* 44 (11), pp. 5844–5853. DOI: 10.1002/2017GL072874.
- Zhang, Rui; Li, Tiegang; Russell, James; Zhou, Yurou; Zhang, Fan; Liu, Zhiyong et al. (2018): High-resolution reconstruction of historical flood events in the Changjiang River catchment based on geochemical and biomarker records. In *Chemical Geology* 499, pp. 58–70. DOI: 10.1016/j.chemgeo.2018.09.003.
- Zhao, Yifei; Zou, Xinqing; Gao, Jianhua; Wang, Chenglong (2017): Recent sedimentary record of storms and floods within the estuarine-inner shelf region of the East China Sea. In *The Holocene* 27 (3), pp. 439–449.
- Zielonka, Tomasz; Holeksa, Jan; Ciapała, Szymon (2008): A reconstruction of flood events using scarred trees in the Tatra Mountains, Poland. In *Dendrochronologia* 26 (3), pp. 173–183. DOI: 10.1016/j.dendro.2008.06.003.

# Acknowledgements

This Thesis is dedicated to my mother and father for showing faith in me and giving me liberty to choose what I desired. I salute you for the selfless love, care, pain and sacrifice you did to shape my life. I wish you could have been here with me. I hope I had made you proud before you left this world.

This Thesis is the culmination of my journey of PhD which was just like climbing a high peak step by step accompanied with encouragement, hardship, trust, and frustration. I realized though only my name appears on the cover of this dissertation, a great many people including my family members, my friends, colleagues and various institutions have contributed to accomplish this huge task.

I am greatly indebted to my research guides Prof. Attilio Castellarin and Dr. Alessio Domeneghetti who accepted me as a PhD student and offered their mentorship, patience and care. This work would not have been possible without their guidance and involvement, continuous support and encouragement throughout this research project. I am extremely grateful for our friendly chats at the end of our meetings and your personal support in my academic and personal endeavours. Under their guidance I successfully overcame many difficulties and learnt a lot. Our morning jog in Rimini will be always a great reference of what team work is.

I would like to thank the external reviewers of the thesis Dr. Guy Schumann and Dr. Maurizio Mazzoleni and the committee for their very useful tips and recommendations for improving the Thesis.

My PhD program was granted by EU Horizon 2020 Marie-Sklodowska-Curie ETN "System-risk". The grant has given me an opportunity to take part in numerous seminars, conferences, workshops and meetings around the world. I am grateful to the 14 talented ESRs for endless memories and fun experiences. This project has given me an incredible chance to meet most brilliant scientists and practitioners from numerous institutions around the world, which consequently reflected on my research. I also would like to say special thank you to Dr. Kai Schröter, without his guidance this project would not have

been the same! Big thanks to Dr. Sergiy Vorogushyn who has helped me when I was in doubt and gave a valuable input in my research. Also, no research is possible without data and resource. For this I extend thanks to the Po River Basin Authority and Civil Protection Agency of Emilia Romagna.

From the bottom of my heart I would like to say big thank you to Prof. Paul Bates and Dr. Jeff Neal for their warm welcome during my secondment at Bristol University. Along with the scientific concepts and practical tips, you have showed me how it is to be truly enthusiastic about the research.

It's my fortune to gratefully acknowledge the support of my friends and colleagues who I was so lucky to meet during this journey who gave me their support and encouragement throughout the PhD. Special thanks goes to DICAM people who have helped, encouraged and supported me whenever I needed it: Francesca, Alessio, Simone, Mattia, Giada, Alberto, Elena, Serena, Lorenzo and others.

I am very grateful to Henry for encouraging me through bright and darker moments and being such a compassionate and caring boyfriend. Thank you for your rock steady support in the final stretch.

Finally, I must express my very profound gratitude to my family and friends for providing me with unfailing support and continuous encouragement throughout my years of studies. This accomplishment would not have been possible without them. Thank you! Grazie! Gracias! Danke! Dank u wel! Дякую! Спаси́бо! Obrigado! Merci!